PERMEABILITY ESTIMATION FROM FRACTURE CALIBRATION TEST ANALYSIS IN SHALE AND TIGHT GAS

A Thesis

by

HAN XUE

Submitted to the Office of Graduate Studies of
Texas A&M University
in partial fulfillment of the requirements for the degree of

MASTER OF SCIENCE

Approved by:

Chair of Committee,	Christine Ehlig-Economides
Committee Members,	Thomas Blasingame
	Walter Ayers
Head of Department,	Daniel Hill

December 2012

Major Subject: Petroleum Engineering

Copyright 2012 Han Xue

ABSTRACT

Permeability estimation in tight and shale reservoirs is challenging because little or no flow will occur without hydraulic fracture stimulation. In the pressure falloff following a fracture calibration test (FCT), radial flow after the fracture closure can be used to estimate the reservoir permeability. However, for very low permeability, the time to reach radial flow can exceed any practical duration. This study shows how to use the reservoir pressure to estimate the maximum reservoir permeability when radial flow is missing in the after-closure response. The approach is straightforward and can also be used for buildup tests. It applies whenever the well completion geometry permits radial flow before the pressure response encounters a real well drainage limits.

Recent developments have blurred the boundary between fracture calibration test analysis and classic pressure transient analysis. Adapting the log-log diagnostic plot representation to the FCT analysis has made it possible to perform before and after closure analysis on the same diagnostic plot. This paper also proposes a method for diagnosing abnormal leakoff behavior using the log-log diagnostic plot as an alternative method for the traditional G-function plot.

The results show the relationship between reservoir permeability and pressure can be used effectively for both estimation of the permeability upper bound when there is no apparent radial flow and for confirming the permeability estimated from apparent late time radial flow. Numerous field examples illustrate this simple and powerful insight.

DEDICATION

To my parents

ACKNOWLEDGEMENTS

I would like to thank my committee chair, Dr. Christine Ehlig-Economides for her dedication and support throughout the course of this research. Also, thanks to my committee members, Dr. Thomas Blasingame, and Dr. Walter Ayers.

I would like to thank also Dr. David Craig for his helpful guidance.

Thanks also to Shell, Apache Canada, Ltd., and EOG Resources, Inc. for providing the data for this research.

Also, thanks to Schlumberger and Chrisman Institute for funding and support.

Thanks also to all friends, colleagues, and the department faculty and staff for making my time at Texas A&M University an invaluable experience.

Finally, thanks to my father, mother, and all my family for their love and encouragement.

NOMENCLATURE

A_f =fracture area, L^2, ft^2

B =formation volume factor, L^3/L^3, RB/STB

b_r =p-intercept on log-log plot

b_N =intercept, Nolte-Shlyapobersky method , $ML^{-1}T^{-2}$

b_M =intercept, slope, method of Mayerhofer, Economides and Ehlig-Economides, dimensionless

s_f =compressibility of fluid in fracture, Lt^2/m, psi-1

c_t =total compressibility, Lt^2/m, psi-1

C_a =adjusted wellbore storage L^4t^2/m, bbl/psi

C_f =fracture conductivity, m^3, md-ft

C_{ac} =after-closure storage, L^4t^2/m, bbl/psi

C_{pf} =propagating-fracture storage, L^4t^2/m, bbl/psi

C_{fbc} =before-closure fracture storage, L^4t^2/m, bbl/psi

E' =plane-strain modulus, m/Lt^2, psi

E =Young's modulus, $ML^{-1}T^{-2}$, psi

F =F-function, dimensionless

F_L =linear flow time function, dimensionless

F_R =radial flow time function, dimensionless

FCT =Fracture Calibration Test

g =loss-volume function, dimensionless

G	=G-function, dimensionless
h	= formation thickness, L, ft
h_f	=fracture height, L, ft
ISIP	=instantaneous shut-in pressure
k	=permeability, L^2, md
k_fw	=fracture conductivity, md-ft
Lf	=fracture half-length, L, ft
m’	=constant derivative level in a log-log plot
m_H	=slope of data on Horner plot, m/Lt^2, psia
m_L	=slope of data on pseudo-linear flow plot, m/Lt^2psia
m_N	=slope, Nolte-Shlyapobersky method , $ML^{-1}T^{-2}$
m_M	=slope, slope, method of Mayerhofer, Economides and Ehlig-Economides, dimensionless
m_R	=slope of data on pseudo-radial flow plot, m/Lt^2, psia
p	=pressure, m/Lt^2, psia
p_{fo}	=falloff pressure, m/Lt^2, psia
Q_i	=injection rate into one wing of the fracture, bbl/min
Rw	=wellbore radius, ft
R_f	=fracture radius, L, ft
r_p	=ratio of permeable to gross fracture area, dimensionless
s	=Laplace transform variable, dimensionless
s_f	=fracture stiffness, m/L^2t^2, psi/ft

S_p =spurt loss coefficient, L, m

t_p =production time, hr

t_e =equivalent time, hr

t_{ebf} =end of bi-linear flow time, hr

V_L =leakoff volume in one wing, L3, bbl

V_w =wellbore volume, L^3, bbl

w_L =Fracture lost width, L, ft

X =rigorous superposition time for variable rate, dimensionless

x =before-closure pressure transient coordinate, dimensionless

x_f =fracture half-length, ft

y =before closure pressure transient coordinate, dimensionless

z =real gas deviation factor, dimensionless

Greek

Δ =difference, dimensionless

μ =viscosity, m/Lt, cp

α_N =fracture growth exponent, dimensionless

τ =superposition time, dimensionless

ϕ = porosity, dimensionless

υ =Poisson's ratio, dimensionless

η =fracture fluid efficiency, %

Subscript

bf	=bilinear flow
c	=closure
D	=dimensionless
e	=end of pumping
ebf	=end of bilinear flow
hf	=hydraulic fracture
r	=reservoir
lf	=linear flow
i	=initial
n	=time step
ne	=time step at the end of the injection

TABLE OF CONTENTS

Page

LIST OF FIGURES

Page

LIST OF TABLES

Page

CHAPTER I

INTRODUCTION

The fracture calibration test (FCT), otherwise known as a minifrac, an injection/falloff test (IFOT) or a diagnostic fracture injection test (DFIT) has become a standard practice before hydraulic fracture main treatment especially in tight gas and shale. Important parameters for hydraulic fracture design and expectation of post-frac production can be estimated from an FCT.

Traditional specialized plot analysis techniques for before- and after- closure replies on finding a straight-line for a portion of data on a straight line for a certain portion of the data, from which parameters such are estimated either from slope of the line or end point values. As such there is a high risk that an apparent straight line on a specialized plot leads to erroneous results. Also, the dependability of the commonly unknown parameters such as closure pressure in constructing these specialized plots causes circular logic which is inefficient since it requires trial and error for the input parameter. Another challenge prevails in After-Closure-Analysis (ACA) of fracture calibration test is the inability to estimate formation permeability when the after closure pseudo-radial flow regime is absent.

Mohamed et al. (2011) introduced using log-log diagnostic plot to perform before and after closure analysis in a unified manner which to some extends eliminates the necessity of multiple piecewise specialized plots. However the diagnosis of abnormal leakoff type was not described.

The objective of this work is to propose method for diagnosing abnormal leakoff using the Log-log diagnostic plot as an alternative method for the traditional G-function plot and to propose an approach for estimating the upper-limit of formation permeability using the permeability-reservoir pressure relationship when radial flow is absent.

The main masks of this work are two-fold. The first is to show how features that impact before and after closure behavior in the falloff data from an FCT appear in the log-log diagnostic plot. Specifically, to

1. Use the 3/2 slope derivative trend to perform before closure analysis to estimate formation minimum stress, leakoff coefficient, and fluid efficiency;
2. Show how to identify and distinguish variable leakoff and storage effects that appear before closure, and
3. Use ¼, ½, and constant derivative trends appearing after closure to estimate formation permeability, fracture conductivity and half-length, and reservoir average pressure;

The second task is to use the relationship between permeability and formation pressure estimation as a way to bound the permeability estimate when radial flow is absent in the falloff response and to validate a permeability estimate from an apparent radial flow response.

This study mainly expands on the Mohamed et al. (2011) log-log diagnostic plot to perform before and after closure analysis. Log-log diagnostic plots of FCT data from representative tight gas and shale formations are used to illustrate before-closure and

after-closure anomalies that have been described using specialized plots in the literature. Each example is shown both on the log-log diagnostic plot and on the specialized plot to illustrate the advantages in using a single universally- applicable log-log plot. In cases when after-closure radial flow is absent, we propose a simple method using the relationship between permeability and reservoir pressure for estimating an upper limit for the reservoir permeability.

In order to enable better data handling and standardized procedure, an Excel Spreadsheet program has been prepared to perform fracture calibration test data diagnosis and analysis. The main functions of the program will be: 1. Data filtering and quality control; 2. Generation of diagnostic and specialized plots; 3. Parameter and estimation. In addition, the Ecrin software by Kappa Engineering will be used for comparison purposes.

CHAPTER II

LITERATURE REVIEW

This chapter reviews information from the literature on fracture calibration test (FCT) analysis. The subsections explain the FCT pressure response chronology and review existing before- and after- closure analysis approaches.

2. 1 Fracture Calibration Test Pressure Response Chronology

Nolte et al. (1997) described several types of tests that may be included in a fracture calibration test. A "mini-falloff "test with a short, low rate-injection in the undisturbed reservoir before a prolonged falloff period for formation transmissibility estimation may precede a second calibration test performed with much higher injection rate and more viscous fluid to characterize fracture behavior. In addition to these two tests, a step-rate test is sometimes conducted before a mini-fracture test to determine fracture extension pressure. (Figure 2. 1) In tight gas or shale gas formation the short and low rate injection-fall off test using slick water as injection fluid is favored because slick water is the injection fluid for the main fracture treatment and because the closure time increases with increased injection volume (Marongiu-Porcu et al. 2011). Sometimes, a step rate test is performed for a prior estimation of the closure pressure, p_c, which can be used to ensure that shut-in period following injection is monitored longer than the complete time of fracture closure. (Gulrajani and Nolte 2000). In this thesis, Fracture Calibration Test (FCT) refers to the mini-falloff test that described in Nolte et al. (1997).

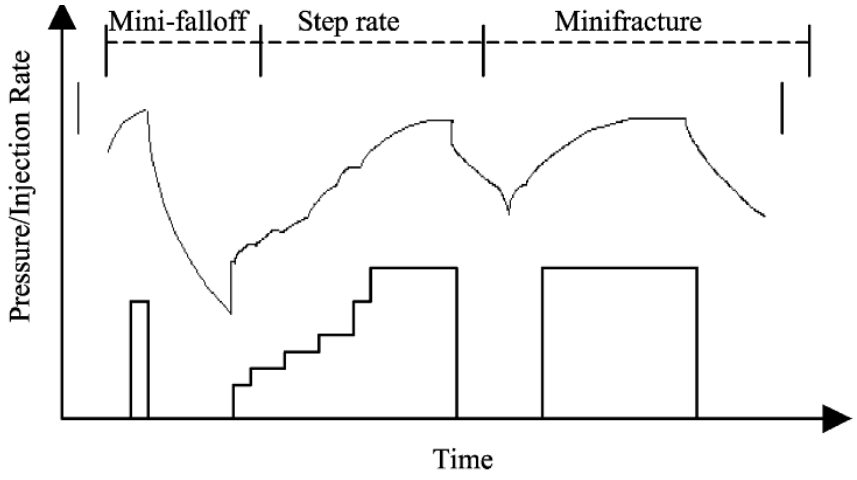

Figure 2.1 Formation Calibration Testing Sequence (Nolte 1997)

In a constant rate fracture calibration test, fracture growth occurring before the end of pumping is followed by a pressure decline that ultimately approaches reservoir pressure. The possible late time pseudo-radial can be analyzed in a manner similar to traditional well testing methods to provide transmissibility and initial reservoir pressure estimation.

2. 2 Before Closure Analysis

A synopsis of Carter (1957) and Nolte (1979) leakoff models is provided in the following sections. The method by Mayerhofer and Economides (1993) and Mayerhofer and Economides (1997) is summarized as an alternative approach.

2. 2. 1 Carter-Nolte Leakoff Model

Early fracture diagnostics techniques were aimed at determination of fracture closure pressure and leakoff coefficient. The first formulation describing fracture fluid leakoff was given by the Carter (1957) equation in which the leakoff coefficient with a unit of

ft/min$^{0.5}$ was developed to quantify the fluid leakoff rate at fracture face. Carter postulated that the fracture fluid loss after shut-in is the summation effect of fluid leakoff and the spurt loss. Nolte (1979) made a simple assumption that during injection, fracture fluid is contributing to the fracture propagation in the reservoir and that the fracture surface area increases according to a power law. He assumed that the fracture area remains constant after the end of pumping. The fracture fluid material balance after shut-in is thus reduced to the following:

$$V_{t_e+\Delta t} = V_i - 2A_e r_p S_p - 2A_e r_p g(\alpha, \Delta t_D) C_L \sqrt{t_e} \text{ , where } \Delta t_D = \frac{\Delta t}{t_e} \quad \text{..... (2.2.1.1)}$$

The equation is based on simple material balance, which allocates the injected fracture fluid either to the initial spurt loss or leakoff through the fracture walls. The average fracture width can be computed from the fracture fluid material balance equation by dividing both sides of the fracture material balance equation by fracture face area. Linear elastic theory indicates that net pressure is proportion to average width as

$$p_{net} = s_f \overline{w} = p_{wf} - p_c \quad \text{..... (2.2.1.2)}$$

where s_f is fracture stiffness. Combining the above equations yields

$$p = (p_c + \frac{s_f V_i}{A_E} - 2r_p s_f S_p) - (2r_p s_f C_L \sqrt{t_e}) g(\alpha, \Delta t_D) = b_N + m_N g(\alpha, \Delta t_D) \quad \text{..... (2.2.1.3)}$$

This equation is the basis of Nolte's pressure decline analysis. The pressure falloff model indicates a linear relation between bottom hole treating pressure and the g-function,

$g(\alpha, \Delta t_D)$, later reformulated by ValkoÂ´ and Economides (1999) as a hyper-geometric function which can only be computed numerically. Two extreme cases for $g(\alpha, \Delta t_D)$ are shown in **Eq. 2.2.1.4** and are widely used to approximate the g-function. The simplified g-function formulation using upper bound values for α = 1and θ = ½ corresponds to negligible leakoff and about 100% fluid efficiency and is widely applied in low permeability formations. In most tight gas and shale cases, the choice for this g-function representation is valid.

$$g(\Delta t_D)\big|_{\theta=1/2} = \begin{cases} (1+\Delta t_D)\sin^{-1}\left(1+\Delta t_D\right)^{-1/2} + {\Delta t_D}^{1/2} & \alpha = 1/2 \\ 4/3((1+\Delta t_D)^{3/2} - {\Delta t_D}^{3/2}) & \alpha = 1 \end{cases} \quad \text{..... (2.2.1.4)}$$

When non-Newtonian filtrate occurs for fracturing fluids exhibiting a power-law-based rheology, θ would deviate from ½ and the following exact form of g-function should be used:

$$g(\Delta t_D, \alpha, \theta) = \frac{1}{\theta}\int_0^1 \left(1+\Delta t_D - \xi^{1/\alpha}\right)^{\theta} d\xi \quad \text{..... (2.2.1.5)}$$

When Δt_D=0, $g_0(\alpha,\theta) = \dfrac{\Gamma(1+\theta)\Gamma(1+\alpha)}{\theta\Gamma(1+\alpha+\theta)}$, where $\Gamma(x)$is the gamma function. (Gulrajani and Nolte 2000)

2. 2. 2 G-function Diagnostic Method for Fracture Closure

The G-function is a representation of the elapsed time after shut-in normalized to the duration of fracture extension. (Barree et al, 2009) The G-function is defined as

$$G(\Delta t_D) = \frac{4}{\pi}[g(\Delta t_D) - g_0] \quad \text{(2.2.2.1)}$$

Barree et al. (2009) presented a consistent analysis of the G-function and its derivative with respect to G-function. He demonstrated through field cases the diagnostic approach for 4 different leakoff types, namely normal leakoff, pressure-dependent leakoff, tip extension as well as transverse storage (or height recession). A straight trend passing through the origin of the G-function plot corresponds to normal leakoff behavior. Barree et al. (2009) summarized four types of leakoff behavior and their signature characteristics on the G-function semi-logarithmic derivative as the following.

1. Normal leakoff
    a. During normal leakoff, the fracture surface area and reservoir system permeability are constant.
    b. Closure diagnosis on G-function plot-- Fracture closure is identified by the departure of the semi-log derivative of pressure with respect to the G-function from the straight line through the origin. The leak-off coefficient is determined from the slope of the line.
2. Pressure-Dependent leakoff
    a. Pressure-dependent leakoff (PDL) can significantly affect the behavior of wells during fracture treating. Pre-frac identification of pressure dependent leakoff enables adjustment of the main fracture treatment design to compensate for this effect. (Baree et al. 1998)

b. PDL occurs when the fluid loss rate changes with pore pressure or net effective stress in the rock surrounding the fracture. This may be caused by a change in the transmissibility of a reservoir fissure or fracture system that dominates the fluid loss rate. PDL may occur when there is substantial stress dependent permeability in a composite dual permeability reservoir. Baree et al (1998) suggest that when fluid is injected at pressures above the minimum in-situ stress either a hydraulic fracture will be induced or a suitably oriented set of pre-existing fissures or weakness planes will open (dilate). As the injected fluid pressure raises further above the minimum principal stress other fissure sets may be activated. Which fissure sets open depends on their orientation with respect to the minimum and maximum stress direction and the fluid pressure applied.

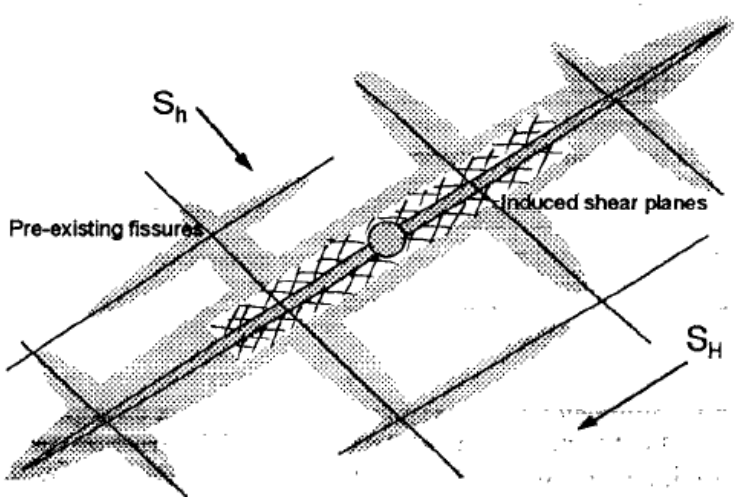

Figure 2.2 Schematic fracture system in hard, fissured rock (Baree et al. 1998)

c. Barree et al.2009 have applied a stress ratio term (R), which relates the available fluid pressure to the minimum and maximum horizontal stress magnitudes to determine the orientation of fractures opening during hydraulic fracturing. For fissure dilation to occur, the stress ratio must exceed a function of the angle between the primary hydraulic fracture (maximum stress direction) and the fissure orientation.

$$\frac{(P_f - S_H) + (P_f - S_h)}{S_H - S_h} = R > -\cos(2\alpha) \quad \text{..... (2.2.2.2)}$$

The plot of R against the angle (α) indicates four regimes (Figure 2.2). For the minimum R value of -1 only fractures orientated in the maximum stress direction with magnitude S_H can open. This includes the primary hydraulic fracture. As the fluid injection pressure rises (increasing R) the orientation angle range for open fissure ranges from 0 to 90 degrees. For R > 1 any fissure, including those perpendicular to the primary fracture, can be dilated and invaded by the injection fluid (Figure 2.3). This analysis is consistent with observed fracture treating behavior in fissured reservoirs which suggests that fissure opening, presumably at some specific orientation, can be associated with a critical open pressure (P_{fo}) that is greater than the fracture closure pressure. In these systems higher treating pressure tends to aggravate any problems associated with fissure reopening, including leakoff, poor proppant mobility and early screen out.

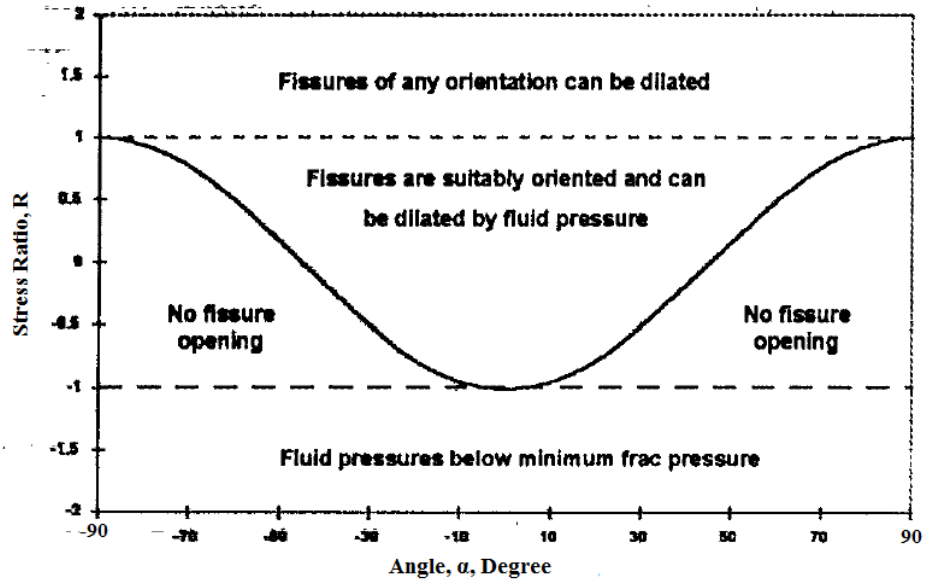

Figure 2.3 Stress ratio plot defines orientation of open fissure. (Barree et al. 1998)

d. Closure Diagnostics on the G-function plot— same with normal leakoff. However, during PDL, Semilog derivative exhibits the characteristic "hump" above the straight line extrapolated to the derivative origin. The end of PDL and critical fissure opening pressure corresponds to the end of hump and beginning of straight line representing matrix dominated leakoff.

3. Fracture Tip Extension

a. Occurs in very low permeability reservoirs. As the pressure declines the fracture width decreases while displacing fluid to the fracture tip, resulting in fracture length extension. When fracture tip extension occurs, the fracture cannot close during the entire falloff.

b. Diagnostics on G-function plot—the G-function derivative fails to develop any straight-line trend. The semi-log derivative starts with large positive

slope, and the slope continues to decrease with shut-in time, giving a concave downward curvature. In this case the closure pressure cannot be determined.

4. Transverse Storage.
    a. Transverse storage occurs when the fluid pressure exceeds the critical fissure-opening pressure and opens a secondary fracture set. As the secondary fractures dilate they create a storage volume for fluid lost from the primary hydraulic fracture. As the fracture storage volume increases, leakoff can also accelerate. As such, PDL and transverse storage are aspects of the same coupled mechanism of fissure dilation. The relative magnitudes of the enhanced leakoff and transverse storage mechanisms determine whether the G-function derivative show PDL or transverse storage. At shut-in the secondary fractures will close before the primary fracture because they are held open against a stress higher than the minimum in-situ horizontal stress. As they close fluid is expelled from the transverse storage volume back into the main fracture, decreasing the normal rate of pressure decline and, in effect, supporting the observed shut-in pressure by re-injection of stored fluid. Accelerated leakoff can still occur at the same time, but if the storage and expulsion exceeds the enhanced leakoff rate, then transverse storage will dominate the response behavior. In many cases a period of linear, constant area, leakoff dominated by constant matrix permeability will occur after the end of transverse storage.

b. Characteristic G-function derivative signature is a “belly” below the straight line through the origin and tangent to the semilog derivative of p_w vs. G at the point of fracture closure.

The transverse storage model requires that a larger volume of fluid must be leaked-off to reach fracture closure than is expected for a single planar constant-height fracture. The time to reach fracture closure is delayed by the excess fluid volume that must be compressed.

2. 2. 3 Before Closure Permeability Estimation

Because leak-off represents flow into the formation, it is logical to consider relating closure behavior to the formation permeability. This approach is complicated when the fracture fluid creates a filter cake designed to minimize leak-off. This section briefly describes the Modified Mayerhofer methods (Valko et al. 1999) for before closure permeability estimation. The Mayerhofer and Economides (1993) method uses an analytical model that accounts for the filter cake created by some fracture fluids to minimize leak-off. Barree et al. (2009) presented an empirical function for permeability estimation derived from numerous simulations of fracture closure

Mayerhofer and Economides Permeability Estimation

The original Mayerhofer and Economides (1993) method to estimate permeability and fracture face resistance from a specialized plot requires a history match of pressure drop and pressure derivative versus time during the shut-in period. The history match algorithm requires varying permeability, fracture face resistance and fracture area until

pressure decline and pressure derivative can be satisfactorily simulated. The modified Mayerhofer method determines the fracture geometry with fracture height and extent from Nolte analysis of the fracture calibration test data. As result, a history match of the pressure falloff is not required to determine fracture extent and the estimated permeability and fracture face resistance is representative, provided the fracture dimensions are realistic.

One of the assumptions and the major limitation of Nolte analysis is that the model assumes a constant leakoff coefficient – which is not always the case in reality. The Mayerhofer et al. (1995) model overcomes Nolte's constant leadoff assumption. It represents the leakoff rate by introducing reference resistance R_0 of the filter cake and the reservoir permeability k_r. Another contribution of Mayerhofer et al. (1995) is that it showed that the pressure drop between the fracture face and the formation is largely reservoir dominated, challenging the then prevalent claim that the pressure response during the FCT is almost totally at the fracture face.

The Mayerhofer et al. (1995) model for pressure decline analysis uses rate convolution to account for pressure dependent fluid loss and couples the resulting rate- and time- dependent skin effect with a transient solution for an infinite-conductivity fracture analogous to the transient pressure behavior for fractured wells in the Cinco-Ley and Samaniego-V. (1981) formulation.

Mayerhofer et al. (1995) demonstrated their method for estimating formation permeability and filter cake resistivity by analyzing the pressure decline following the injection test in a fracture calibration test. The method is intended for a reservoir

containing a slightly compressible fluid such as oil and requires preparing a graph of y_n vs. x_n from the equations shown in Table 2.1. To accommodate compressible fluid such as natural gas Craig and Blasingame (2006) reformulated the before-closure pressure-transient analysis in terms of adjusted pseudo-pressure and adjusted pseudo-time.

Table 2.1 Equations for before-closure pressure transient analyisis -- Mayerhofer Method(Craig and Blasingame 2006)

Description	Pressure and Time	Adjusted Pseudopressure and Adjusted Pseudotime
Basic Equation	$y_n = b_M + m_M x_n$	$(y_{ap})_n = b_M + m_M (x_{ap})_n$
y_n or $(y_{ap})_n$	$y_n = \dfrac{(p_w)_n - p_i}{d_n\sqrt{t_n}\sqrt{t_{ne}}}$	$(y_{ap})_n = \dfrac{(p_{aw})_n - p_{ai}}{(d_{ap})_n\sqrt{t_n}\sqrt{t_{ne}}}$
x_n or $(x_{ap})_n$	$x_n = \left[c_1 \left[\dfrac{d_{ne+2}}{d_n}\left(\dfrac{t_n - t_{ne+1}}{t_n t_{ne}}\right)^{1/2} + \sum_{j=ne+3}^{n} \dfrac{[d_j - d_{j-1}]}{d_n}\left(\dfrac{t_n - t_{j-1}}{t_n t_{ne}}\right)^{1/2} \right] + \dfrac{c_2}{d_n t_{ne}^{3/2}}\left[1 - \left(1 - \dfrac{t_{ne+1}}{t_n}\right)^{1/2}\right] \right]$	$(x_{ap})_n \equiv \left[c_{ap1} \left[\dfrac{(d_{ap})_{ne+2}}{(d_{ap})_n}\left[\dfrac{(t_a)_n - (t_a)_{ne+1}}{t_n t_{ne}}\right]^{1/2} + \sum_{j=ne+3}^{n} \dfrac{[(d_{ap})_j - (d_{ap})_{j-1}]}{(d_{ap})_n}\left(\dfrac{(t_a)_n - (t_a)_{j-1}}{t_n t_{ne}}\right)^{1/2} \right] + \dfrac{c_{ap2}(t_a)_n^{1/2}}{(d_{ap})_n t_n^{1/2} t_{ne}^{3/2}}\left[1 - \left(1 - \dfrac{(t_a)_{ne+1}}{(t_a)_n}\right)^{1/2}\right] \right]$
d_j or $(d_{ap})_j$	$d_j = \dfrac{p_{j-1} - p_j}{t_j - t_{j-1}}$	$(d_{ap})_j = \dfrac{(c_t)_i}{(c_t)_j}\left[\dfrac{(p_a)_{j-1} - (p_a)_j}{(t_a)_j - (t_a)_{j-1}}\right]$
c_1 or c_{ap1}	$c_1 = \sqrt{\dfrac{\mu}{\phi c_t}}$	$c_{ap1} = \sqrt{\dfrac{\mu_i}{\phi c_{ti}}}$
c_2 or c_{ap2}	$c_2 = S_f w_L \sqrt{\dfrac{\mu}{\phi c_t}}$	$c_{ap2} = S_f w_L \dfrac{B_{gi}}{(B_g)_{ne}}\sqrt{\dfrac{\mu_i}{\phi c_{ti}}}$
b_M	$b_M = \dfrac{1}{2\pi}\dfrac{R_0}{r_p S_f}\dfrac{1}{t_{ne}}$	$b_M = \dfrac{1}{2\pi}\dfrac{R_0}{r_p S_f}\dfrac{1}{t_{ne}}$
m_M	$m_M = \dfrac{1}{\sqrt{\pi}}\dfrac{1}{r_p S_f \sqrt{k}}$	$m_M = \dfrac{1}{\sqrt{\pi}}\dfrac{1}{r_p S_f \sqrt{k}}$

After creating the graph, permeability is calculated from the slope, m_M, of the resulting straight line using the following equation:

$$k = \left[\frac{2(141.2)(0.02878)(24)}{5.615} \frac{1}{r_p S_f m_M} \right]^2 \quad \text{..... (2.2.3.1)}$$

Fracture-face resistance is calculated from the intercept, b_M, as

$$R_0 = \frac{5.615}{\pi(141.2)(24)} r_p S_f t_{ne} b_M \quad \text{..... (2.2.3.2)}$$

G-Function Permeability Estimate

The Barree et al. (2009) empirical correlation is based on the observed G-function time at fracture closure:

$$k = \frac{0.0086 \mu_f \sqrt{0.01 p_z}}{\varphi c_t \left(G_c E r_p / 0.038 \right)^{1.96}} \quad \text{..... (2.2.2.2)}$$

In order to account for abnormal leak-off behavior Eq. 2.2.2.3 the observed closure time must be corrected by multiplying by the storage ratio, r_p. Under transverse storage Barree et al. 2009 indicated that the magnitude of r_p can be determined by taking the ratio of the area under the G-function semilog derivative up to the closure time, divided by the area of the right-triangle formed by the tangent line through the origin at closure. For normal leakoff and PDL the value of r_p is set to 1 even though the ratio of the areas will be greater than 1 for the PDL case. It is possible that closure time for PDL leakoff is proportional to the composite system permeability including both the matrix and fractures. For severe case storage r_p can be as low as 0.5 or less.

2. 3. After Closure Analysis

A summary of the most accepted after-closure analysis method is provided in this chapter. For after-closure radial flow analysis, most of the analysis is based on Gu et al. (1993) impulse test analysis, from which reservoir transmissibility can be estimated. The period following fracture closure and preceding the onset of pseudo-radial flow can exhibit reservoir pseudo-linear flow. Nolte (1997) established the analytical solution for linear flow adapting the heat transfer formulation. Numerous after-closure analysis specialize plots were created based on this two theories.

The sections also dedicates to the most recently development in which Mohamed et al. (2001) implemented the conventional well test method in after-closure analysis.

2. 3. 1 Gu et al. Impulse Test Solution for Describing After Closure Behavior

The theory and analysis of the impulse-fracture test are based on the instantaneous point-source solution to the diffusivity equation. For the case of injection or withdrawal of fluid from a reservoir with a finite thickness h, the pressure response is given by

$$\Delta p(r,t) = \frac{V_i \mu}{4\pi k h}\left(\frac{e^{\frac{-\phi c_t \mu r^2}{4k\Delta t}}}{\Delta t}\right) \quad \text{..... (2.3.1.1)}$$

When injection duration is short compared to the shut-in time, Δt, the injection can be approximated as the instantaneous point sauce.

$$\Delta p(r,t) = \frac{V_i \mu}{4\pi k h}\left(\frac{1}{\Delta t}\right) \quad \text{..... (2.3.1.2)}$$

The after-closure analysis first developed by Gu et al.(1993) suggests applying impulse test analysis to FCT data in the same manner it applies for instantaneous injection times-- provided that the duration of injection is much shorter than the falloff period. The permeability estimation depends only on the injected volume and does not depend on the pumping schedule or the properties of the injected fluids. In particular, they used the following approximation for Horner time:

$$\ln\left(\frac{t_c+\Delta t}{\Delta t}\right)\rightarrow\frac{t_c}{\Delta t}\approx\frac{t_c}{t};t>>t_c \quad \text{..... (2.3.1.3)}$$

where t is the total time of the falloff plus the injection time, and noting that

$$(p(t)-p_i)\rightarrow m_H\frac{t_c}{t}=\frac{\mu(V_i/t_c)}{4\pi kh}\frac{t_c}{t};t>>t_c \quad \text{..... (2.3.1.4)}$$

permeability is estimated from is the slope, m_H, of a straight trend on the graph of p versus t_c/t:

$$k=\frac{\mu(V_i/t_c)}{4\pi hm_H} \quad \text{..... (2.3.1.5)}$$

2. 3. 2 Benelkadi Method –F-function Plot for Closure Pressure Determination

Benelkadi and Tiab (2004) concluded that the pressure first derivative with respect to total time of the falloff duration for after closure analysis from Gu et al. (1993) has an exponential form that characterizes the pressure response within the reservoir and that the onset of the exponential occurs at the closure time.

The late –time pressure decline evolves a radial flow, thus allowing the reservoir pressure to be determined with Cartesian plot. The after-closure radial flow regime is a

function of injected volume, reservoir pressure, formation transmissibility, and closure time. Their relationship is provided in the following equations.

$$p(t) - p_r = m_R F_R(t, t_c) = m_R F^2 \quad \text{..... (2.3.2.1)}$$

$$F(t) = \sqrt{\left[1 + (t - t_c)/\chi t_c\right]} - \sqrt{\left[(t - t_c)/\chi t_c\right]}, \text{ where } \chi = 16/\pi^2 \quad \text{..... (2.3.2.2)}$$

Modified method for permeability determination by use of after-closure radial flow analysis

$$\Delta p = \frac{\pi V_i \mu}{16 k h t_c} F^2 \quad \text{..... (2.3.2.3)}$$

$$\log(\Delta p) = \log(F^2) + \log(m_R) \quad \text{..... (2.3.2.4)}$$

$$\log\left(\frac{d\Delta p}{dF^2}\right) = \log(m_R) \quad \text{..... (2.3.2.5)}$$

$$m_R = \frac{\pi V_i \mu}{16 k h t_c} \quad \text{..... (2.3.2.6)}$$

For the pressure difference vs. F^2, the above equations indicate that the radial flow is characterized by a unit-slop line. The intercept with p-axis is m_R at $F^2=1$. Therefore, the reservoir transmissibility is determined from

$$\frac{kh}{\mu} = \frac{251000 V_i}{m_R t_c} \quad \text{..... (2.3.2.7)}$$

Since only one unit-slope line can across the Δp-axis at point m_R, to determine the reservoir pressure, the value of the assumed reservoir pressure is varied until the

pressure difference curve overlies the drawn unit-slope line. Note that the time zero is set at the beginning of pumping.

The main limitation of the proposed method is that the unit slope straight line can be observed only if the exponential term in Eq. 2.3.1.1 is equal to unity; that is

$$e^{\frac{-\phi c_t \mu r^2}{4k\Delta t}} = 1 \quad \text{..... (2.3.2.8)}$$

At long time t and/or very low permeability k, or very large values of radius r Eq. 2.3.1.2 is a good approximation of Eq. 2.3.1.1, with less than 1% error. However, if the exponential term is closer to 0.1, the approximation can introduce up to 10% error in permeability estimation. (Benelkadi and Tiab 2004)

2. 3. 3 Nolte (1997) Time Function Diagnostics

Nolte et al. (1997) focused on the description of after-closure pseudo-linear flow regime. The period following fracture closure and preceding the onset of pseudo-radial flow can exhibit reservoir pseudo-linear flow. Assuming the pressure in the fracture is essentially constant during injection, the pressure decline after closure behaves as the thermal decay. A linear-flow Cartesian plot is developed as a counterpart of the Horner plot. The linear flow time-function was then expressed in equivalent forms in Talley et al. (1999).The reservoir linear flow gives insight on fracture geometry and can be used to validate or question the before-closure analysis. Closure time and leakoff coefficient should be predetermined from before closure analysis to apply this method. Pressure decline for pseudo-radial flow is provided in the following equation expressed using the radial flow time function, F_R.

After-Closure Pseudo-Radial Flow

$$p(t) - p_r = m_R F_R(t, t_c)$$ ……...…….. **(2.3.3.1)**

$$F_R(t, t_c) = \frac{1}{4}\ln(1 + \frac{\chi t_c}{t - t_c}), \chi = \frac{16}{\pi^2} \cong 1.6$$ …….. **(2.3.3.2)**

A Cartesian plot of pressure versus the radial flow time function yields reservoir pressure from the y-intercept and its slope m_R permits reservoir transmissibility estimation.

$$\frac{kh}{\mu} = 251000\left(\frac{V_i}{m_R t_c}\right)$$ ……..…….. **(2.3.3.3)**

Where k, h, m expressed in oil field units, t_c in minutes and V_i is injected volume.

After-Closure Pseudo-Linear Flow

In the absence of spurt loss, it resembles a heat transfer problem. The pressure difference can be expressed similarly as:

$$p(t) - p_r = m_L F_L(t, t_c)$$ ……..…….. **(2.3.3.4)**

$$F_L(t, t_c) = \frac{2}{\pi}\sin^{-1}\sqrt{\frac{t_c}{t}}, t \geq t_c$$ …….. **(2.3.3.5)**

$$m_L = C_T\sqrt{\frac{\pi\mu}{k\phi c_t}}$$ ……..……...……..…….. **(2.3.3.6)**

$$p(t) - p_r = C_T\sqrt{\frac{\pi\mu}{k\phi c_t}}\frac{2}{\pi}\sin^{-1}\sqrt{\frac{t_c}{t}}, t \geq t_c$$ ……..……..…….. **(2.3.3.7)**

where C_T is the total leakoff coefficient.

Fracture half-length is determined from the time of transition from linear to radial-flow. The fracture length determined from this method can be compared to that determined from the conventional, pre-closure analysis. (Talley et al. 1999)

One of the drawbacks of pseudo-linear flow analysis is that the guess of reservoir pressure, p_r, used in construction of the flow regime plot severely influences the slope and magnitude of the pressure difference curves. The pressure first order derivative with respect to after closure falloff duration, because of the difference function used to generate it, is not affected by the initial guess of reservoir pressure.

2. 3. 4 Soliman et al. (2005) Formulation

Soliman et al. (2005) developed the after-closure analysis technique using analogous technique for conventional well test analysis. They postulated three types of the possible after closure flow regimes—pseudo-radial flow, pseudo-bilinear flow or/and pseudo-linear flow. The parameters that are sensitive to each respected flow regime are quantified if possible.

Pseudo-radial Regime.

After-closure pressure follows pseudo-radial flow behavior when the created fracture is fairly short and no, or little, residual fracture conductivity remains. In addition to the short fracture, this would require a higher formation permeability and lower formation compressibility. The area affected by pseudo-radial flow is far enough such that the fracture appears almost as a cylinder. For low permeability formation, if the pumping rate is low and well is shut-in for a sufficient long period, pseudo-radial flow regime will

probably be observed if the fracture eventually close. To reach the pseudo-radial flow, the dimensionless time should exceed 1. Time in hours is determined from Eq. 2.3.4.1

$$t \geq \frac{3.792 \times 10^3 \phi \mu c_t L_f^2}{k} hr \quad \text{..... (2.3.4.1)}$$

Eq. 2.3.4.2 describes the behavior of pressure during pseudo-radial flow.

$$p_{fo} - p_i = \frac{1694.4 V \mu}{kh} \frac{1}{t_p + \Delta t} \quad \text{..... (2.3.4.2)}$$

The equation implied that the specialized plot of $\log(p_{fo} - p_i)$ vs. $\log(t_p + \Delta t)$ would render a straight line trend with slope of -1.0. Furthermore, given injection volume, fluid viscosity and fracture height, the permeability can be estimated from the intercept, b_r of the log-log plot. (Soliman et al. 2005)

$$k = \left(\frac{1694.4 V \mu}{b_r h} \right) \quad \text{..... (2.3.4.3)}$$

Bilinear Flow Regime

If the created fracture is long, or if it did not completely close, thereby maintaining some residual conductivity, it is possible that to observe a bilinear flow regime instead. The bilinear flow regime is controlled by the pressure drop caused by the linear flow inside fracture as well as the formation just surrounding the fracture. The relation governs bilinear flow of this particular condition are presented in Eq. 2.3.4.4

$$p_{fo} - p_i = \frac{264.6 V \mu^{0.75}}{h} \left(\frac{1}{\phi c_t k} \right)^{0.25} \frac{1}{\sqrt{k_f w_f}} \left(\frac{1}{t_p + \Delta t} \right)^{0.75} \quad \text{..... (2.3.4.4)}$$

The equation implied that the specialized plot of $\log(p_{fo} - p_i)$ vs. $\log(t_p + \Delta t)$ would render a straight line trend with slope of -3/4. The last point on the straight line may be used to calculate an upper bound of formation permeability.

$$b_r = 264.6\frac{V}{h}(\mu)^{0.75}\left(\frac{1}{\phi c_t k}\right)^{0.25}\frac{1}{\sqrt{k_f w_f}} \quad \text{..... (2.3.4.5)}$$

$$k = 264.6\frac{V}{h}\frac{\mu}{b_r}\frac{1}{(2.637t_{ebf})^{0.25}} \quad \text{..... (2.3.4.6)}$$

Linear Flow Regime

If the fracture stays open with a high dimensionless conductivity, a linear flow regime may be observed. This is a fairly rare occasion. However, it may happen if the formation permeability is low. Another condition would be the fracture staying open for a fairly long time.

$$p_{fo} - p_i = \frac{31.05V}{4h}\left(\frac{\mu}{\phi c_t k L_f^2}\right)^{0.5}(\frac{1}{t_p + \Delta t})^{0.5} \quad \text{..... (2.3.4.7)}$$

To sum up, Soliman's analysis method for After-closure analysis is the following: First, create derivative graph by plotting log ($p_{fo} - p$) vs. log ($t_p + \Delta t$) and its semilog Derivative. Then, observe slope of the derivative straight line that data eventually follow. If the slope is -1, the fracture was properly closed at closure, and pseudo-radial flow regime will dominate the fluid flow behavior during the shut-in

period. If the slope is -0.75 or -0.25, the fracture stayed open during the falloff period, and bilinear flow or linear flow regime is expected.

A specialized plot method provided by Soliman et al. (2005) is to plot log-log graph of pressure difference, p_{wf}-p_i, vs. the reciprocal of elapsed time, 1/ (t_e+Δt). The characteristic slope would be the absolute value as in log ($p_{fo} - p$) vs. log ($t_p + \Delta t$) for respective flow regime1.

Table 2.2 Flow Regime Identification from semi-log derivative curve. Soliman et al (2005)

Log-log Graph	Pre-closure		Post Closure		
tdp/dt vs. t	Bilinear	linear	Bilinear	Pseudo-linear	Pseudo-radial
	1/4	1/2	-3/4	-1/2	-1

2. 3. 5 Horner Analysis for Permeability Estimation in Buildup/Falloff Analysis

The conventional Horner analysis for buildup and falloff uses a semi-logarithmic plot of observed pressure vs. Horner time, (t_p+Δt)/ Δt with all times in consistent units. The Horner plot is not a diagnostic plot, but can be used to estimate reservoir pressure and reservoir permeability if radial flow presents. The formation permeability can be estimated from the corresponding assumed radial flow period on the straight line trend. The extrapolated reservoir pressure can be estimated from the extrapolated straight line trend to the pressure for Horner time of 1 for an infinite acting system.

$$p_{ws} = p_i - \frac{162.6qB\mu}{kh}\log\frac{t_p + \Delta t}{\Delta t} \quad \text{..... (2.3.5.1)}$$

The permeability can be estimated as

$$k = \frac{70.6qB_0\mu_0}{m'h} \quad \text{..... (2.3.5.2)}$$

in which m' is the value of semi-log slope.

If variable rate production history or injection scheme precedes a shut-in period, the substitution of the production/injection time t_p for the material balance time, t_e is necessary to account for the variable rate convolution. The material balance time is the total production/injection at the end of injection or production history normalized by the last rate Eq. (2.3.5.3).

$$t_e = \frac{N_p}{q_{last}} \quad \text{..... (2.3.5.3)}$$

In case that last production/injection rate is abnormal, the actual superposition time function, Eq. (2.3.5.4) should be used for x-variable on Horner Plot instead of the simplified equivalent time. The data should be graphed in Cartesian scale instead of semilog scale.

$$X = \frac{q_1}{q_{n-1}}\ln(\frac{t}{t-t_1}) + \frac{q_2}{q_{n-1}}\ln(\frac{t-t_1}{t-t_2}) + \frac{q_3}{q_{n-1}}\ln(\frac{t-t_2}{t-t_3})... \quad \text{..... (2.3.5.4)}$$

2. 3. 6 Formation Pressure Estimation from the FCT

After closure the FCT behavior is like that of any injection falloff transient. Whenever the FCT is conducted in an undepleted formation, extrapolation of a late-time trend to infinite time provides estimation for the formation pressure. For example, the extrapolation of the radial flow line on a Horner plot yields the extrapolated pressure, p*, which will approximate p_i in new wells in never-produced reservoirs. Marongiu-Porcu et

al. (2011) estimated the extrapolated pressure directly from the FCT logarithmic derivative on the log-log diagnostic plot as

$$p_i \sim p^* = -m' \ln\left(\frac{t_e + \Delta t_{slope=0}}{\Delta t_{slope=0}}\right) - \Delta p(\Delta t_{slope=0}) + ISIP \quad \text{..... (2.3.6.1)}$$

Rock mechanics dictates that the poroelastic equation for estimating in-situ horizontal minimum stress is the following

$$\sigma_{\min} = \left\lfloor \frac{\nu}{1-\nu}\left(\sigma_z - \alpha_v P_i\right)\right\rfloor + \alpha_h P_i + \sigma_t \quad \text{..... (2.3.6.2)}$$

Where σ_z = overburden stress, psi

υ=Posson's ratio

α_v=vertical Biot's parameter =1

α_h=horizontal Biot's parameter =1

σ_t= external tectonic stress, psi

$\sigma_{\min}$ =formation minimum stress

Assuming that external tectonic stress is zero, rearrange the relation, Equation (2.3.6.3) is obtained. This relationship indicated that the reservoir average pressure can be roughly estimated from the relationship between closure stress and a uniaxial strain given by

$$p_i = \frac{\sigma_{\min} - \left(\frac{\upsilon}{1-\upsilon}\right)\sigma_z}{1 - \left(\frac{\upsilon}{1-\upsilon}\right)} \quad \text{..... (2.3.6.3)}$$

Nolte et al. (1997) postulated that after closure linear flow resembles heat transfer and pressure difference can be expressed as:

$$p(t) - p_r = m_L F_L(t, t_c) \quad \text{(2.3.6.4)}$$

where the time function F_L is given by Eq. (2.3.3.5)

With this relation, the most convenient way to estimate reservoir pressure given linear flow regime is simply compose a Cartesian plot of BHP vs. F_L and extrapolate the pressure data corresponding to the linear flow time frame to F_L =0.

2. 4 Craig and Blasingame New Fracture Injection/Falloff Model and Type Curve Matching

Craig and Blasingame (2006) presented a new single-phase fracture injection/falloff model accounting for fracture creation, closure and after-closure diffusion. The model accounts for fracture propagation as time-dependent storage, and the rigorous fracture-injection/falloff dimensionless pressure solution for a case with a propagating fracture, constant before-closure storage, and constant after-closure storage are derived. Especially, Craig and Blasingame (2006) presented two limiting case solutions when a fracture propagates, or an existing fracture dilates, during an injection with a short dimensionless injection time. Before-closure reservoir pressure solutions in the Laplace domain as

$$\overline{p}_{bcD} = \frac{\overline{p}_{fD}}{1 + s^2 C_{bcD} \overline{p}_{bcD}} \quad \text{(2.4.0.1)}$$

where Dimensionless before –closure storage is defined as

$$C_{bcD} = \frac{5.615}{2\pi}\frac{C_{bc}}{\phi c_t h L_f^2}$$ ……. **(2.4.0.2)**

in which C_{bc} [bbl/psi] is the before-closure storage coefficient written as

$$C_{bc} = c_w V_w + \frac{2}{5.615}\frac{A_f}{S_f}$$ ……. **(2.4.0.3)**

P_{fD} is the finite- or infinite-conductivity fracture solution.

The after-closure limiting case solution is also a slug test solution, but including variable storage. The Laplace solution is written as

$$\bar{p}_{acD} = \frac{\bar{p}_{fD}}{1 + s^2 C_{acD}\bar{p}_{acD}}$$ ……. **(2.4.0.4)**

where Dimensionless after –closure storage is defined as

$$C_{acD} = \frac{5.615}{2\pi}\frac{C_{ac}}{\phi c_t h L_f^2}$$ ……. **(2.4.0.5)**

in which C_{ac} [bbl/psi] is the after closure storage coefficient written as

$$C_{ac} = c_w V_w + 2c_f V_{fr}$$ ……. **(2.4.0.6)**

Craig and Blasingame (2006) proposed a type-curve analysis method for analyzing all falloff data from the end of the injection through fracture closure, pseudo-linear flow, and pseudo-radial flow. This quantitative type-curve method requires that both initial reservoir pressure and fracture half-length are known. When pseudo-linear or pseudo-radial flow periods are observed, the initial reservoir pressure can be definitively

determined. Estimates of fracture half-length, however, will have more uncertainty, which can create errors in the calculated transmissibility.

2. 5. Log-Log Diagnostic Method for Before and After Closure Analysis

In modern well-test interpretation, log-log diagnostic plots of the pressure change and the semilog superposition derivative function are used identify flow regimes from straight derivative trends with characteristic slopes and levels from which important well or reservoir parameters can be directly computed.

Mohamed et al. (2011) showed that the pressure derivative trend just before closure has slope 3/2, and Marongiu-Porcu et al. (2011) gave a rationale for why this occurs and used the diagnostic plot introduced by Mohamed et al. (2011) to identify closure pressure, quantify the leak-off coefficient, and estimate permeability and the fracture geometry.

The Marongiu-Porcu et al. (2011) interpretation consists of the following steps:

1. Initial assumption of fracture geometry (PKN or radial) based on height containment analysis from a gamma ray log.
2. The point ($\Delta p_c'$, t_c) at the end of the 3/2 slope trend in the derivative defines the closure time, and closure stress is given by the pressure at that time.
3. Values for m_N and b_N are computed using a derivative value $(\Delta t, \Delta p')_{pc}$ found on the 3/2 slope trend.

$$m_N = \frac{\Delta p'}{2\Delta t_D^{5/2}\tau(1-\tau^{1/2})} \qquad \text{..... (2.5.0.1 a)}$$

$$b_N = p_w - m_N \frac{4}{3} t_D^{3/2}\left(\tau^{3/2} - 1\right) \quad \text{..... (2.5.0.1 b)}$$

Then the leakoff coefficient, fracture area, fracture width, and fluid efficiency are estimated from Table 2.3.

Table 2.3 Fracture Calibration Test analysis model based on the Nolte (1979)

	PKN α=4/5	KGD α=2/3	Radial α=8/9
Leakoff coefficient, C_L	$\frac{\pi h_f}{4\sqrt{t_e E'}}(-m_N)$	$\frac{\pi x_f}{2\sqrt{t_e E'}}(-m_N)$	$\frac{8R_f}{3\pi\sqrt{t_e E'}}(-m_N)$
Fracture Extent	$x_f = \frac{2E'V_i}{\pi h_f^2 (b_N - p_C)}$	$x_f = \sqrt{\frac{E'V_i}{\pi h_f (b_N - p_C)}}$	$R_f = \sqrt[3]{\frac{3E'V_i}{8(b_N - p_C)}}$
Fracture Width	$\overline{w}_e = \frac{V_i}{x_f h_f} - 2.830 C_L \sqrt{t_e}$	$\overline{w}_e = \frac{V_i}{x_f h_f} - 2.956 C_L \sqrt{t_e}$	$\overline{w}_e = \frac{V_i}{R_f^2 \frac{\pi}{2}} - 2.754 C_L \sqrt{t_e}$
Fluid Efficiency	$\eta_e = \frac{\overline{w}_e x_f h_f}{V_i}$	$\eta_e = \frac{\overline{w}_e x_f h_f}{V_i}$	$\eta_e = \frac{\overline{w}_e R_f^2 \frac{\pi}{2}}{V_i}$

4. Permeability is estimated from a constant derivative level, m', characteristic of pseudo-radial flow:

$$k = \frac{70.6qB\,\mu}{m'h} \quad \text{..... (2.5.0.2)}$$

5. The fracture half-length can be estimated when a ½ slope derivative trend occurs between the closure time and the onset of pseudo-radial flow using the equation

$$x_f = \left(\frac{4.064qB}{m_{lf} h}\right)\left(\frac{\mu}{k\phi c_t}\right)^{0.5} \quad \text{..... (2.5.0.3)}$$

with $m_{lf} = 2\Delta p'/\sqrt{\Delta t}$ for a point $(\Delta t, \Delta p)_{lf}$ on the ½ slope derivative trend.

6. Fracture conductivity estimation from bilinear flow using Cinco-Ley finite conductivity fracture model

The bilinear flow to hydraulic fracture the pressure difference is proportional to the fourth root of shut-in time, and the log-log semi-log superposition will present a ¼ slope. With a known permeability, the fracture conductivity $k_f w$ (can be obtained using Equation (2.5.0.6).

$$\Delta p = m_{bf}\sqrt[4]{\Delta t} \quad \text{..... (2.5.0.4)}$$

$$\Delta p' = \frac{1}{4} m_{bf}\sqrt[4]{\Delta t} \quad \text{..... (2.5.0.5)}$$

$$k_f w\sqrt{k} = \left(\frac{44.1\Delta qB\mu}{m_{bf}h}\right)^2\left(\frac{1}{\phi\mu c_t}\right)^{0.5} \text{ where } m_{bf} = 4\Delta p'/\sqrt[4]{\Delta t} \quad \text{..... (2.5.0.6)}$$

with $m_{lf} = 4\Delta p'/\sqrt{\Delta t}$ for a point $(\Delta t, \Delta p)_{lf}$ on the 1/4 slope derivative trend.

7. Initial reservoir pressure can be estimated from the constant derivative level in the pseudo-radial flow regime and a value of Δp and Δt during pseudo-radial flow, using

$$p^* \sim p_i = -m'\ln\left(\frac{t_e + \Delta t_{slope=0}}{\Delta t_{slope=0}}\right) - \Delta p\left(\Delta t_{slope=0}\right) + ISIP \quad \text{..... (2.5.0.7)}$$

where the instantaneous shut in pressure, ISIP, is located on a Cartesian plot of falloff pressure just after the end of injection.

2.6 Chapter Summary

Numerous existing approaches for FCT analysis use specialized plots each featuring a specific flow regime to analyze various elements of the falloff behavior. The exception is the approach by Marongiu-Porcu et al. (2011) that uses the same log-log diagnostic plot used for standard pressure transient analysis. The next chapter will show how the same plot reveals the behavior described in this chapter and displays the important trends in a global context that avoids erroneous parameter estimations based on apparent straight lines on specialized plots.

CHAPTER III

DIAGNOSTIC DERIVATIVE EXAMPLES

Chapter II explained before- and after- closure theories and their respective analysis methods. For before-closure analysis, Barree et al. (2009) investigated the existing fracture injection/falloff diagnostic methods categorized by three leakoff models, i.e. normal leakoff (Constant-area and constant-permeability leakoff), pressure dependent leakoff and transverse storage on well-known diagnostic plots such as the G-function plot.

This chapter begins with a simplified math proof and visualization of why a 3/2 slope on the pressure superposition derivative represents normal leakoff behavior on the log-log diagnostic plot. Then, the second section showcases field case examples to demonstrate how the three types of leakoff behavior can be distinguished on the log-log diagnostic plot. Specifically, the characteristic slope patterns on the superposition derivative for the three leakoff types are explained. The final section illustrates how the relationship between permeability and formation pressure can be used to determine an upper bound for the formation permeability when an independent estimate for the formation pressure is available.

3.1 Log-Log Diagnostic for Constant Area Poroelastic Fracture Closure

The advantage of graphing the pressure superposition derivative on the log-log plot for flow regime study is that the slope of the derivative curve reflects the exponent of the time term in a pressure response model. Or in mathematical terms:

$$p_D \sim t_D^m \Rightarrow dp_D / d(\ln(t_D)) = t_D dp_D / d(t_D) \sim m t_D^m, \quad \text{..... (3.1.0.1)}$$

As mentioned in Chapter II, Valko and Economides (1995) reformulated and popularized the analytical expression for the g-function that was introduced by Nolte (1979) in his well-known power law fracture surface growth postulation. Equation (2.2.1.3) shows the Nolte (1979) pressure decline model for fracture poro-elastic closure suggesting that the bottom-hole pressure decreases linearly with the g-function until the fracture finally closes, after which the pressure falloff will depart from this linear trend. The pressure profile with respect to $g(\alpha, \Delta t_D)$ is as in Equation (2.2.1.3)

The g-function that was reformulated by Valko and Economides (1999) involves a hyper-geometric function which can only be computed numerically. The formulation is given by Equation (2.2.1.5). When $\Delta t_D = 0,\ g_0(\alpha, \theta) = \dfrac{\Gamma(1+\theta)\Gamma(1+\alpha)}{\theta\Gamma(1+\alpha+\theta)}$, where $\Gamma(x)$is the gamma function. (Gulrajani. N. S. and Nolte 2000)

Two extreme case for $g(\alpha, \Delta t_D)$can be written as Eq. (2.2.1.4) and are widely used to approximate the g-function:

$$g(\Delta t_D)\big|_{\theta=1/2} = \begin{cases} (1+\Delta t_D)\sin^{-1}(1+\Delta t_D)^{-1/2} + {\Delta t_D}^{1/2} & \alpha = 1/2 \\ 4/3((1+\Delta t_D)^{3/2} - {\Delta t_D}^{3/2}) & \alpha = 1 \end{cases} \quad \text{..... (2.2.1.4)}$$

The simplified formulation of the g-function for $\alpha = 1$and $\theta = ½$ given by the second Equation 2.2.1.4 represents the upper bound behavior corresponding to negligible leakoff and about 100% fluid efficiency and is appropriate for low permeability formation applications including most tight gas and shale slick-water cases..

Noting that this g-function expression has a term of dimensionless time with a power raised to 3/2 case makes it intuitive that the log-log representation of Carter leakoff will appear as a straight trent with slope 3/2 on the pressure superposition derivative

To demonstrate the above comment we note that the semilog derivative of the second equation is given by

$$p_{ws} \propto g_0(\alpha, \theta)$$

$$\Delta p' = \frac{dp}{d\ln\tau} = \tau\frac{\mathrm{dp}}{\mathrm{d}\tau} \propto \tau\frac{dg(\Delta t_D)\big|_{\theta=1/2}}{d\tau} = \tau\frac{\tau}{(\tau\text{-}1)^2}\times\left(\frac{1}{\tau\text{-}1}+1\right)^{0.5}\text{-}\left(\frac{1}{\tau\text{-}1}\right)^{0.5}\Big)$$

Where $\tau = \dfrac{\Delta t}{\Delta t + t_e}$ ..... **(3.1.0.3)**

Figure 3.1 is a graph of Eq. 3.1.3. For $0.1 < \Delta t < 100$, $\tau\dfrac{\mathrm{dp}}{\mathrm{d}\tau} \propto 1.46\,\Delta t^{\frac{3}{2}}$,

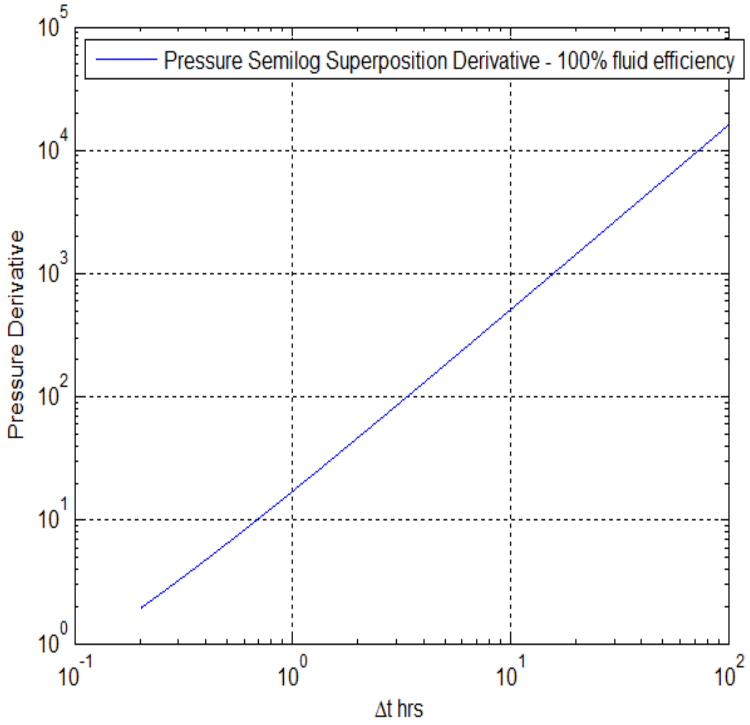

Figure 3.1 Pressure derivative vs. Δt for poro-elastic closure-low leakoff

Similarly, for high leakoff, or low fluid efficiency scenario given by the first equation

$$\frac{dp}{d\ln\tau} = \tau\frac{\mathrm{dp}}{\mathrm{d}\tau} \propto \tau\frac{dg(\Delta t_D)\big|_{\theta=1/2}}{d\tau} = \tau[\frac{\sin^{-1}(\frac{\tau-1}{\tau})^{0.5}}{(\tau\text{-}1)^2} + 0.5(\tau\text{-}1)^{-1.5} + 0.5(\tau\text{-}1)^{0.5})]$$

Where $\tau = \dfrac{\Delta t}{\Delta t + t_e}$ ..... **(3.1.0.5)**

For the same range of Δt, Figure 3.2 shows a line with $\tau\dfrac{\mathrm{dp}}{\mathrm{d}\tau} \propto 1.509$ for $0.1 < \Delta t < 100$. In both cases, the derivative trend has a slope of about 3/2.

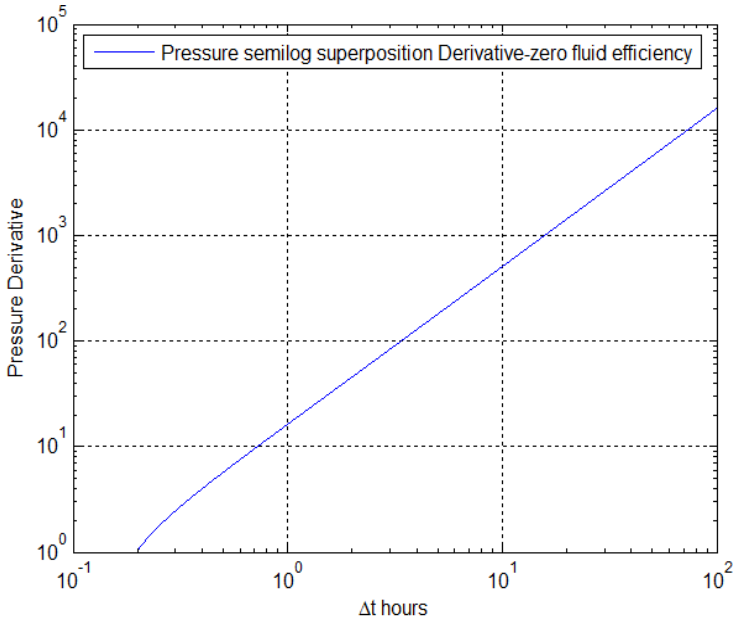

Figure 3.2 Pressure derivative vs. Δt for poro-elastic closure-high leakoff

Under non-Newtonian filtration occuring for fracturing fluids exhibiting a power-law-based rheology, θ deviates from ½ and the exact form of g-function should be used. However, since the exact g-function is bounded by the two equations, its semilog derivative will also follow a 3/2 slope trend.

Figure 3.3 shows the comparison of two diagnostic plots for normal leakoff (constant-area and constant-permeability leakoff) behavior. The graph on the left of Figure 3.3 shows the field data plotted on G-function plot whereas the log-log plot of pressure change from Instantaneous Shut-in Pressure (ISIP) and pressure superposition derivative vs. shut-in time for the same data set is shown on the right of Figure 3.3.

The created hydraulic fracture closure on G-function plot is diagnosed by identifying the departure of the semi-log derivative of pressure with respect to G-function from the straight line through the origin. In this case, the closure time is

identified at G=19.42 hr, which correspond to shut-in time at fracture closure, Δt_c= 7.95 hr. The corresponding bottomhole pressure value determines closure pressure or the value of formation minimum stress. In this case p_c = 11,830 psi. There are many techniques commonly used to determine p_c such as step rate test and flow back test. The method for determining closure pressure used in this work is focused on shut-in pressure decline after the fracture calibration test.

Following the technique described in the previous section, on the log-log plot, hydraulic fracture closure diagnosis is identified at the end of the 3/2 slope and the corresponding pressure, in this case of value 11,830 psi is the closure stress for the main fracture. The two diagnostic plots exhibit exactly same diagnosis for fracture closure. In addition to the before closure information, for this particular case, the log-log plot also shows the pressure response eventually goes to radial indicated when derivative becomes level at shut-in time of around 25 hours, and the derivative level of which can be used to estimate reservoir transmissibility. Such after-closure information is not possible to obtain from G-function plot only. Other specialized plots are required for after-closure analysis using traditional methods.

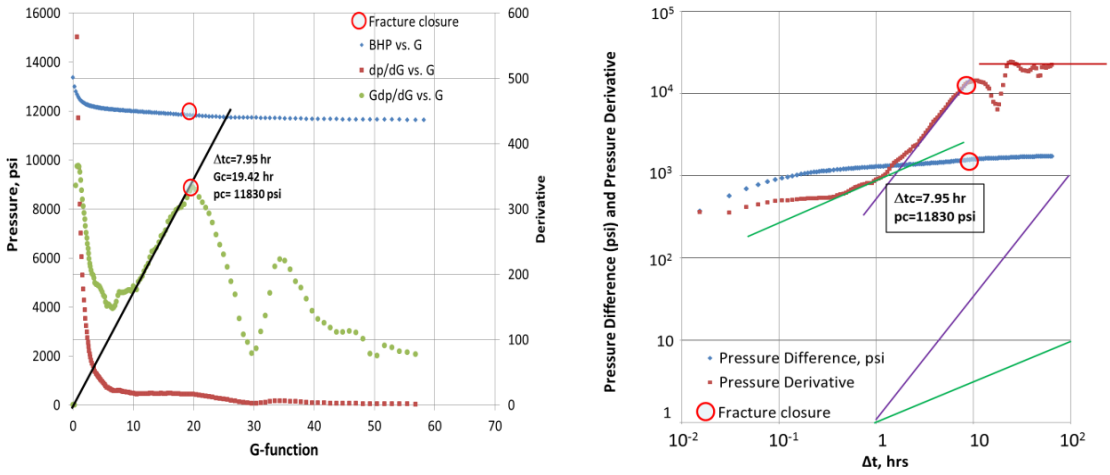

Figure 3.3 Normal leakoff behavior--G-function, log-log pressure superposition derivative

3.2 Diagnostic Examples for Three leakoff Modes

When the data no longer follow pressure poro-elastic closure model, the pressure superposition derivative would no longer follow the 3/2 trend. Thus the deviation from the characteristic 3/2 slope on derivative curve is the indication of fracture closure. However, the following three situations could compromise or obscure the characteristic 3/2 slope for fracture closure identification:

- Pressure dependent leak-off;
- Transverse storage from natural fracture/induced fracture dilation or existing fracture reopening; and/or
- Height recession from bounding layers (does not apply to shale).

In this section, two field examples are shown to demonstrate how abnormal leakoff behavior impacts the standard logarithmic derivative slope on the log-log scale.

3.2.1 Pressure-dependent Leakoff Behavior on Diagnostic Plots

Pressure dependent leakoff (PDL) could greatly influence the behavior of wells during main hydraulic fracture treatment. To make informed decisions regarding stimulation design, fracture calibration test is needed to indicate the presence of pressure dependent leakoff. As briefly described in Chapter II, PDL occurs when the fluid loss rate changes with pore pressure or net effective stress in the rock surrounding the fracture. When fluid is injected at pressures above the minimum in-situ stress either a hydraulic fracture will be induced or a suitably oriented set of pre-existing fissures or weakness planes will open (dilate). As the injected fluid pressure rises further above the minimum principal stress other fissure sets may be activated. Which fissure sets open depends on their orientation with respect to the minimum and maximum stress direction and the fluid pressure available.

Figure 3.4 shows the comparison of two diagnostic plots for case of pressure dependent leakoff. On the left it shows the G-function plot representation, and the log-log plot for the same example is shown on right.

As for normal leakoff, the hydraulic fracture closure during PDL is diagnosed on the G-function plot by the departure from a straight line through the origin in the semi-log G-function derivative. However, in this case the derivative exhibits a characteristic "hump" above the straight line. The end of PDL corresponds to critical fissure opening pressure and appears at the end of hump, which is also the beginning of straight line that represents matrix dominated leakoff.

In Figure 3.4 the fissure closure time is diagnosed on the G-function plot is at $G_{c,fissure}$ = 12.9, which correspond to 4.47 hr and a fissure closure stress value of 11350 psi. The hydraulic fracture closure time is diagnosed on G-function plot is at $G_{c,hf}$ = 13.33, which correspond to closure time = 5.15 hr and a closure stress value of 11313 psi. The difference between the two stress values, 37 psi, is the value of the stress contrast.

The log-log plot, on the right of Figure 3.4 shows an approximate 3/2 slope for the time ranging from about 0.7 to 1.1 hr after which the slope drops slightly. The pressure derivative trend eventually returns to 3/2 slope for a very short duration of time before bending toward a relatively long ½ slope trend at the hydraulic fracture closure time. The fissure closure timing is identified at the beginning of the 3/2 slope trend at Δt= 4.47 hr that ends in fracture closure. This diagnosis is consistent with that from the G-function plot.

An alternative analysis is suggested by Figure 3.5. Instead of indicating fissure closure at the start of the G-function straight line, it may be more logical to identify it at the end of an earlier G-function line drawn with a dashed line in both figures. This interpretation implies that PDP behavior is a transition between 2 closure events and indicates a higher fissure closure pressure of 11,598 psi. With this interpretation the signature PDP behavior is defined on the G-function plot by identification of 2 lines and on the log-log diagnostic plot as a succession of two 3/2 slope trends.

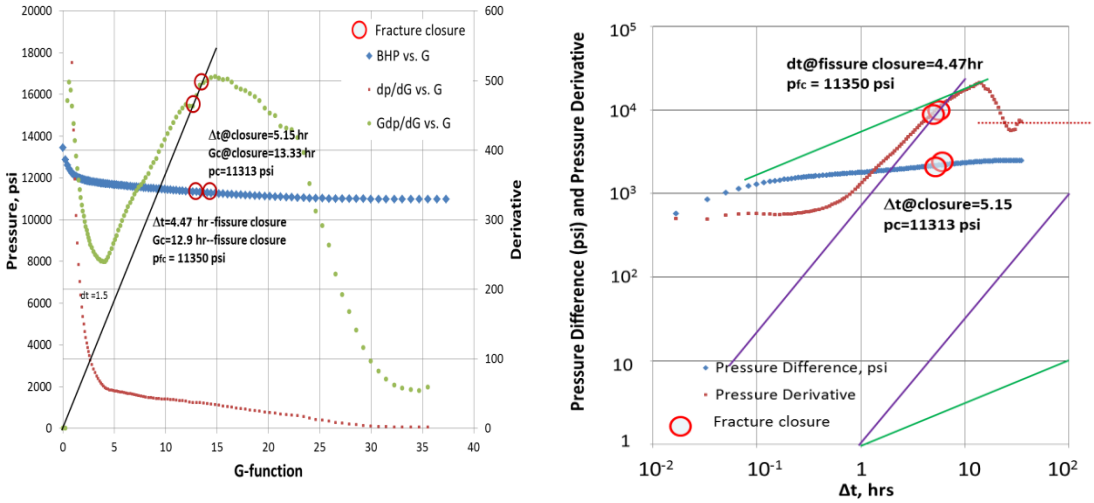

Figure 3.4 Pressure dependent leakoff behavior--G-function, log-log pressure superposition derivative

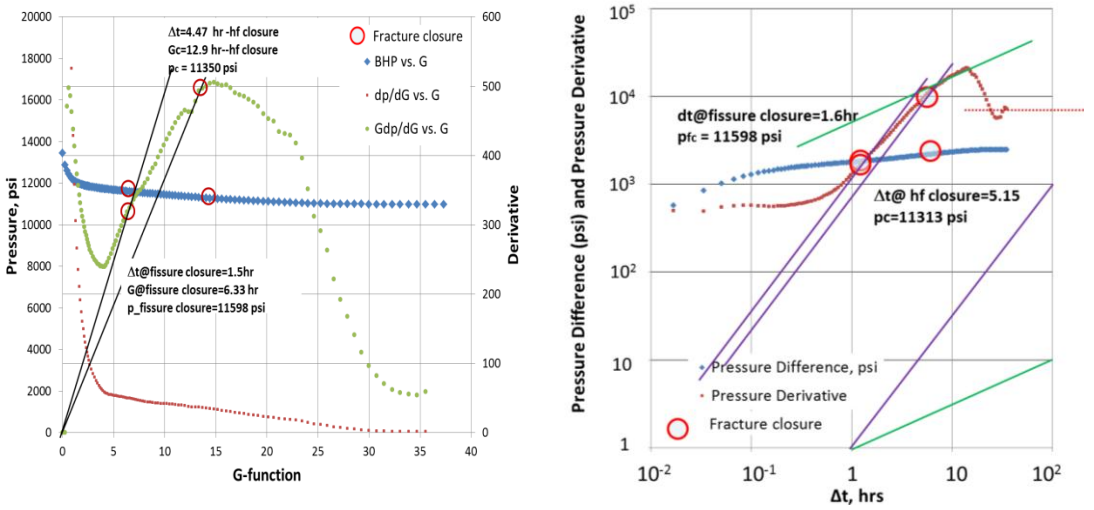

Figure 3.5 Alternative interpretation -- multiple closure--G-function, log-log pressure superposition derivative

3.2.2 Transverse Storage Behavior on Diagnostic Plots

Figure 3.6 shows the comparison of two diagnostic plots for case of transverse storage behavior. On G-function plot, the G-function derivative exhibits a characteristic “belly”

below the straight line extrapolated from origin to the derivative which is a strong indication of the transverse storage effect. The end of the storage effect is at the tangent to the G-function derivative and is normally interpreted as the closure time. In this case $G_c = 9.89$, which corresponds to closure shut-in time = 3.03 hr and closure pressure of 11,823 psi.

Because there is no identifiable poroelastic closure trend, neither the G-function nor the log-log diagnostic plot shows a line. Instead, closure pressure is found at the tangent to the bending behavior seen just after a steeply climbing G-function derivative trend. On the log-log plot on the right of Figure 3.6 the logarithmic derivative shows a steep upward trend, and closure time and pressure can be picked when the tangent to the derivative has a slope of 3/2. As such, in this case the closure shut-in time is identified at Δt= 3h and the hydraulic fracture closure pressure, p_c=11,822 psi.

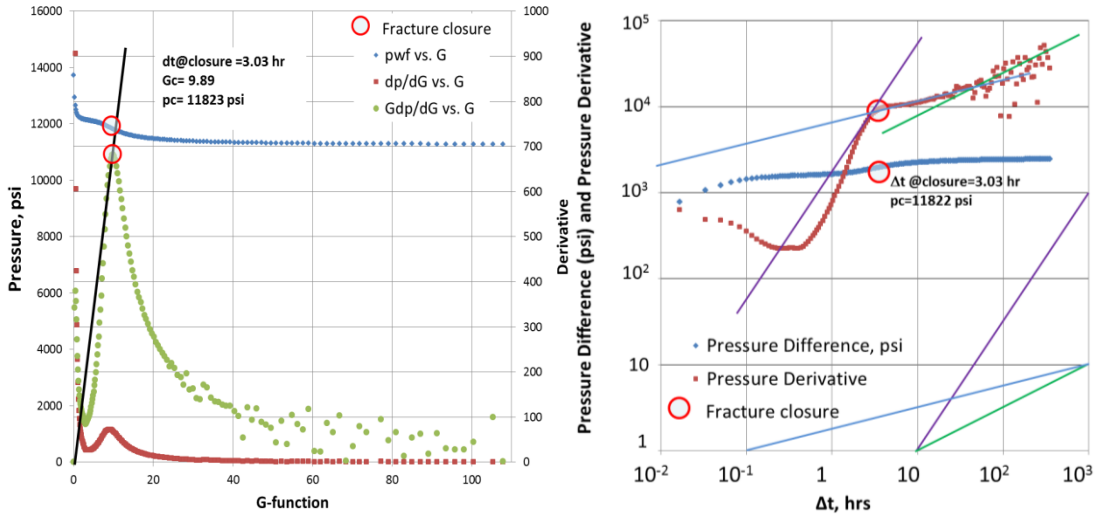

Figure 3.6 Transverse storage leakoff behavior--G-Function, log-log pressure superposition derivative

3.3 Permeability Estimation from Formation Pressure

From the review of existing after-closure analysis, it can be concluded that no matter what specialized plot is used, permeability is estimated from late time bilinear (Soliman et al. 2005), linear (Nolte 1997) or, in most cases, radial flow. Ways to estimate reservoir pressure provided in many of the specialized plot techniques were discussed in Section 2.3.5 of Chapter II.

When radial flow is absent, which is a common problem in many FCTs in shale, the conventional approaches for permeability estimation would not be applicable. Likewise, an approach using bilinear flow requires an independent estimate for the fracture conductivity or meeting the condition that the end of bilinear flow is known (Soliman et al. 2005), and an approach using linear flow requires an independent estimate for the fracture half-length, and these, as well, only apply when the bilinear or linear flow regime appears.

The above simple observations inspire an idea to use a known reservoir pressure value to estimate an upper bound for the formation permeability using the radial time function extrapolation on which the Horner plot is based.

The procedure to implement p_i-k relation for permeability estimation from assumed formation pressure

1. Estimate formation pressure.
    a. From external source such as pore pressure gradient.
    b. From Eq 2.3.6.2 using vertical stress, Poisson ratio, and closure stress estimated from the FCT

c. From Linear Flow extrapolation

From Eq. 2.3.6.3 using after closure linear flow if present in the FCT response. The slope of the Nolte (1997) linear flow function specialized plot can be determined directly from the slope of the straight line m_{lf} from two points (F_{L1}, p_1) and (F_{L2}, p_2)

Then formation pressure can be estimated using the point $\Delta p(\Delta t_{lf})$ as

$$p_i \sim p_{lf}^* = p_1 + \frac{p_2 - p_1}{F_{L2} - F_{L1}} \times F_{L1} \quad \text{..... (3.3.0.1)}$$

d. From Linear Flow pressure difference and semi-log derivative

Using Soliman et al. 2005 method, after-closure analysis requires a log-log graph of the pressure difference, p_i-p_{ws}, and the well testing pressure derivative versus the total shut-in time. During pseudo-linear flow, both curve should be parallel and exhibit negative ½ slope. Further more, pressure difference curve should double the value of the derivatie curve during this timeframe. This determination of initial reservoir pressure is an iterative process, and the pressure difference value would not double the derivative curves during linear flow until the initial reservoir pressure is correct.

2. Estimate an upper bound for the formation permeability using the last recorded falloff pressure. One way to do this is to plot the FCT falloff data on a Horner plot. If radial flow was present, the end of the falloff data would show a line with Horner slope, m that extrapolates to the formation pressure p_i. Instead, we

construct this line using the externally-determined value for formation pressure and use the slope of this line to estimate the formation permeability. Figure 3.7 illustrates the procedure. On the left is a Horner plot of falloff data. Highlighted on the plot are 2 red points: the last recorded falloff pressure and the externally determined value for formation pressure. The equation for the line between the 2 red points is shown on the plot. On the right is a zoom on the end of the plot. The slope of the line gives m' = 2.303m. In reality, the slope, m', can be determined without actually constructing the Horner plot as

$$m' = \frac{p_{last} - p_i}{\ln\left(\frac{t_e + \Delta t_{last}}{\Delta t_{last}}\right)} \qquad \text{..... (3.3.0.2)}$$

The upper bound permeability is computed as

$$k = \frac{70.6qB\ \mu}{hm'} \qquad \text{..... (3.1.0.3)}$$

where m' is the slope of the straight-line connecting last falloff pressure and the assumed pressure.

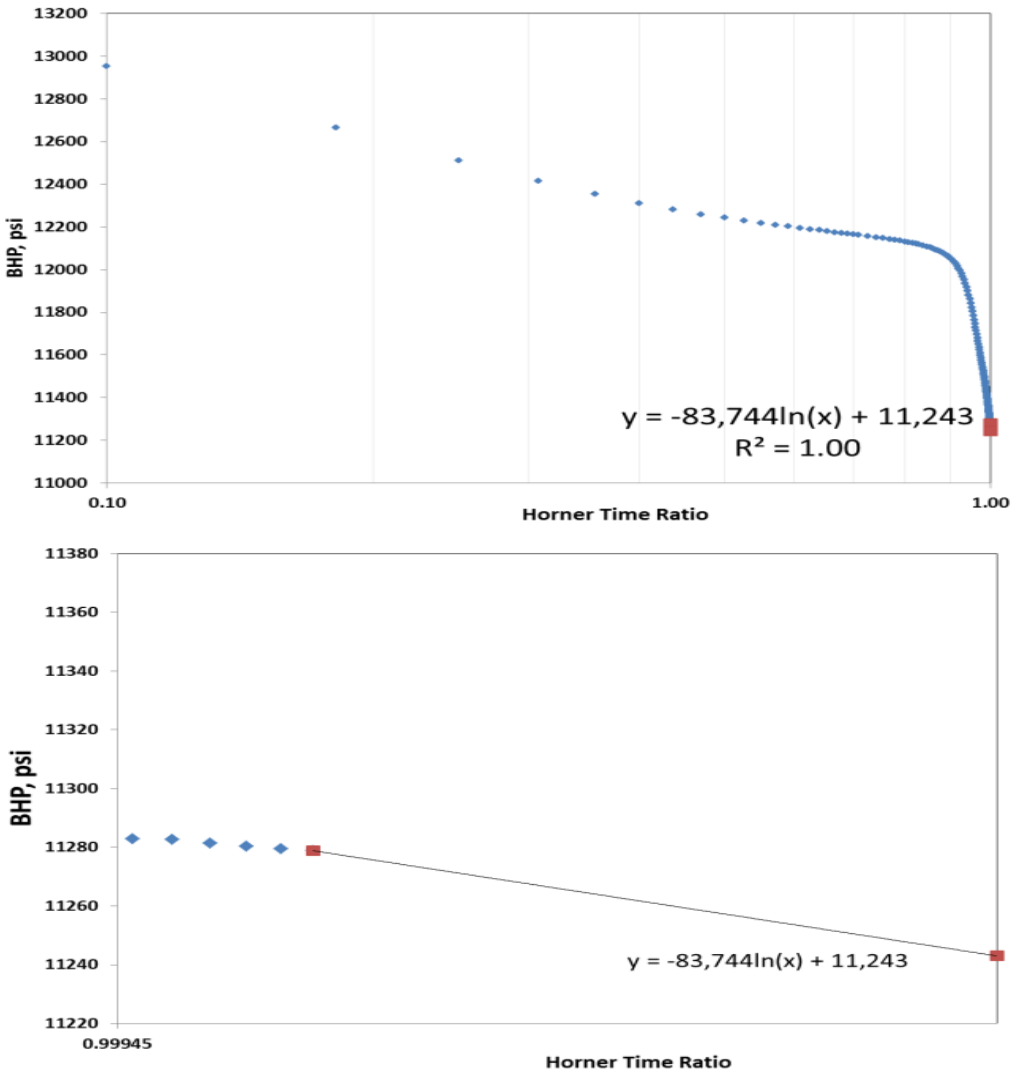

Figure 3.7 Horner plot and zoom to demonstrate p_i-k relationship method for permeability estimation

In case that last production/injection rate is abnormal, the actual superposition time function, Eq. 3.1.0.9 should be used for x-variable on Horner Plot instead of the simplified equivalent time. (Figure 3.8)The data should be graphed in Cartesian scale instead of semilog scale.

$$X = \frac{q_1}{q_{n-1}} \ln\left(\frac{t}{t-t_1}\right) + \frac{q_2}{q_{n-1}} \ln\left(\frac{t-t_1}{t-t_2}\right) + \frac{q_3}{q_{n-1}} \ln\left(\frac{t-t_2}{t-t_3}\right) \ldots \quad \textbf{(3.1.0.9)}$$

From this plot, permeability can still be estimated using the k-pi relation, (3.1.8) only the m' is calculated with the following formula:

$$m' = \frac{p_{last} - p_i}{X_{last}} \quad \textbf{(3.1.0.10)}$$

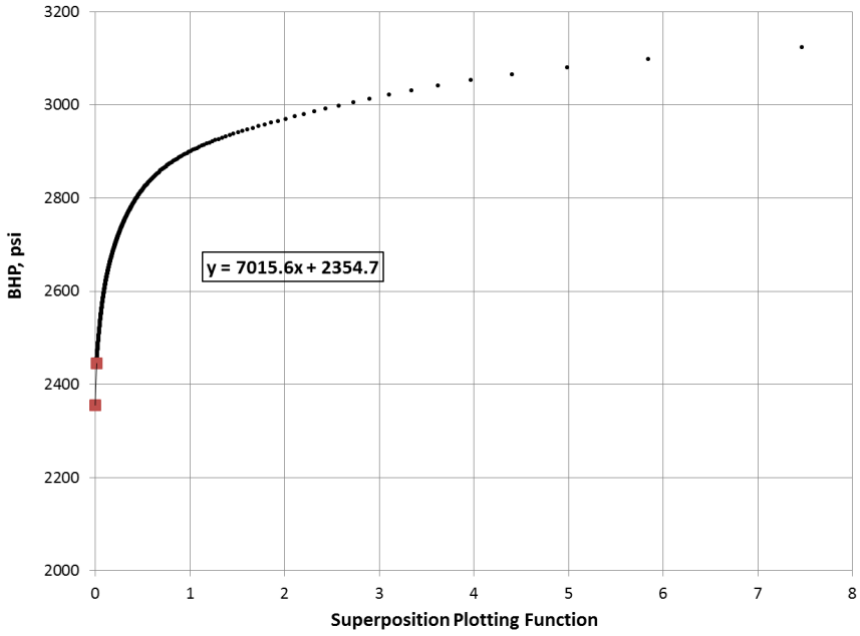

Figure 3.8 Bottomhole pressure vs. superposition plotting function

3.4 Chapter Summary

Three field data examples were shown to illustrate how common closure behaviors appear on the log-log diagnostic plot. These demonstrate that the log-log analysis method provides a closure pressure value consistent with what would be

estimated with the well-known G-function plot. The cases included are normal constant-area and constant permeability leakoff, pressure dependent leakoff and transverse storage. An alternative estimate is provided for fissure closure pressure from pressure dependent leakoff.

The key original contribution of this work is the estimation of an upper bound formation permeability using an external estimate for the initial formation pressure that applies even when no evidence of radial flow is found in the FCT response. The next chapter will demonstrate application of this method on field data.

CHAPTER IV

FIELD DATA APPLICATIONS

Chapter III briefly described the diagnosis of three leakoff behaviors, i.e. normal leakoff, pressure dependent leakoff, and transverse storage, on the log-log diagnostic plot. The characteristic slope signatures on the superposition derivative were illustrated using field examples.

This chapter elaborates on the before- and after- closure analysis on 5 field cases. In Particular, the utility of the relationship between permeability and formation pressure estimation as a way to bound the permeability estimate is explained and demonstrated in cases when radial flow is absent in the falloff response. The field case study of one well from Mesaverde Sandstone formation will include a buildup test analysis. With both a fracture calibration test and drawdown/buildup completed sequentially, a direct comparison of the buildup and falloff interpretation is possible.

Field Cases shown are 3 from Haynesville Shale, 1 from Horn River Shale, and 1 from Mesaverde Sandstone.

4.1 Haynesville Shale Formation Characterization

This section begins with background information on the Haynesville shale providing shale properties and typical well completion and the baseline parameters required for the FCT analysis.

Then FCT field data from three cased horizontal wells in Haynesville shale will be used to demonstrate the unified before- and after-closure analysis on the log-log plot.

4.1.1 Field Background

The Haynesville is an organic-rich shale, Upper Jurassic in age, and located in the North Louisiana Salt Basin, and East Texas. The Haynesville Shale is overlain by the Bossier Shale, which in turn is overlain by the Cotton Valley Sandstone. It is underlain by the Cotton Valley limestone in Texas and the Smackover limestone in Louisiana (Thompson 2010). Figure 4.1 shows the Type log and stratigraphic column for the Haynesville shale and adjacent formations. Abnormal high pressure and great thickness make the Haynesville shale a prolific formation. The Haynesville shale play has true vertical depth (TVD) greater than 11,000 ft, and the productive interval of the Haynesville shale can have a gross thickness between 75 and 400 ft, temperature greater than 300 F, and extraordinarily high pore pressure gradient, up to 0.95 psi/ft. Average porosity in the formation is 0.07; water saturation is approximately 30%.

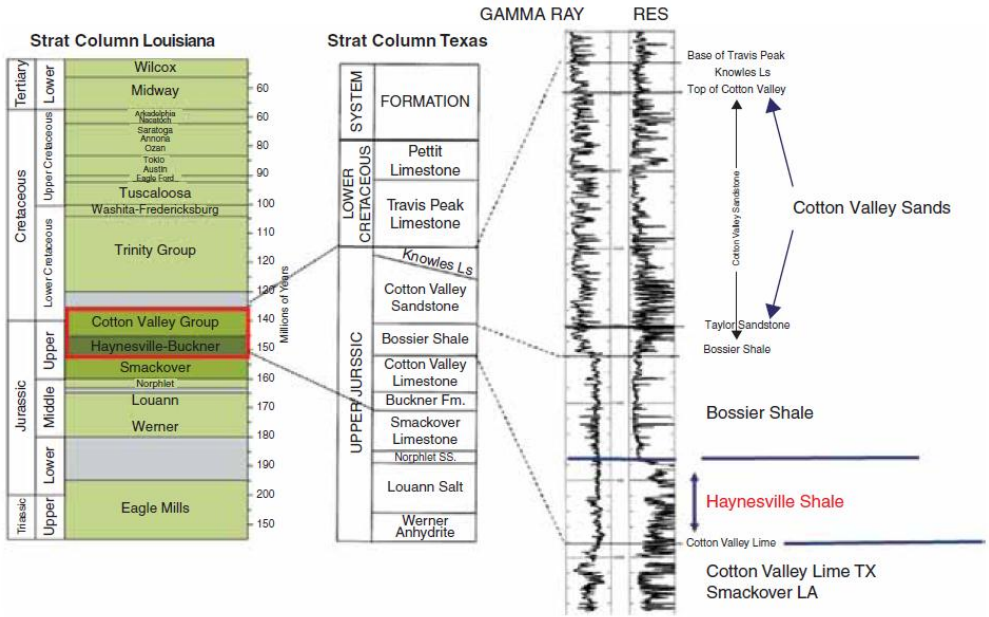

Figure 4.1 Haynesville shale and adjacent formation (Thompson, 2010)

The early conjecture about the natural fracture network in Haynesville analogous to the Barnett shale has been proved to be unrealistic. In fact, evidence shows that even if fractures are present in the Haynesville-Bossier shale system, they are typically cemented and cannot directly contribute to the productivity of the well, unless reactivated during stimulation. The reactivated fractures are typically limited to the vicinity of the stimulated fracs and do not extend far (Younes et al. 2010).

The baseline parameters for Haynesville shale FCT analysis are summarized in Table 4.1 based on information found in the literature and an available data set.

Table 4.1 Input parameters for Haynesville shale fracture calibration Test

Properties	**Value**	**Unit**
Gas Specific Gravity, sg_g	0.70	
Gas Viscosity, μ_g	0.038	cp
Formation Total Compressibility, c_t	2.98×10^{-05}	psi-1
Formation Porosity, ϕ	7	%
Water Saturation, S_w	30	%
Young's Modulus, E'	6.00×10^{6}	
Poisson's ratio, ν	0.33	
Formation Height, h	150	ft
Formation Temperature	320	F

4.1.2 Haynesville Shale Well A

A fracture calibration test was conducted at the toe of the cased horizontal well. The FCT perforation interval is between 15,833 to 15,838 feet (measured depth, MD) with a perforation density of 6 short per foot (SPF) and perforation phasing of 1, which yields 30 perforation holes in one single cluster.

The injection was performed by pumping fresh water, at an average rate of 5 bbl/min for 0.22 hours. The initial pressure on the wellhead was 5364 psi. The formation initially broke down at pressure and rate of 15,078 psi and 5.2 bpm (barrel per minute). The instantaneous shut-in pressure (ISIP) is observed at 12,686 psi which yields a fracture gradient of 1.09 psi/ft. The bottomhole pressure decline was monitored for 0.5 hours.

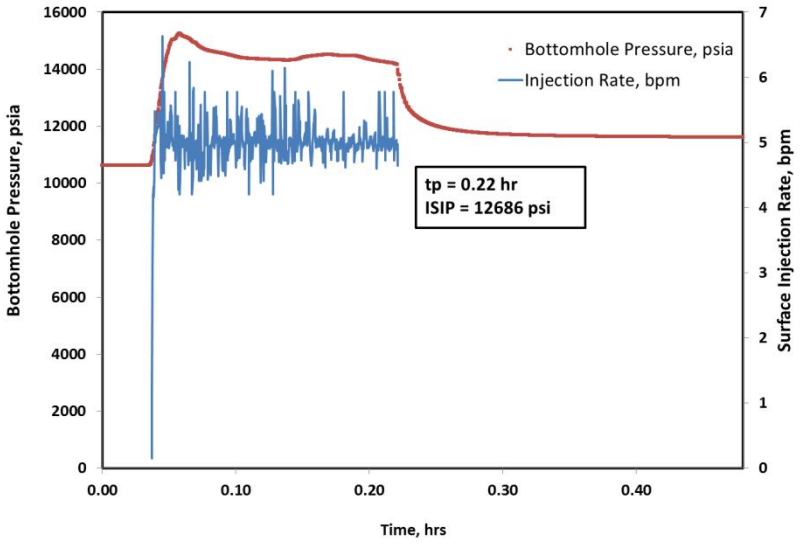

Figure 4.2 Bottomhole pressure and injection profile for Haynesville Well A

Before Closure Analysis

Figure 4.3 shows the log-log diagnostic plot for Well A. The prominent 3/2 slope trend is visible for more than a logarithmic cycle, and a clear departure from this trend is identified at $\Delta t_c = 0.0156$ hour, yielding closure pressure of 12102 psia. The closure pressure value is also the value for the formation minimum stress.

The G-function plot diagnosis yields coherent estimation of closure time and pressure, indicated at the end of the signature straight-line of pressure semi-logarithic derivative with respect to G-function. The characteristic 3/2 slope on the log-log plot and the straght line trend through origin on the G-function plot until to the point of fracture closure indicates classic normal leakoff mode. Duirng normal leakoff, the fracture area is constant and the reservoir rock appears homogeneous.

The small injected volume may not have been sufficient for the fracture to grow in height to the shale thickness, in this case, 150 ft. Thus we assume radial fracture geometry for this case.

Initial reservoir pressure can be estimated from the closure stress and the uniaxial strain relationship

Assuming Poisson's ratio, $\upsilon = 0.2$, and an overburden stress, $\sigma_z = 12686$ psi (1.06 psi/ft overburden stress). From before-closure analysis, it is known that $\sigma_{min} = 12102$ psi. From Eq. (2.3.6.2) the initial reservoir pressure estimate is $p_i = 11908$ psi.

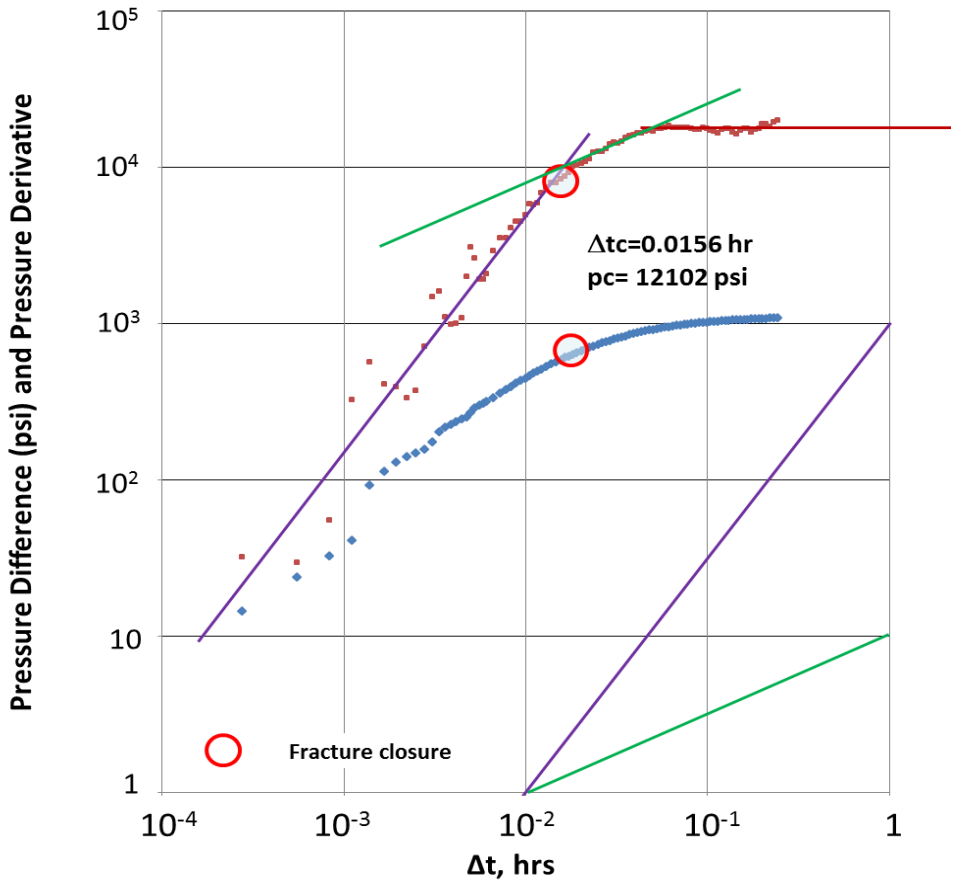

Figure 4.3 log-log diagnostic plot for data of Haynesville Well A FCT test

Fracture geometry and leakoff coefficient estimation from Before-closure analysis

The Nolte (1979) method for before-closure analysis requires an estimate of fracture half-length and lost fracture width because of fluid leakoff, w_L. Fracture half-length and lost width can be estimated from a graph of bottomhole pressure versus the loss-volume function, $g(\alpha, \Delta t_D)$ provided the fracture geometry is homogeneous and the "no spurtloss" assumption is met. The slope of the line through the before-closure data is m_N=-71.6 psi and the intercept is b_N = 12834 psi.

With the log-log plot, the calculation of m_N and b_N can be directly obtained from the log-log plot using the method described by Marongiu-Porcu et al. (2011), thus eliminating the necessity of constructing the BHP vs. $g(\alpha, \Delta t_D)$ plot. The method was described in Section 2.5.

In order to estimate fracture geometry by the time of the fracture closure, substitute m_N = -71.6 psi and b_N = 12834 psi in the equations for radial geometry provided in Table 2.3,The fracture radius R_f is obtained as 14 ft. The leakoff coefficient can be subsequently evaluated to be $C_L = 0.0057 \ \ ft/\sqrt{\min}$ and fracture average width at the end of pumping is 0.0025 ft (0.03 inch) with fluid efficiency, η, of 86.5%.

For mere comparison purpose, if PKN fracture geometry is assumed, then the fracture half-length from before-closure analysis is obtained as 0.11ft.

Permeability Estimation from Before Closure analysis

The Barree, et al. (2009) empirical correlation in Eq. (2.2.2.2) provides a permeability estimate of 0.0042 md. The storage ratio r_p in normal leakoff cases is 1. This particular permeability estimation is color-coded in orange in Figure 4.4 along with the logarithmic derivative level it represents.

After Closure Analysis

The after-closure pressure response is dominated by the final fracture geometry existing at the closure time. The purpose of the after-closure analysis is to determine reservoir permeability, fracture geometry, and pressure from the late time FCT response. The after

closure analysis theory is presented in Chapter II. As illustrated in Figure 4.4, Haynesville Shale Well A has both linear and radial occurs after closure, indicated by a ½ slope derivative trend followed by a flat trend.

Radial Flow Regime Analysis

The presence of the radial flow regime allows direct estimation of reservoir transmissibility, kh, from Equation (3.3.0.3).

In this case, the late time apparent derivative level m' = 17828 psi. By substituting the values for the known parameters, the value of the kh product is obtained as 0.5904 md-ft.

If the radial fracture geometry is assumed as in previous discussion, permeability should be estimated with h =2 R_f, and the formation effective permeability to gas is estimated to be 0.0213 md. This estimation is very high for shale. If PKN fracture geometry is assumed and fracture height is same as the formation height, then the permeability is estimated to be 0.004 md, which is a more reasonable estimation.

The initial reservoir pressure estimated from the derivative level in the pseudo-radial flow regime m' and corresponding values of Δp and Δt, using Equation (2.5.0.4) is 11660 psi independent of the fracture geometry.

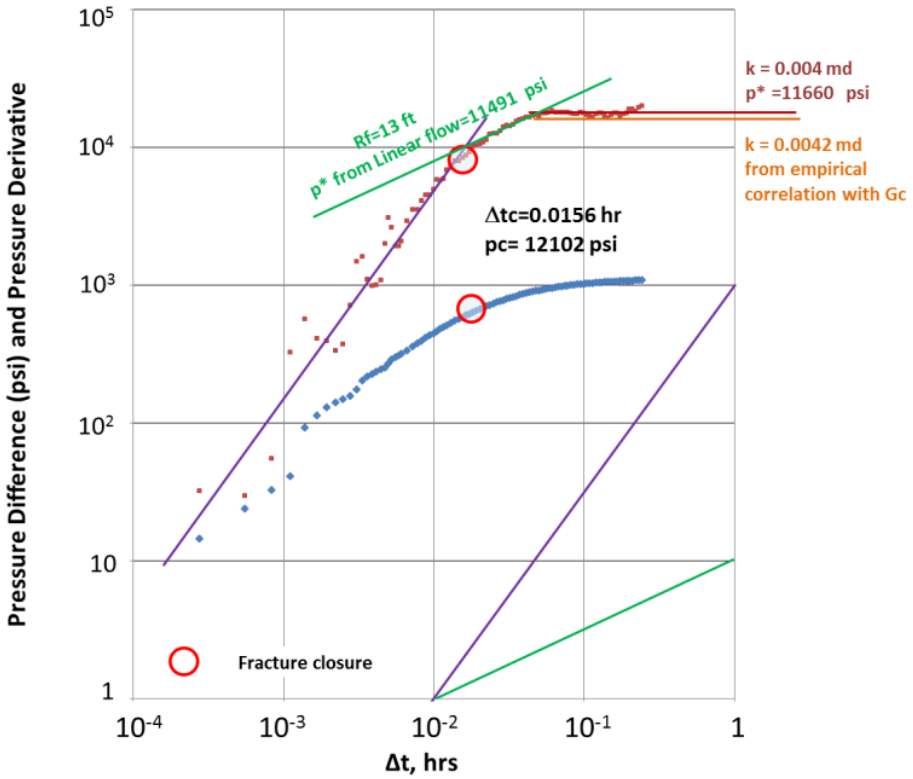

Figure 4.4 Log-log diagnostic plot with ACA for data of Haynesville Well A FCT

Linear Flow Regime Analysis

Selecting the point (0.0356, 15493) from the ½ slope derivative trend in Figure 4.1.2.5, the fracture radius is computed using Eq. (2.5.0.3) as 1.8 ft. Then directly from the same derivative point Eq. (3.3.0.2) provides an estimate for formation pressure of 11491psi.

Reservoir permeability and average pressure estimation from radial flow using other methods

For mere comparison purpose, the radial flow period is analyzed with the Soliman et al. 2006 radial flow specialized plot shown in the Appendix. With given injection volume, fluid viscosity and fracture height, the permeability is estimated from

the y-axis intercept, b_r. The formation pressure is obtained by trial and error until the pressure difference, $p(\Delta t)- p_i$ overlaps the derivative curve on a single negative unit slope for the portion of the data that correspond to radial flow. The resulting estimates are p_i = 11563 psi and permeability k = 0.006 md (PKN geometry) k=0.032 md (Radial geometry).

Reservoir Pressure Estimation from Linear Flow

Nolte 1997 method for linear flow analysis was described by Eqs. (2.3.6.3) and (2.3.6.4). The linear extrapolation to F_L= 0 yields an extrapolated pressure value of 11491 psi.

Nolte 1997 did not explain how to estimate permeability from this relation. However the pressure value estimated from linear flow allows the estimation of permeability using the reservoir pressure and permeability relation. The details of this method will be explained in the next field example.

Observation and Discussion

This example compares closure pressure, permeability, and formation pressure estimations directly determined from the log-log diagnostic plot to those determined from specialized plot analyses. As long as the specialized lines correspond to correct flow regime trends identified on the diagnostic plot, the results will be quite similar.

4.1.3 Haynesville Shale Well B

A fracture calibration test was conducted on the toe of the cased horizontal well at an average true vertical depth of 12500 ft. The injection was performed by pumping

20 bbl of fresh water, at an average rate of 2.2 bbl/min in a time interval of 7 minutes (Figure 4.5). The ISIP is observed at 13738 psi. The bottomhole pressure decline was monitored for 350 hours.

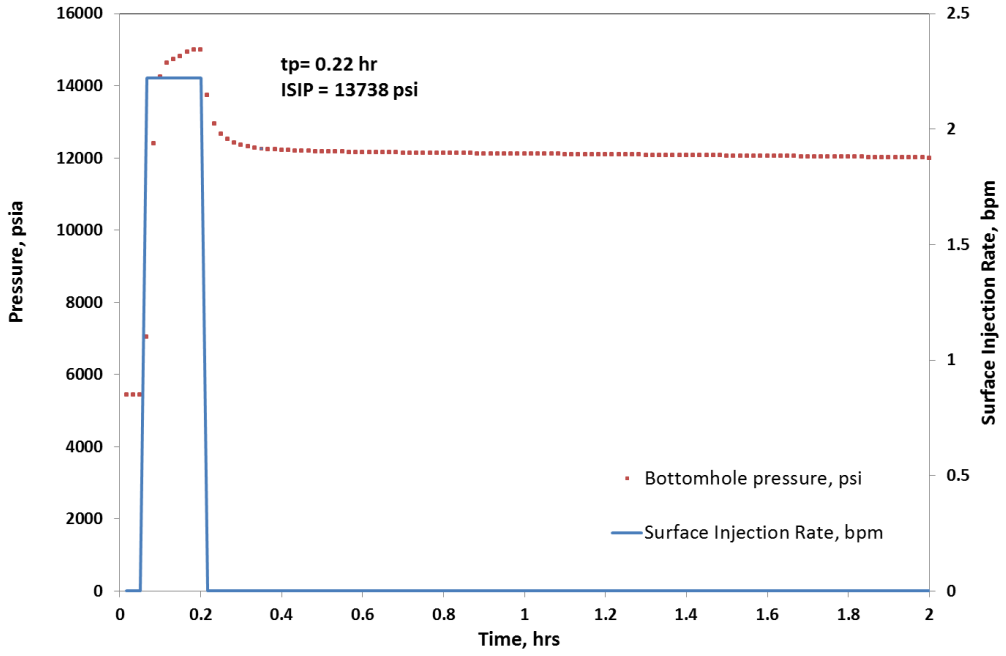

Figure 4.5 Bottomhole pressure and injection profile for Haynesville Well B

Before Closure Analysis

The log-log diagnostic plot for this example is shown in Figure 4.6. In this case the behavior shows a steep derivative trend with greater than 3/2 slope characteristic of transverse storage. The hydraulic fracture closure time is identified at the interception of the derivative curve with a 3/2 slope straight-line that is tangent to the derivative curve. As such, in this case the closure shut-in time is identified at $\Delta t = 3$hr and the hydraulic fracture closure pressure, $p_c = 11822$ psi. On G-function plot, the semi-log derivative curve exhibits the characteristic "belly" below the straight line extrapolated from origin

to the derivative which is a strong indication of transverse storage effect. The end of the storage effect is indicated by the departure of the tangent line on the semilog derivative curve. In this case $G_c = 9.89$, which corresponds to closure shut-in time = 3.03 hr. The closure pressure is 11823 psi. The two analysis methods show consistent estimates.

Another feature that distinguishes the case from the previous example is that the after-closure behavior does not show a flat level trend on semi-log derivative curve. Instead, soon after closure it shows a long duration bilinear flow period with derivative slope 1/4 followed by linear flow with derivative slope 1/2. In this case, the initial formation pressure can be estimated from the closure pressure using Eq. (2.3.6.2) or from the linear flow period using Eq. (3.3.2). This case is actually quite challenging due to lack of radial flow after closure which means that there is no definitive indication of the permeability. The permeability estimation from permeability-reservoir pressure relationship becomes crucial.

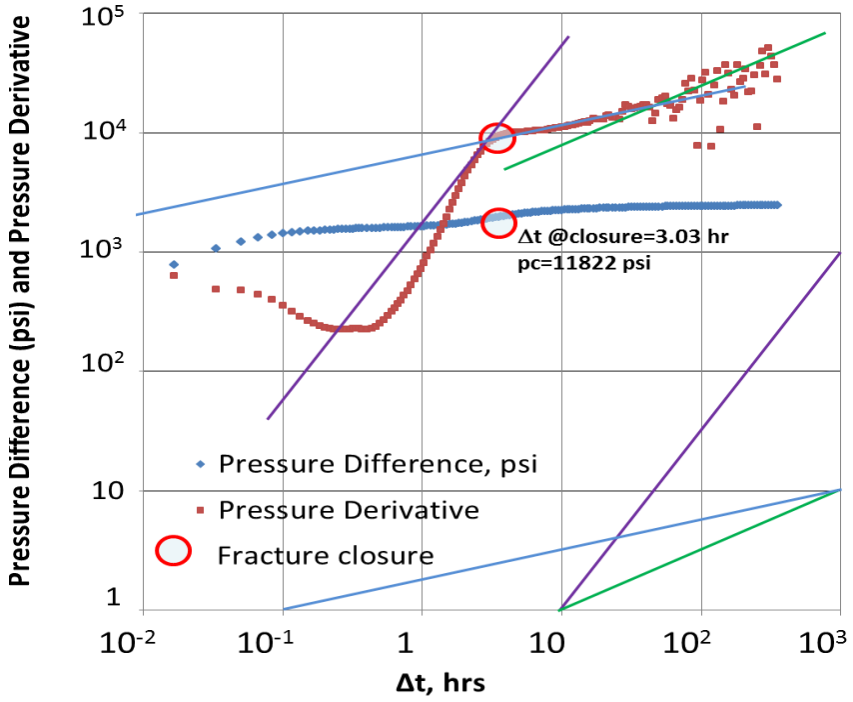

Figure 4.6 log-log diagnostic plot for data of Haynesville Well B FCT test

Nolte's pressure decline model for before-closure analysis (2.2.1.3) requires constant-fracture geometry and constant-permeability leakoff. Only with normal leakoff there exists the linear relation between bottom hole treating pressure and g-function. Since this case presents abnormal leakoff for which the total permeability is changing with the closure of the natural fracture/induced fracture, it is not surprising that the plot of bottom-hole pressure versus the loss-volume function, $g(\alpha, \Delta t_D)$ does not yield a straight-line trend. Thus the Nolte before closure analysis is inapplicable in this case. As a result fracture geometry cannot be estimated from before-closure analysis. Thus we have to count on after-closure analysis for fracture geometry estimation.

Permeability Estimation from Before Closure analysis

Using the Baree et al. (2009) G-function construction, r_p is estimated as 0.9. Then using Eq. (2.2.2.2) the estimated permeability is 0.0427 md.

Formation Pressure Estimation from Closure Pressure

Apply equation (2.6.3.2) with assumed Poisson's ratio $\nu = 0.2$, assuming overburden stress 1 psi/ft; it yields an estimate for formation pressure of 11597 psi.

After-Closure Analysis

As mentioned previously the Haynesville Shale Well B shows bilinear flow after closure followed by linear flow. The absence of radial flow prevents direct estimation of permeability, but an upper bound permeability estimate is possible using the Horner line approach explained in Section 3.3.

The Horner line approach requires an estimate for the formation pressure. The before closure estimate using the closure pressure was 9906 psi. Alternatively, using Eq. (3.3.0.2) the linear flow regime allows estimation of the reservoir pressure as 11243 psi.

With an estimate for the formation pressure, Eq. (3.3.0.3) enables estimation of the Horner line slope, m', and permeability is calculated from Eq. (3.1.0.8) as 0.0000178 md from the before closure pressure estimate and 0.00068 md from the after closure pressure estimate. The permeability estimation and the derivative level represent the permeability level from k-p_i relation are labeled and color coded in green in Figure 4.7.

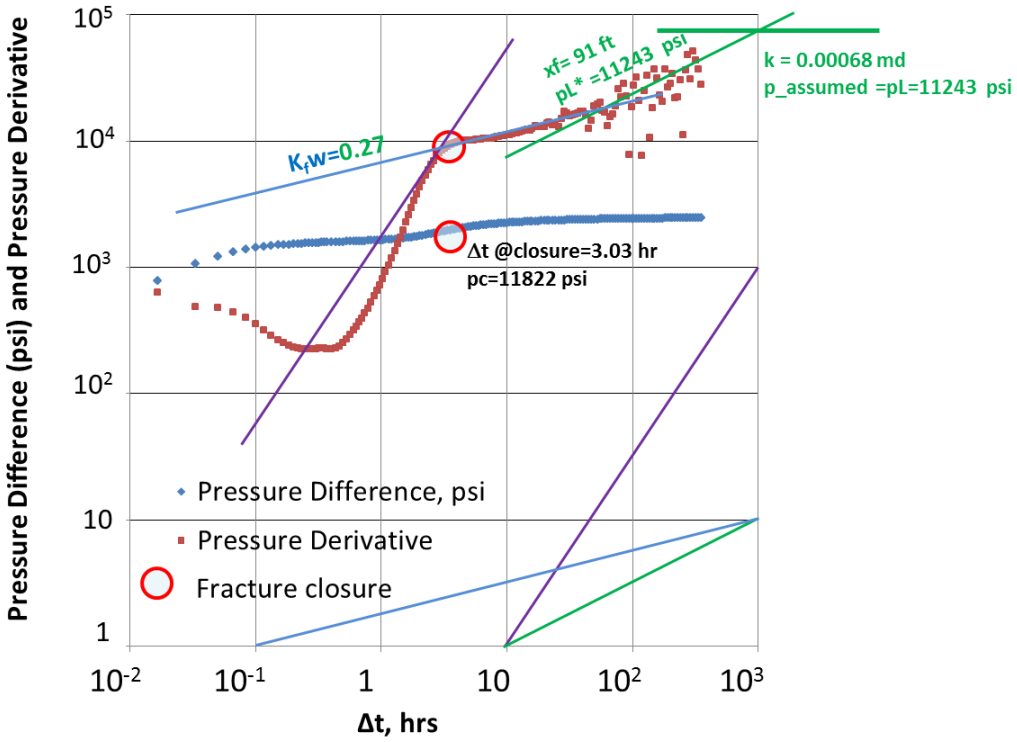

Figure 4.7 Log-log diagnostic plot with ACA for data of Haynesville Shale Well B

Formation linear flow can be used to determine fracture half-length if PKN geometry is assumed. Also, extrapolated reservoir pressure can be obtained from Nolte plot. With the permeability (k=0.00068 md from PKN model) known, the fracture half-length, x_f can be estimated from Marongiu-Porcu (2011) method to be 91 ft.

The standard logarithmic derivative data point, (81, 22127) on ½ slope is used to compute the fracture half-length.

Bilinear Flow Regime Analysis

According to Soliman et al. (1995), the cause of bilinear flow regime could be when created fracture is long, or if it did not completely close, thereby maintaining some residual conductivity. From the before closure analysis, there is indication of possible

induced fracture that could potentially cause finite-conductivity fracture as fluid in the surrounding induced fracture/reopened natural fracture flows linearly into the fracture. The presence of bilinear flow indicates that the flow regime is controlled by the pressure drop caused by the linear flow inside fracture and the pressure drop caused by the linear flow in the induced fracture/reopened natural fracture just surrounding the fracture. Compared to a more conventional interpretation, that bilinear is caused by the effect of linear flow to formation besides the linear flow inside of hydraulic fracture, natural fractures/induced fractures feeding hydraulic fracture would be a more feasible explanation in comparison in this case, since a well usually does not flow without fracture in Shale. With the permeability value estimated from k-p_i relation, the fracture conductivity can be solved. The value of fracture conductivity $k_f w$ is labeled in Figure 4.7.

Formation Permeability Estimation from Bilinear Flow Using Soliman et al. 2005 Impulse Solution

If assuming the fracture falloff period follows the impulse test solution, relation governs bilinear flow of this particular condition is presented Eq. (2.3.4.4) according to Soliman et al. (2005).The equation implied that the specialized plot of $\log(p_{fo} - p_i)$ vs. $\log(t_p + \Delta t)$ would render a straight line trend with slope of -3/4. The last point (end of bilinear flow) on the straight line may be used to calculate an upper bound of formation permeability. b_r is the intercept of pressure difference with the y-axis (on log-log corresponding to t=1). Here b_r =1600 and end of bi-linear flow time, t_{ebf} =17.87 hr. b_r is a function of permeability, the relation is expressed in Equation (2.3.4.5). With Equation

(2.3.4.6), k = 0.00032 md. The estimation and its representative derivative level are color-coded in orange and label in Figure 4.7.

Discussion

This field case shows feature of before closure transverse storage effect, after closure bilinear-linear flow.

The transverse storage effect could potentially relate to induced fracture or reopening existing natural fracture. The storage effect would delay the fracture closure timing and thus necessitate that all of the relation depending on closure time as input be adjusted by the storage ratio $r_{p.}$ The lack of radial flow makes it crucial to utilize the permeability-formation average pressure relation.

The existence of bilinear flow facilitates the estimation of not only fracture conductivity, $k_f w$, using Cinco-Ley finite conductivity fracture model, but the alternative estimation of reservoir permeability can be obtained using bilinear flow as well.

4.1.4 Haynesville Shale Well C

The fracture calibration test was performed on the toe stage of a cased horizontal well at TVD of 12296 ft. A set of three perforation clusters of respectively 4ft, 4 ft and 2 ft was opened via TCP guns. The perforation density is 12-SPF resulting 120 (48+48+24) holes open to flow. The FCT was performed by pumping 20 bbl of fresh water, at a constant rate of 3.3 bbl/min for 6.6 minutes. (Figure 4.8) The bottomhole pressure decline was monitored for 67 hours.

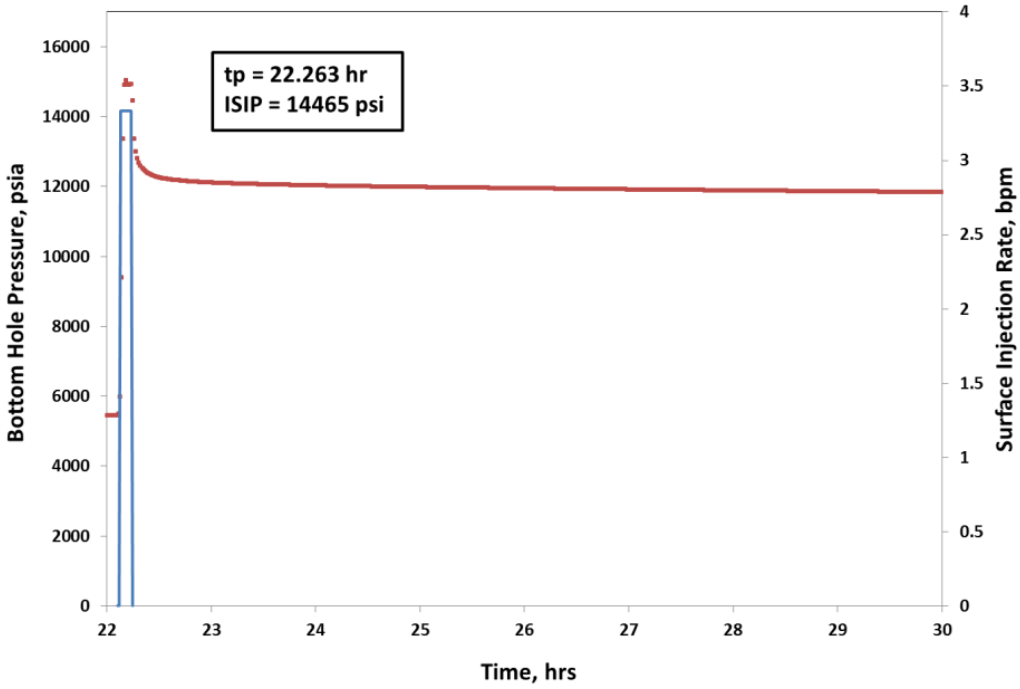

Figure 4.8 Bottom-hole pressure and Injection Scheme profile for Haynesville Well C

Before Closure Analysis

Figure 4.9 shows the log-log diagnostic plot for the pressure falloff data. The characteristic 3/2 slope indicate nomal leakoff. A clear departure from this trend is identified at $\Delta t = 7.95$ hour, yielding closure pressure/formation minimum stress at the time of 11830 psia. The feature that distinguishes the case from the previous example is that the linear flow is absent. A steep valley appears on the semi-log superposition derivative for half a cycle and in late time the derivative gets flat indicating reaching the radial flow. The lack of linear flow make it imperative to make use of the before closure analysis to obtain fracture half-length (or fracture radius assuming radial fracture geometry). The normal leakoff diagnosis is coherent with the G-function plot diagnosis.

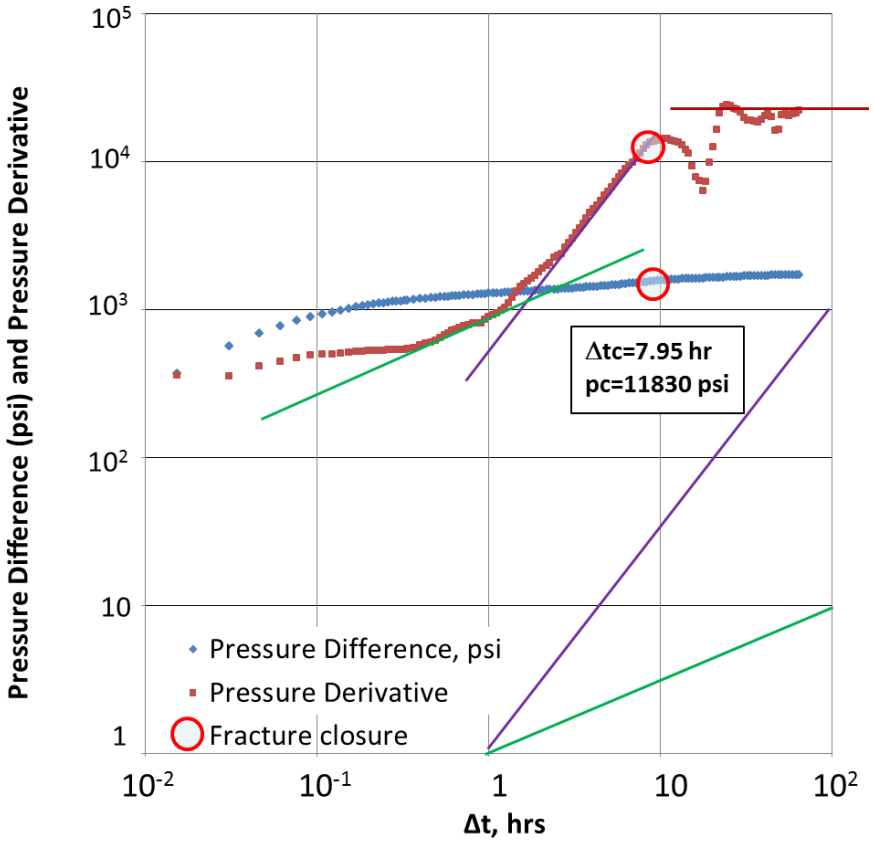

Figure 4.9 log-log diagnostic plot for data of Haynesville well C FCT

Initial reservoir pressure can be estimated from the closure stress and the uniaxial strain relationship

Assuming Poisson's ratio, $\upsilon = 0.25$, and an overburden stress, $\sigma_z = 12296$ psi (assuming 1.0 psi/ft overburden stress). From before-closure analysis, it is known that $\sigma_{min} = 10952$ psi. From Eq. (2.3.6.2) the initial reservoir pressure estimate is $p_i = 11597$ psi.

Fracture geometry and leakoff coefficient estimation from Before-closure analysis

The Nolte (1979) method for before-closure analysis requires an estimate of fracture half-length and lost fracture width because of fluid leakoff, w_L. Fracture half-

length and lost width can be estimated from a graph of bottomhole pressure versus the loss-volume function, $g(\alpha, \Delta t_D)$ provided the fracture geometry is homogeneous and the Shlyapobersky assumption is met. The slope of the line through the before-closure data is m_N=-22 psi and the intercept is b_N = 12198 psi.

With the log-log plot, the calculation of m_N and b_N can be directly obtained from the log-log plot using the method described by Marongiu-Porcu et al. (2011), thus eliminating the necessity of constructing the BHP vs. $g(\alpha, \Delta t_D)$ plot. The method was described in Section 2.5.

In order to estimate fracture geometry by the time of the fracture closure, substitute m_N = -22 psi and b_N = 12198 psi in the equations for radial geometry provided in Table 4.1.

This example is complicated by the fact that there were 3 perforation clusters that possibility creates more than one fracture. The before-closure modeling has been performed for two simplified schematic configurations:

a) Only one radial fracture has been created by the total diversion of the injected fluid throughout only one of the three clusters of perforations:

   The fracture radius R_f is obtained as 66 ft assuming Young's modulus, E'=6×10^6 psi. Leakoff coefficient can be subsequently evaluated to be C_L=0.000915 $ft/\sqrt{\min}$ and fracture average width, $\overline{w_e}$ =0.08 inches with fluid efficiency, η =92%

b) The injected fluid has been equally diverted among the three clusters, corresponding in three identical radial fracture s with the same fracture fluid efficiency and same leak-off coefficient.

The fracture radius R_f is obtained as 46 ft assuming Young's modulus, E'=6×10^6 psi. Leakoff coefficient can be subsequently evaluated to be C_L=0.000635 $ft/\sqrt{\min}$ and fracture average width, $\overline{w_e}$ =0.06 inches with fluid efficiency, η=92%

Permeability Estimation from Before Closure analysis

The Barree, et al. (2009) empirical correlation in Eq. 2.2.2.2 provides a permeability estimate of 0.00236 md.

In Equation (2.2.2.2), p_z is the invaded zone pressure, which is the same value of the pressure difference at the time of closure; $r_{p,}$ is the storage ratio, represents the amount of excess fluid that must be leaked off to reach fracture closure when the fracture geometry deviates from the normally assumed constant-height planar fracture. The storage ratio in normal leakoff cases is 1. This particular permeability estimation is color-coded in orange in Figure 4.10 along with the logarithmic derivative level it represents.

After-Closure Analysis

Haynesville Shale Well C only has both radial flow occurs after closure, indicated by a horizontal level on derivative.

Radial Flow Regime Analysis

The presence of the radial flow regime allows direct estimation of reservoir transmissibility, kh, from Equation (3.3.0.3).

In this case, the late time apparent derivative level m' = 382533 psi. By substituting the values for the known parameters, the value of the kh product is obtained as 0.5193 md-ft.

If the radial fracture geometry is assumed as in previous discussion, we estimate the shale permeability as k= 0.00415 md assuming one created fracture and k= 0.0022 md for three created fracture suing the previously-determined value for kR_f divided by 3 to account for only 1/3 of the injected volume for each fractures.

Permeability Estimation from Horner Plot

Assumed formation pressure from Before Closure

The Horner line approach requires an estimate for the formation pressure. The before closure estimate using the closure pressure was 11,597 psi. With an estimate for the formation pressure, Eq. (3.3.0.3) enables estimation of the Horner line slope, m', and permeability is calculated from Eq. (3.1.0.8) as 0.0034 md from the before closure pressure estimate. The permeability estimation and the derivative level represent the permeability level from k-p_{ave} relation are labeled and color coded in blue in Figure 4.10.

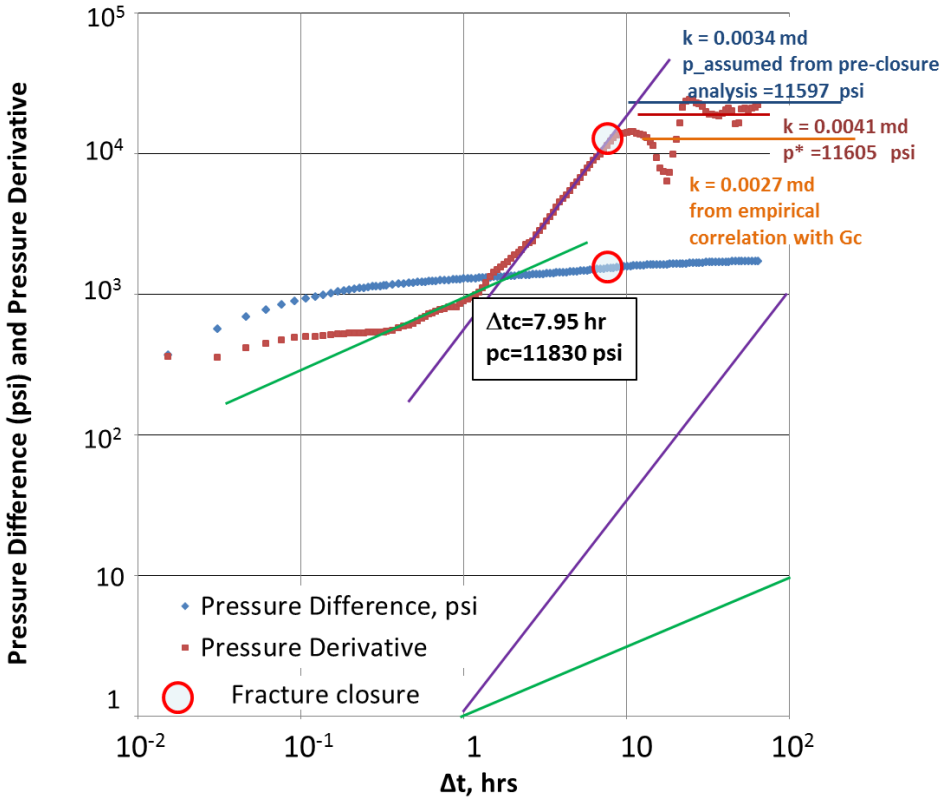

Figure 4.10 log-log diagnostic plot with ACA for data of Haynesville Shale Well C

Reservoir permeability and average pressure estimation from radial flow using Impulse solution methods

For mere comparison purpose, the radial flow period is analyzed with the radial flow specialized plot shown in the appendix. Assuming the fracture injection/falloff follows impulse solution, a specialized plot of $\log(p_{fo} - p_i)$ vs. $\log(t_p + \Delta t)$ renders a straight line trend with slope of -1.0 in late time for radial flow regime, which is a signature for radial flow (Soliman et al. 2006). With given injection volume, fluid viscosity and fracture height, the permeability is estimated from the y-axis intercept, b_r, in this case is 2500 psi. (Equation 2.3.4.3) P_i is obtained by adjusting its own value until

pressure difference overlaps the derivative curve on a single negative unit slope. The p_i estimated by trial and error using compose the plot is 11608 psi and permeability k = 0.004 md. This estimation is in good agreement with the one estimated using the conventional well testing method.

Discussion

This field case study demonstrates the power of combining before and after closure analysis. With the absence of after-closure linear flow, the geometry can be estimated from before closure analysis if before closure analysis conforms to the Shlyapobersky assumptions. The multiple-perforation complicates the case in terms of the distribution of fracture fluid, which subsequently influences the estimation of individual fracture dimension as well as permeability.

4.2 Horn River Shale Field Case Example

In this section, one well with FCT performed in Horn River Shale is used to demonstrate the not uncommon multiple closure effect and its representation on the log-log diagnostic plot.

The section begins by providing the background information on the Horn River shale from the geologic aspect, and then the baseline parameters for Horn River shale will be specified based on information found in the literature and an available data set.

4.2.1 Horn River Basin Background

Horn River Basin is the biggest shale gas field in Canada located between British Columbia and the North Western Territories**.** The shale in Horn River Basin is in Middle and Upper Devonian ages and is comparable to the Barnett shale in aspects of depth, porosities, productivity, and shale qualities. However, the basin contains multiple potential shales including the Carboniferous- Devonian Muskwa, Otter Park, Klua and Evie formations. The Horn River formations were deposited on a continental shelf during a period of rapid sea level rise. Generally the deposits are described as grey to black, organic rich, pyritic, variably calcareous to siliceous shale. Low sedimentation rates and increased subsidence resulted in a starved, anoxic basin, creating favorable conditions for preserving the organic rich shale sediments of the Horn River. The basin has been developed extensively since 2006 using multi-traverse fractured horizontal wells. (Reynolds et al. 2010)

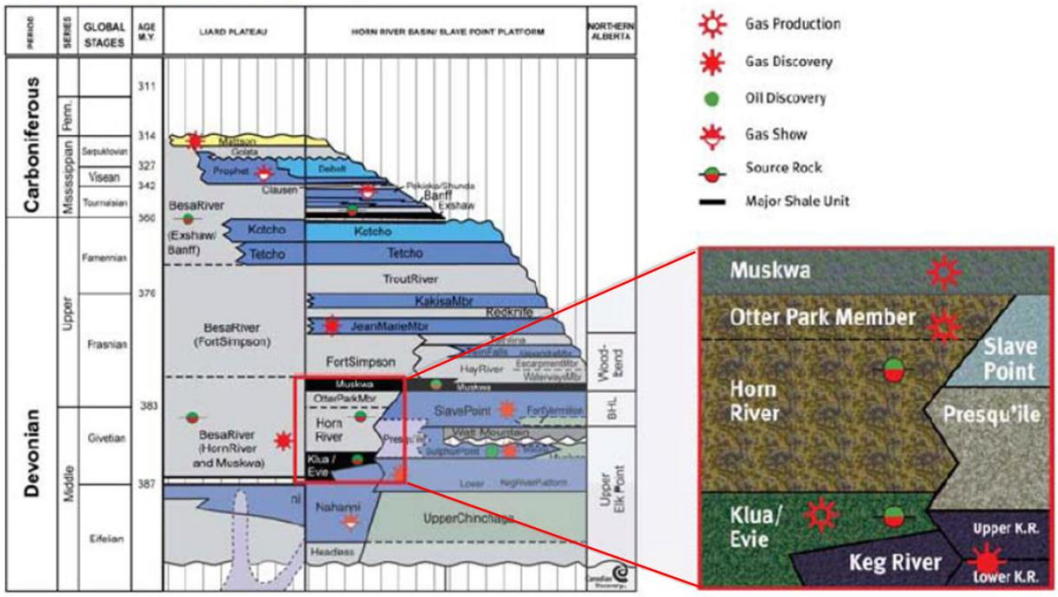

Figure 4.11 Horn River in the Devonian Age, showing the different source rocks that compose it (Reynolds et al. 2010)

Shale formation properties

The Horn River Basin shale is considered as high temperature and over pressured with an average temperature of 350°F and initial pressure of around 5500-7250 psi (Reynolds et al. 2010) or 0.6-0.8 psi/ft equivalent pressure gradient. Average porosity in the Muskwa formation is 0.058. The formation properties are summarized in Table 4.2

Table 4.2 Input parameter for Horn River shale well Z FCT analysis

Properties	Value	Unit
Gas Viscosity, μ_g	0.027	cp
Formation Total Compressibility, c_t	1.06×10^{-04}	psi^{-1}
Formation Porosity, ϕ	5.8	%
Water Saturation, S_w	25	%
Young's Modulus, E'	6.00×10^{6}	
Formation Height, h	360	ft
Formation Temperature	320	F

4.2.2 Horn River Shale Well Z

The fracture calibration test was performed on the toe stage with a single perforation at 9264 ftTVD in Klua formation at a cased horizontal well. The FCT was performed by pumping 77.15 bbl of slickwater for 3.7 minutes (Figure 4.12). The ISIP is observed at 11236 psi, which yielded a fracture gradient of 1.21 psi/ft of. The bottomhole pressure decline was monitored for 400 hours.

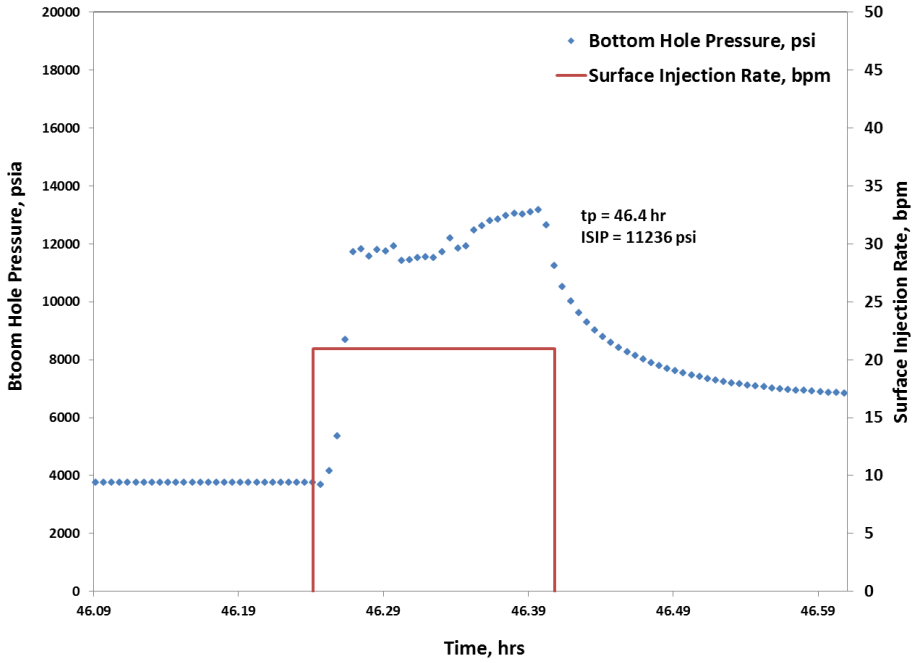

Figure 4.12 Bottom-hole pressure and Injection Scheme profile -- Well Z

Before Closure Analysis

The log-log diagnostic plot (Figure 4.13) shows the pronounce 3/2 slope trend on the pressure derivative curve for more than a logarithmic cycle, and a clear departure from this trend is identified at $\Delta t = 5.32$ hour, yielding closure pressure at the time of 5834 psia. The G-function plot shows coherent diagnosis of closure time and pressure, indicated at the end of the signature straightline following pressure semi-logarithic derivative with respect to G-function. The characteristic 3/2 slope on the log-log plot and the straght line trend through origin on the G-function plot indicate classic constant fracture geometry and constant permeability normal leakoff model. Duirng normal leakoff, the fracture area is constant and the reservoir rock appears homogeneous.

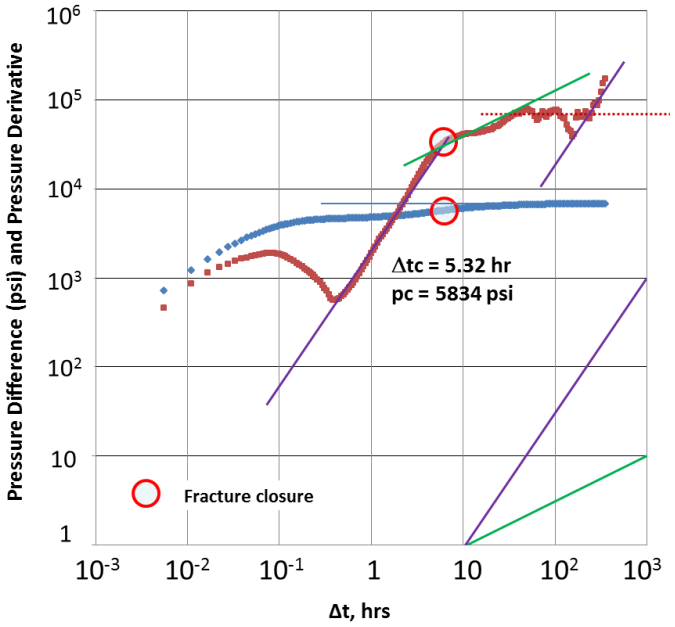

Figure 4.13 log-log diagnostic plot for data of Horn River Well Z FCT

Table 4.2 shows reservoir and fluid properties used for the analysis. In this case, it is known that Poisson's ratio, υ=0.2, and an overburden stress, σ_z=11234 psi. From before-closure analysis, it is known that σ_{min} =5654 psi. Use the relationship between initial reservoir pressure and closure stress, the initial reservoir pressure is estimated to be p_i = 3654. The estimated initial reservoir pressure from closure stress should be considered as a guide only.

Apply Equation (4.1.2.1), the initial reservoir pressure is estimate to be p_i = 3654 psi. The estimated initial reservoir pressure from closure stress should be considered as a guide only.

With the log-log plot, the calculation of m_N (slope of the bottom-hole pressure decline with respect to the loss-volume function $g(\alpha, \Delta t_D)$ during poro-elastic closure)

and b_N (intercept) are obtained by applying the Equations at fracture closure, thus eliminates the necessity of constructing the BHP vs. $g(\alpha, \Delta t_D)$ plot. The estimation in this case are m_N = -88.35 psi and the intercept b_N = 6909.3 psi.

To estimate fracture geometry by the time of the fracture closure, substitute m_N=-88.35 psi and the intercept is b_N = 6909 psi in the equations for radial flow provided in Table 4.2, the fracture geometry and fluid efficiency etc. can be obtained.

a) Assuming Radial Fracture geometry

   The fracture radius R_f is obtained to be 92 ft assuming Young's modulus, E'=6×10^6 psi. Leakoff coefficient can be subsequently evaluated to be C_L=0.0046 $ft/\sqrt{\min}$ and fracture average width, $\overline{w_e}$ =0.35 inches with fluid efficiency, η=90%

b) Assuming PKN Fracture geometry. The fracture height, h_f is obtained as 221.85 ft. Leakoff coefficient can be subsequently evaluated to be C_L=0.002 $ft/\sqrt{\min}$ and fracture average width, $\overline{w_e}$ =0.97 inches with fluid efficiency, η=88%

Permeability Estimation from Before Closure analysis

By applying the empirical correlation described in previous sections, using the input in Table 4.2, the permeability is estimated to be 0.0023 md for p_z= 5581 psi and r_p=1.

$$k = \frac{0.0086\mu_f\sqrt{0.01p_z}}{\varphi c_t\left(G_c E r_p / 0.038\right)^{1.96}} \quad \text{..... (4.1.2.4)}$$

After Closure Analysis

Radial Flow Analysis

The level of the derivative during pseudo-radial flow gives an estimate for $kh=2kR_f$=0.8162 md-ft. The permeability estimation assuming PKN geometry is k= 0.0023 md. The permeability estimation (PKN Geometry) from pressure derivative is color-coded red and labeled on Figure 4.14. From the before closure analysis, the R_f= 92 ft and the permeability estimation is k= 0.0044 md. The permeability estimation (Radial Geometry) is color-coded red and labeled on Figure 4.15.

Reservoir permeability and average pressure estimation from radial flow using Impulse solution methods

For mere comparison purpose, the radial flow period is analyzed with the radial flow specialized plot shown in the Appendix. Assuming the fracture injection/falloff follows impulse solution, . The permeability estimation for radial geometry is k = 0.004 md and k = 0.0016 md for PNK geometry. These estimations are in good agreement with the one estimated using the conventional well testing method. The p_i estimated by trial and error using compose the plot is 4400 psi.

Linear Flow Regime Analysis

Formation linear flow can be used to determine fracture half-length. Also, extrapolated reservoir pressure can be obtained from linear flow using Nolte plot. With the permeability (k=0.0023 md from PKN model) known, the fracture half-length can be conveniently estimated in this case since the linear flow is present.

Where $m_{lf} = 2\Delta p' / \sqrt{\Delta t}$ =26813 and $\Delta p'$ represents the value of the logarithmic derivative at a time which in this case is 35554 at Δt =7.03 when the derivative slope is ½ . x_f can be obtained from this relation and in this case is estimated to be 17.36 ft.

Reservoir Pressure estimation from Linear Flow Nolte 1997 ACA Plot

With the linear extrapolation using Nolte 1997 linear flow model, the reservoir pressure estimated from Nolte linear flow is 4268 psi.

Permeability Estimation from Horner Plot

The extrapolated average formation pressure from Nolte (1997) linear flow function plot is 4268 psi. A permeability estimation can be obtained from slope of the line connecting the last recorded falloff pressure to the estimated reservoir pressure on buildup test analysis. The permeability estimation is 0.0004 md and is labeled and color coded in green Figure 4.14 and Figure 4.15.

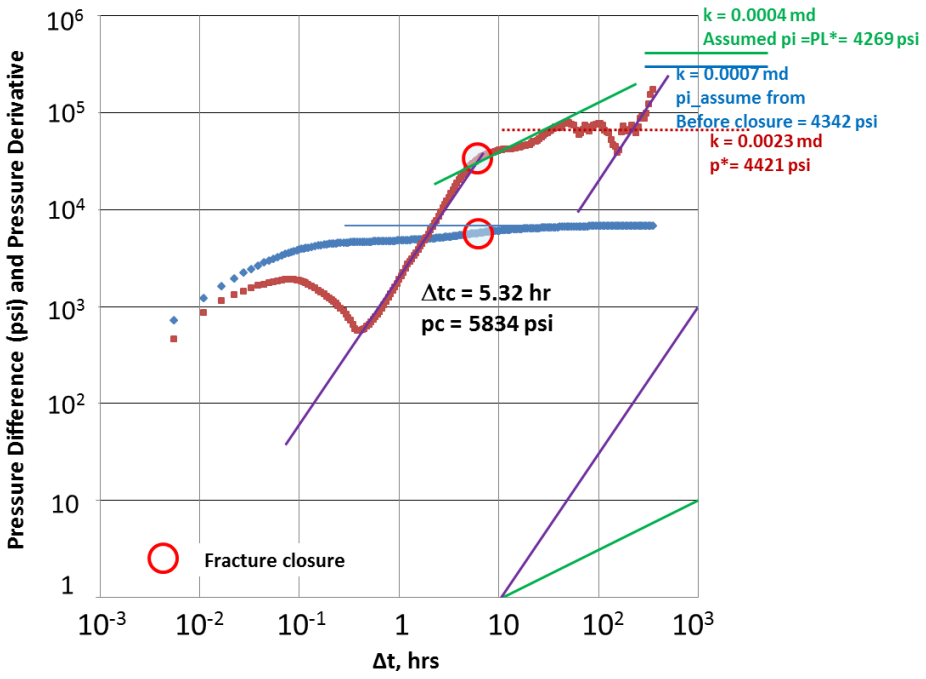

Figure 4.14 log-log plot with permeability estimation (PKN) HR well Z

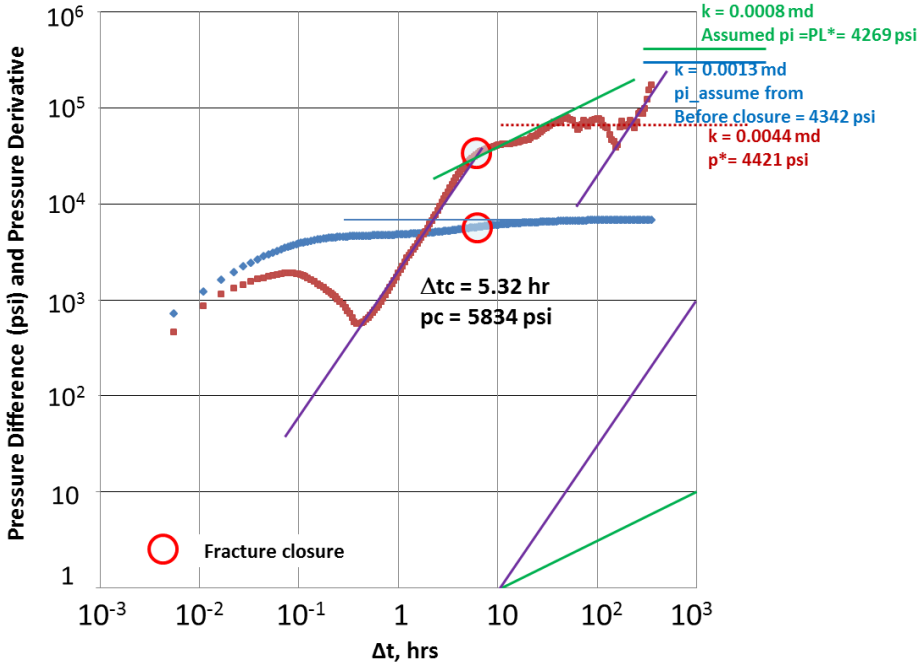

Figure 4.15 log-log plot with permeability estimation (Radial) HR well Z

Observations

The most apparent feature of this case is the advent of multiple closures. Though there are many possibilities that could potentially cause the effect, it is not well studies yet. Of all four wells that performed FCT on the same pad with well Z, all of them exhibit multiple closure effect.

4.3 Mesaverde Tight Gas Well

The Mesaverde formation is a late Cretaceous formation. Well GM produced from 20 low-permeability Mesaverde sands in Piceance Basin that separated from an adjacent sandstone reservoir by impermeable and high stress shale and mudstone formations (Craig et al. 2006). Some formation properties are summarized in Table 4.3.

Table 4.3 Input parameter for the Mesaverde well GM FCT

sg_g	0.63
μ_g (cp)	0.0175
c_t (psi^{-1})	0.0002
ϕ (%)	10
S_w (%)	50
h_{net} (ft)	12
Plane Strain Modulus, E'	5208333.3
Formation Temperature (F)	160

A fracture calibration test (FCT) was completed in a relatively thin sandstone reservoir with gross thickness of 14 ft. The sandstone reservoir was perforated at 4954 feet, and the FCT was executed in the target zone with compatible 1% KCl treated water. 17.69 bbl of water was injected at an average rate of 3.3bbl/min for 5.3 minute. The entire fracture-injection/falloff sequence is shown in Figure 4.16. Injection was stopped

at 0.086 hour and the instantaneous shut-in pressure is estimated at corresponding BHP at 3143 psi. The falloff period shown in Figure 4.16 extended for 16.10 hours beyond the end of pumping.

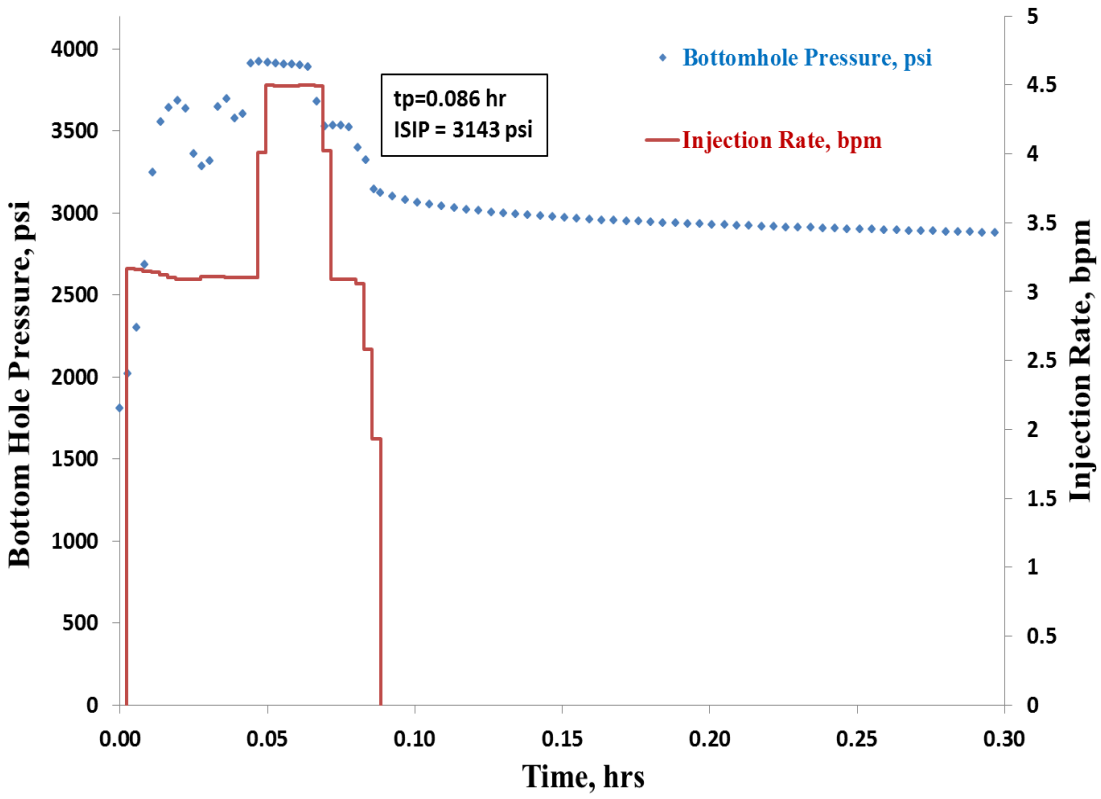

Figure 4.16 Injection Rate and Pressure Falloff Profile - Well GM

Following the falloff period, the plug was removed, and all 20 layers produced for 168 hours prior to a 15 day pressure buildup. With both an FCT and a drawdown/buildup sequence completed sequentially, direct comparison of the buildup and falloff interpretations is possible.

Log-log diagnostic plot

The fact that the injection scheme for this case is a variable rate injection with significantly lower last injection rate which renders the Horner approximation inapplicable, it is imperative to use the rigorous superposition time function given by

$$X = \frac{q_1}{q_{n-1}}\ln(\frac{t}{t-t_1}) + \frac{q_2}{q_{n-1}}\ln(\frac{t-t_1}{t-t_2}) + \frac{q_3}{q_{n-1}}\ln(\frac{t-t_2}{t-t_3})... \quad \text{..... (4.3.1)}$$

The log-log diagnostic plot for this case consists of a pressure difference vs. shut-in time Δt curve and the superposition derivative curve, dp/dX vs. Δt is equivalent to $\tau dp/d\tau$ vs. Δt when the Horner equivalent time approximation is applicable.

Before Closure Analysis

As in the previous cases, the first step is to identify the leakoff type and hydraulic fracture closure. It is observed from Figure 4.18 that following the before closure linear flow (1/2 slope on the superposition derivative curve) is a period in which the derivative curve exhibits slightly less than 3/2 slope. As explained in the second field example in Chapter III, it is a characteristic of Pressure dependent leakoff behavior. The end of the less than 3/2 slope trend or the beginning of the 3/2 trend is the indication of fissures closure, the fissure closure time is Δt= 0.33 with fissures closure stress =2836 psi. Hydraulic Fracture closure is observed at Δt= 0.46 hour and the closure stress is 2790 psi. Figure 4.17 contains the G-function plot for the fracture injection/falloff sequence. Pressure dependent leakoff is diagnosed through the characteristic hump on the semi-log derivative trend. The closure is diagnosed at the end of the linear trend on the semi-log derivative curve at G_c=4.45. The closure timing is consistent with the log-log diagnostic.

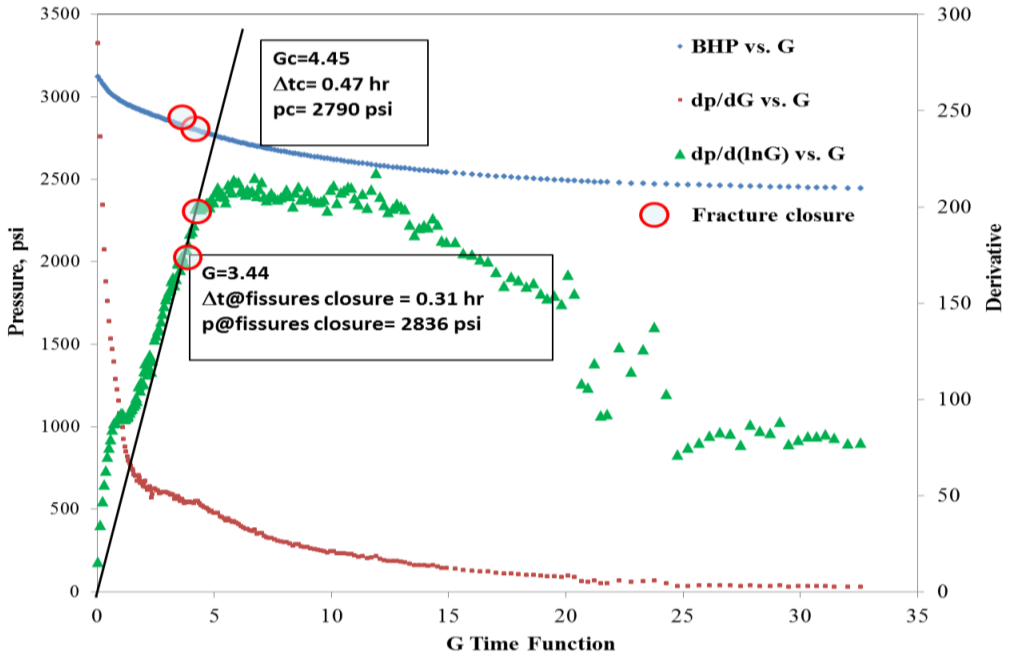

Figure 4.17 G-function diagnostic plot for data of Mesaverde Well GM FCT

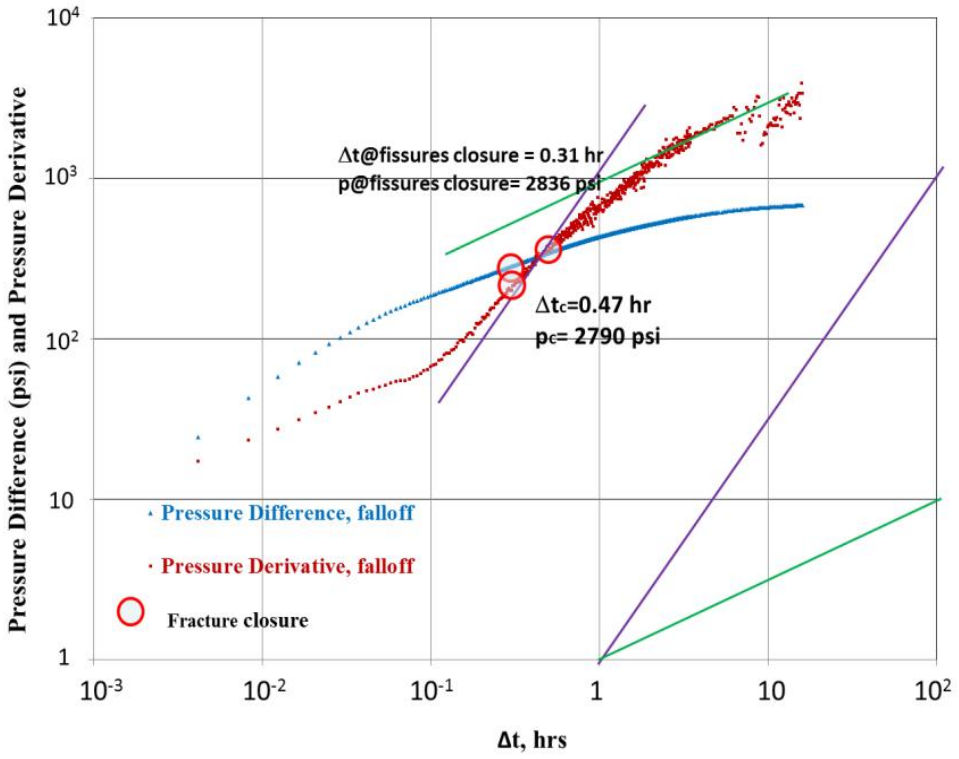

Figure 4.18 Log-log diagnostic plot for data of Mesaverde Well GM

The initial reservoir pressure can be estimated from the closure stress and the uniaxial strain relationship, Equation (2.6.3.2). Assuming an overburden stress, σ_z =4954, with poisson's ratio and plane strain modulus given as υ=0.15, the initial reservoir pressure estimate is p_i= 2326.3 psi.

Lithology suggests the PKN fracture geometry model. In a similar manner as in the previous cases, fracture half-length and width are estimated using a point on the second 3/2 slope trend as indicated by Marongiu-Porcu et al. 2011. The slope of the line through the before-closure data is m_N=-91 psi and the intercept is b_N = 3100 psi. Fracture half-length is calculated from the intercept assuming Young's modulus, E=5×10^6 psi, and fracture height h_f =14 ft assuming the fracture has PKN geometry. The estimated fracture half-length, x_f = 122 ft. The width at the end of pumping is 0.06 inch. The leakoff coefficient is estimated as C_L=0.00011 ft/min$^{0.5}$ and fluid efficiency η = 81.6%.

Permeability Estimation from Before Closure analysis

Apply the empirical correlation, Equation (2.2.2.2)**.** With storage ratio r_p estimated to be 1.1 due to slight pressure dependent leakoff. The permeability estimate is k = 0.0032 md.

After Closure Analysis

The absence of radial flow prevents direct estimation of permeability, but an upper bound permeability estimate is possible using the Superposition plot line approach explained in Section 3.3

Permeability Estimation from BHP vs. Superposition Time Function Plot

The Superposition plot line requires an estimate for the formation pressure. The before closure estimate using the closure pressure was 2326.3 psi. Alternatively, using Eq. (3.3.0.2) the linear flow regime allows estimation of the reservoir pressure as 2356.6 psi. The reservoir pressure estimated from the Soliman et al. (2005) linear flow analysis method is p_i=2360 psi.

With an estimate for the formation pressure, Eq. (3.3.0.10) enables estimation of the Superposition Function line slope, m', and permeability is calculated from Eq. (3.1.0.8) as 0.026 md from the before closure pressure estimate and 0.035 md from the after closure pressure estimate. Figure 4.18 shows the BHP vs. Superposition Time Function Plot for the falloff period. The last falloff pressure is connected with a straight-line with the assumed pressure value on Superposition plotting function X=0. The estimate for the upper bound for the formation permeability for assumed pressures from before closure is color-coded in blue and the permeability estimation from linear flow extrapolated pressure is color-coded in green and labeled in Figure 4.20.

In comparison, if the Horner approximation is used, Eq. (3.3.0.3) would give the value of Horner line slope m', and permeability is calculated from Eq. (3.1.0.8) as 0.026 md from before closure pressure estimation and 0.034 md from the after closure pressure estimate. The results are very coherent with previous estimation using the Superposition Function line slope.

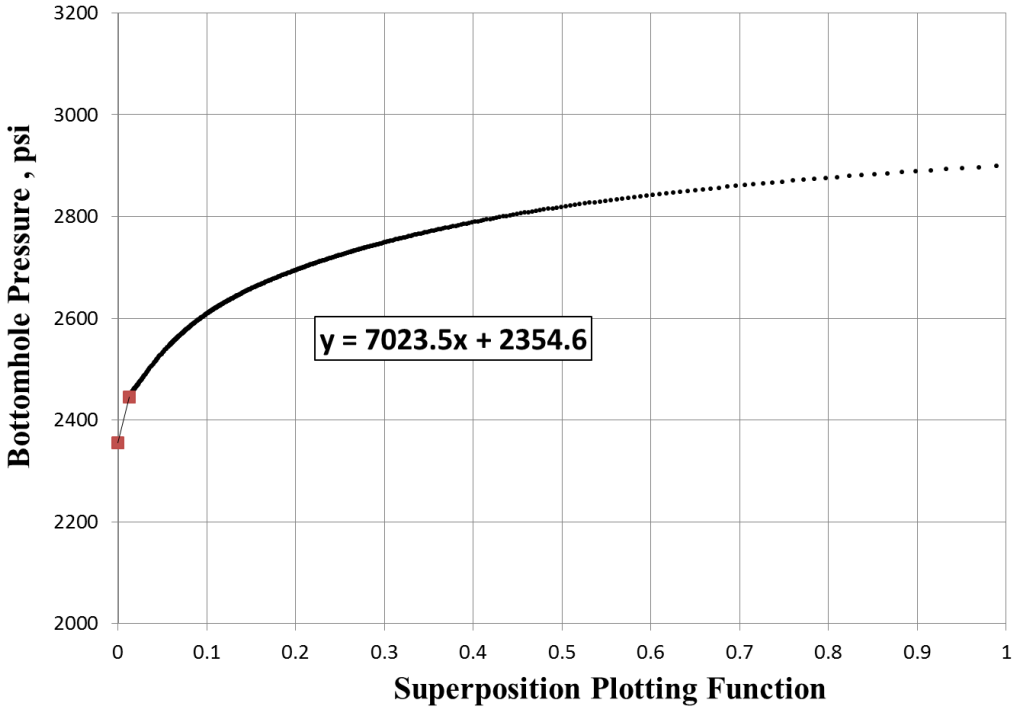

Figure 4.19 BHP vs. Superposition Time function - falloff, Well GM

Linear Flow Regime Analysis

Formation linear flow can be used to determine fracture half-length assuming PKN fracture geometry. Also, extrapolated reservoir pressure can be obtained from Nolte plot. With the permeability (k=0.034 md from k-p_i relation using PKN model) known, the fracture half-length can be conveniently estimated in this case since the linear flow present right after fracture closed. The formation linear Flow in the reservoir dominated by flow to an effectively infinitely conductivity fracture is characterized by (2.5.0.3). Where $m_{lf} = 2\Delta p' / \sqrt{\Delta t}$ and $\Delta p'$ represents the value of the logarithmic derivative at a time Δt when the derivative slope is ½. x_f can be obtained from this

relation. Using the data point on ½ after closure trend on the derivative curve (5, 2212), the fracture half-length assuming PKN geometry can be estimated to be 88.7 ft (with permeability estimation with assume pressure from Linear Flow extrapolation) and 107 ft (with permeability estimation with assumed pressure from before closure)

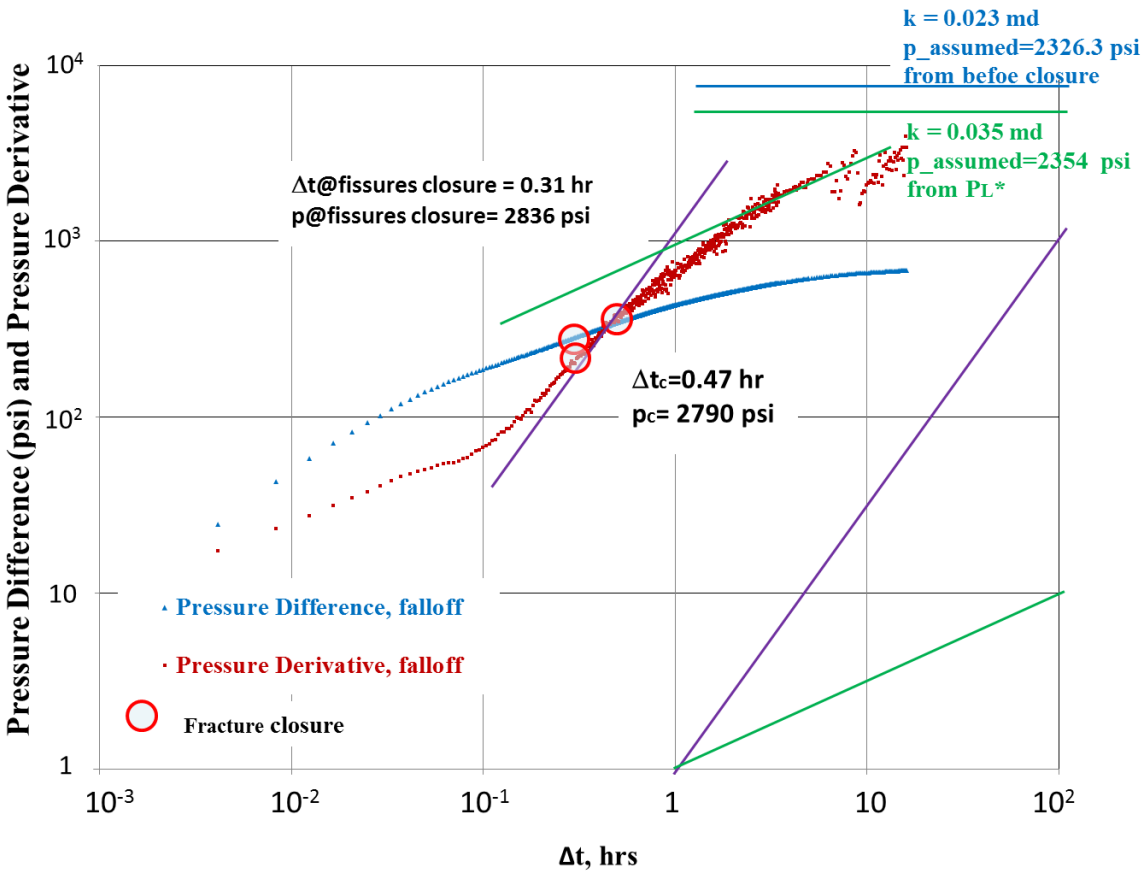

Figure 4.20 Log-log diagnostic plot with permeability estimation -- well GM

Buildup Test Analysis

Following the falloff period, the well was flowed at 100Mscf/D for141.7 hrs, then lowered at 98 Mscf/D for the next 24.3 hrs, then lowered at 60 Mscf/D for the next 0.6 hrs and finally lowered at 50 Mscf/D for the final 0.1 hrs before shutting the well in for a pressure buildup test lasting 14.95 days. (Figure 4.21)

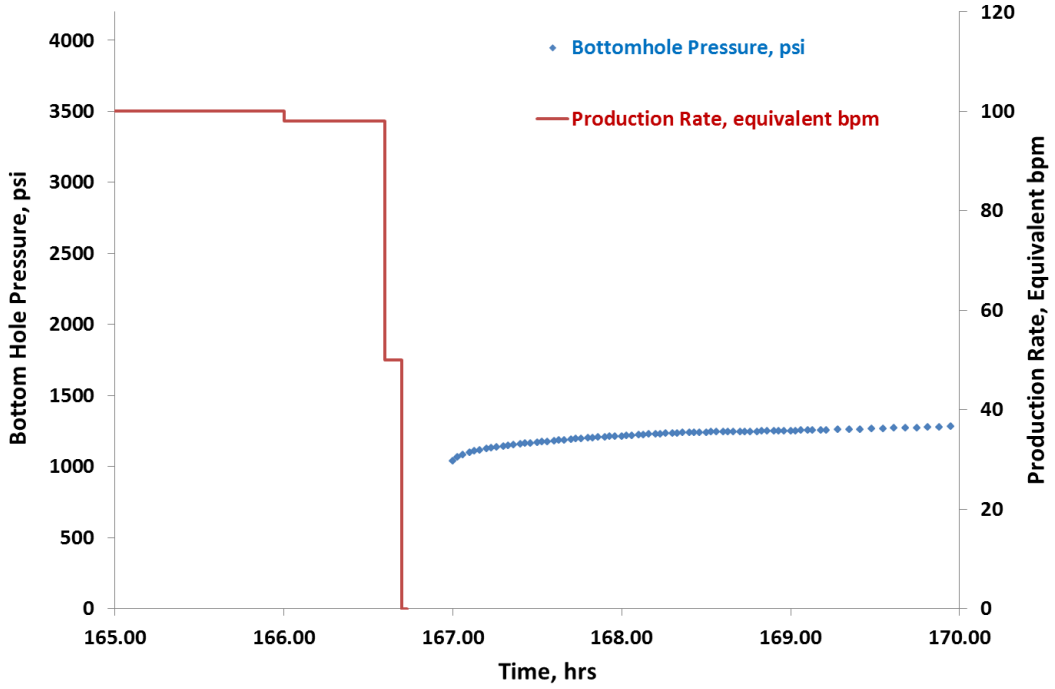

Figure 4.21 Production history and buildup sequence (zoom)

Craig and Blasingame (2006) used their type-curve method to match this buildup, which provided a reservoir permeability of 0.012 md, a fracture half-length of 121 ft and a fracture conductivity of 18 md-ft.

Log-log diagnostic plot

Similar to the FCT test, due to the fact that last production rate is much lower than the average production rate, it is imperative to use rigorous superposition time

function instead of the equivalent time approximation in creating the pressure derivative curve.

Figure 4.22 shows the FCT diagnostic plot and pressure buildup pressure difference and derivative curves on the same log-log plot. It is observed that in between 4 hr <Δt <10hr, the two derivative curves appear almost parallel. After adjusting the buildup pressure derivative curve with the rate history, the two curves overlay quite compellingly upon the pressure falloff derivative curve during after-closure pseudo-linear flow (Figure 4.23). Marongiu-Porcu et al. 2011 indicated that this provided an empirical proof of the validity of the analysis method for fracture calibration test based on the use of the log-log diagnostic plot.

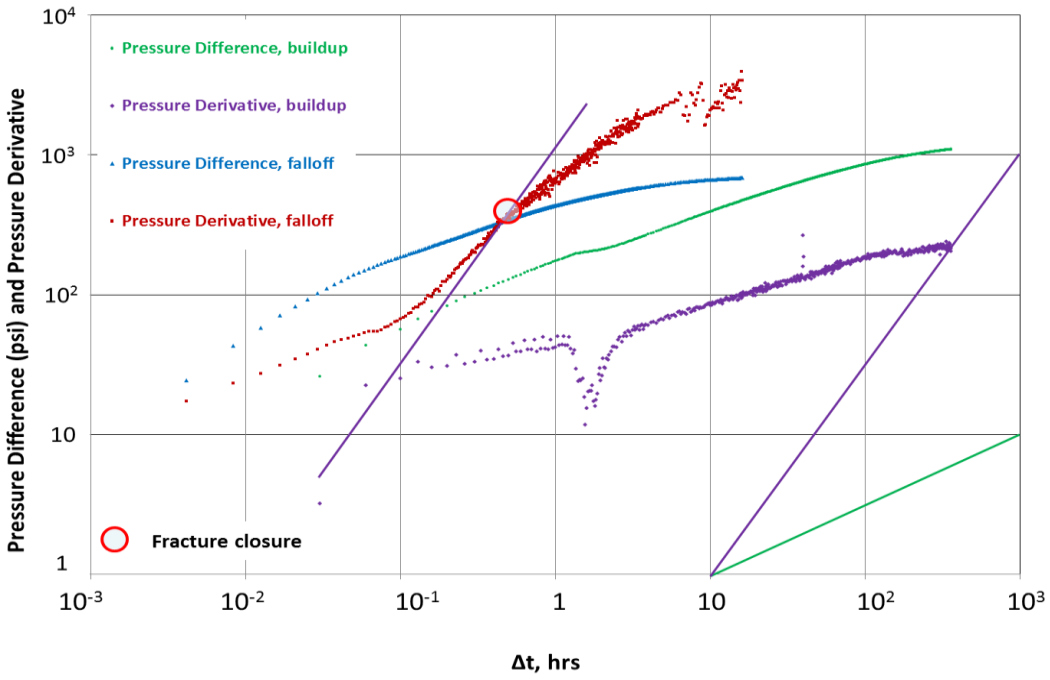

Figure 4.22 Log-log diagnostic plot with falloff and buildup data

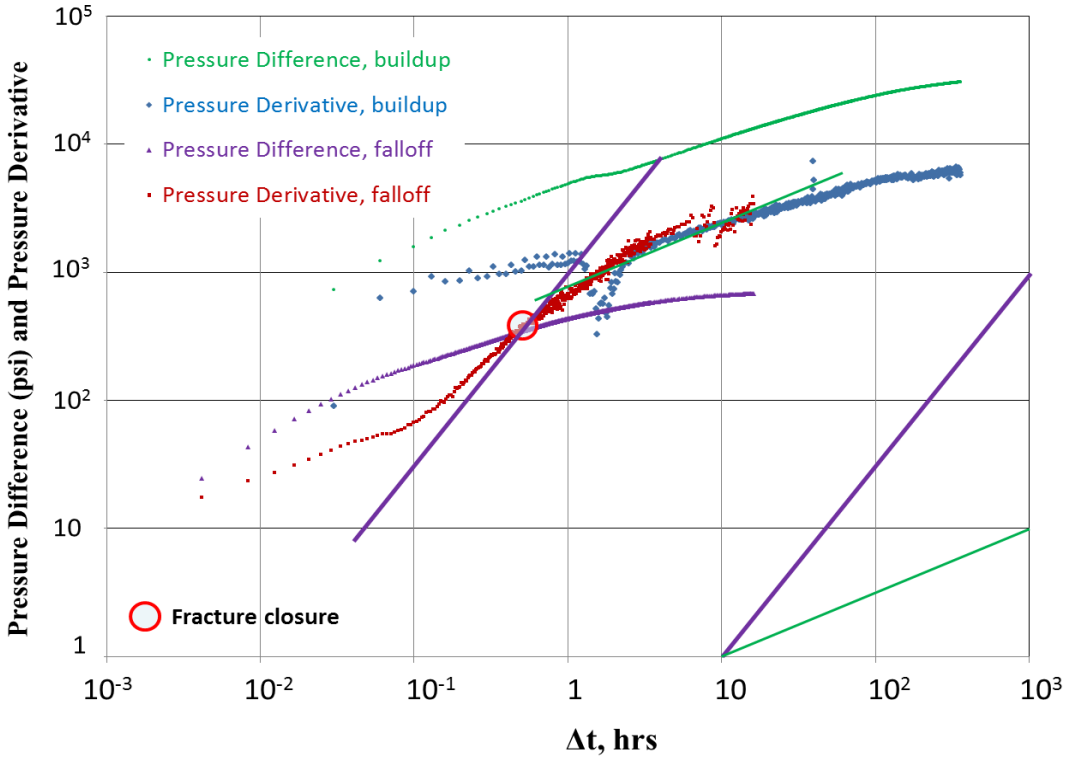

Figure 4.23 Log-log diagnostic plot with falloff and shifted buildup data, well GM

New method for estimating initial reservoir pressure for buildup test adapting FCT conventional method--Adjusted Nolte et al. 1997 method

Benelkadi reviewed Nolte's method for after-closure linear flow and he pointed out that the permeability and reservoir pressure values were insensitive to changes of a seemingly important input which was the closure pressure i.e. for different assumptions on closure pressure the derived k and P_i were practically constant. This was due to the fact that radial flow started a significant amount of time after closure had occurred. (Benelkadi et al., 2003) In the new ACA method that Benenkadi proposed, the F function (or F_L function, they are effectively the same) is applied from shut in (start of

fall off assuming that the reference time, which is supposed to be the closure time in the original Nolte's after closure method, is now the shut in time.

If we adapt Benenkadi's philosophy that P_i is insensitive to the input of t_c when using the extrapolation on F_L plot to estimation formation permeability as long as the range of data used are far enough from the closure time, then we can use shut-in time as the reference time to create a "Nolte Linear Flow" plot for linear flow period shut-in period the reservoir average pressure can be extracted from the linear flow plot. The method can not only be used in pressure falloff, but also in buildup. In this manner, the p_i extrapolated from the linear flow Plot is 2385 psi.

Permeability Estimation from k-p_i relation

The extrapolated formation pressure from Nolte (1997) linear flow function plot is 2385.3 psi. A permeability estimate can be obtained from Equation (3.1.0.10) assuming that the production prior to the buildup is mostly contributed from the sand layer that has been fractured from the FCT. Figure 4.23 illustrate the straight-line connecting the last buildup pressure with the assume initial reservoir pressure. The upper limit estimation using this method is k=4.95 md. The permeability estimation and the derivative level represent the permeability level are labeled and color coded in blue in Figure 4.24.

In comparison, if the Horner approximation is used, Eq. (3.3.0.3) would give the value of Horner line slope m', and permeability upper-limit is calculated from Eq. (3.1.0.8) as 4.28 md using the linear flow extrapolated pressure. The effect of rate history before the buildup test is significant. Therefore, in this case, using rigorous superposition function for analysis is necessary.

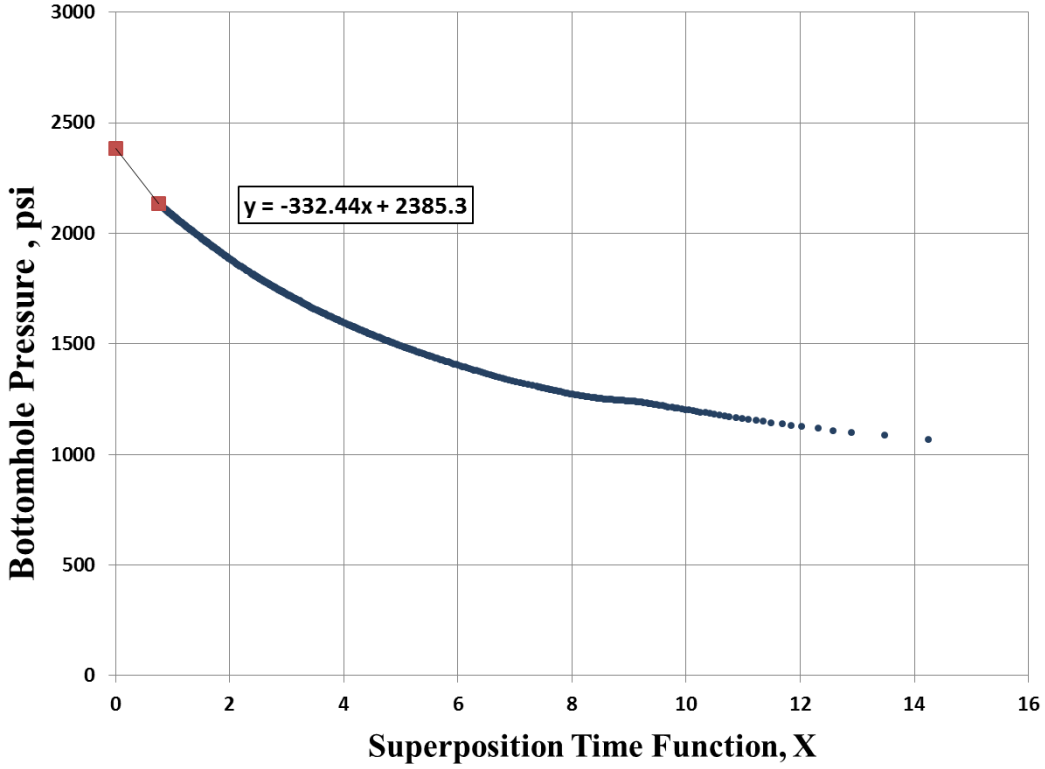

Figure 4.24 BHP vs. superposition time function - buildup, well GM

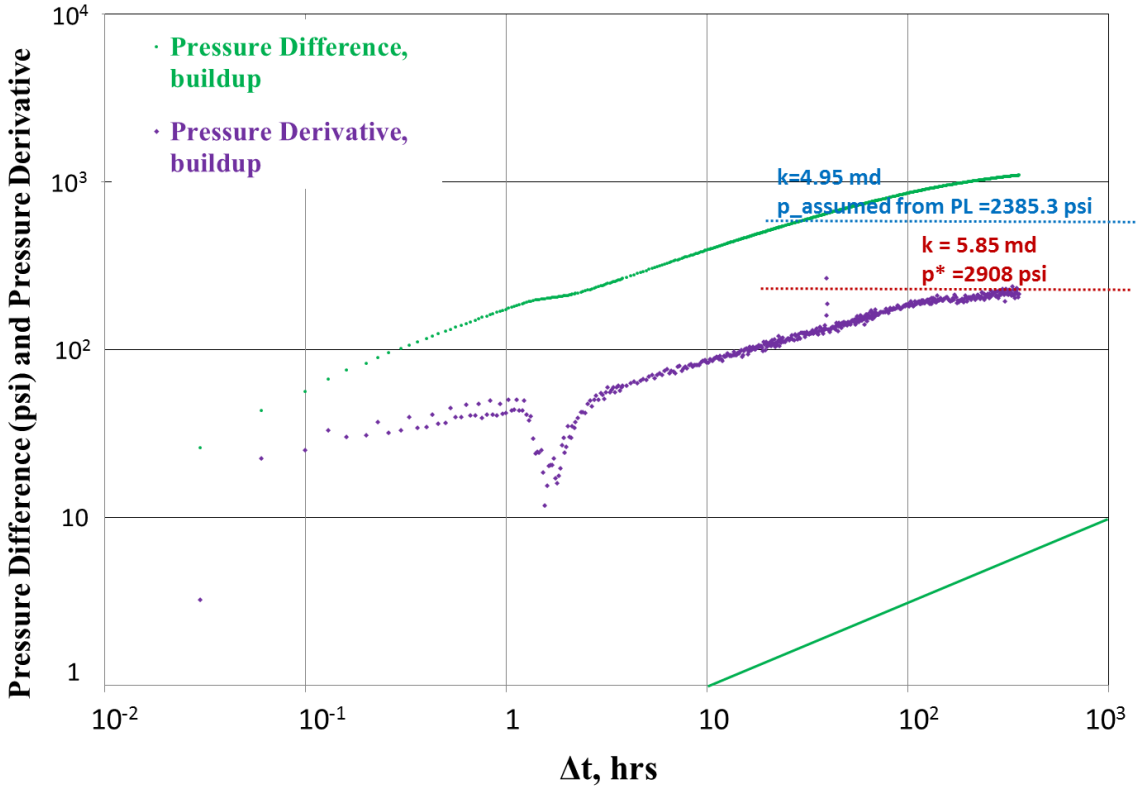

Figure 4.25 log-log diagnostic plot buildup data with analysis– Mesaverde Well GM

Figure 4.26 illustrates the portion of Figure 4.24 showing the slope connecting last buildup pressure with the assumed initial reservoir pressure. In figure 4.26, It is clear that the buildup is not long enough to be closely approaching radial flow for the "derivative level" method for permeability-thickness estimation to be applicable. The superposition function value for the last buidup data is 0.7, which is very far away superposition function X=0. Recall that the last data on FCT falloff period is located on X=0.01 (Figure 4.19). The relative large value of X results a relative small slope which leads to high upper-limit of permeability estimation. If the buildup is longer so that superposition plotting function X is close to 0, as seen in Figure 4.26, then the slope used

to estimate upper bound of permeability would be higher, so that the upper bound permeability would be much lower. Figure 4.26 shows the potential pressure profile on the superposition function plot indicated by the dashed red line. The maroon colored slope is the slope for permeability upper limit estimation if the buildup is longer for to the scenario shown on the plot. As it clearly shows in Figure 4.26, the longer the buildup, the lower the upper limit of permeability estimation or the narrow the range of the uncertainty in permeability estimation. The fact that the buildup is too short causes the overestimation of permeability. The other reason that contributes to the overestimation of permeability can be that the gas productions are taken place in all 20 sand layers and the production from the unfractured layers cannot be ignored. The properties for other layers beside the one that performed FCT are unknown. These k-h estimations are based on assumption that other layers of formation possess effectively same properties.

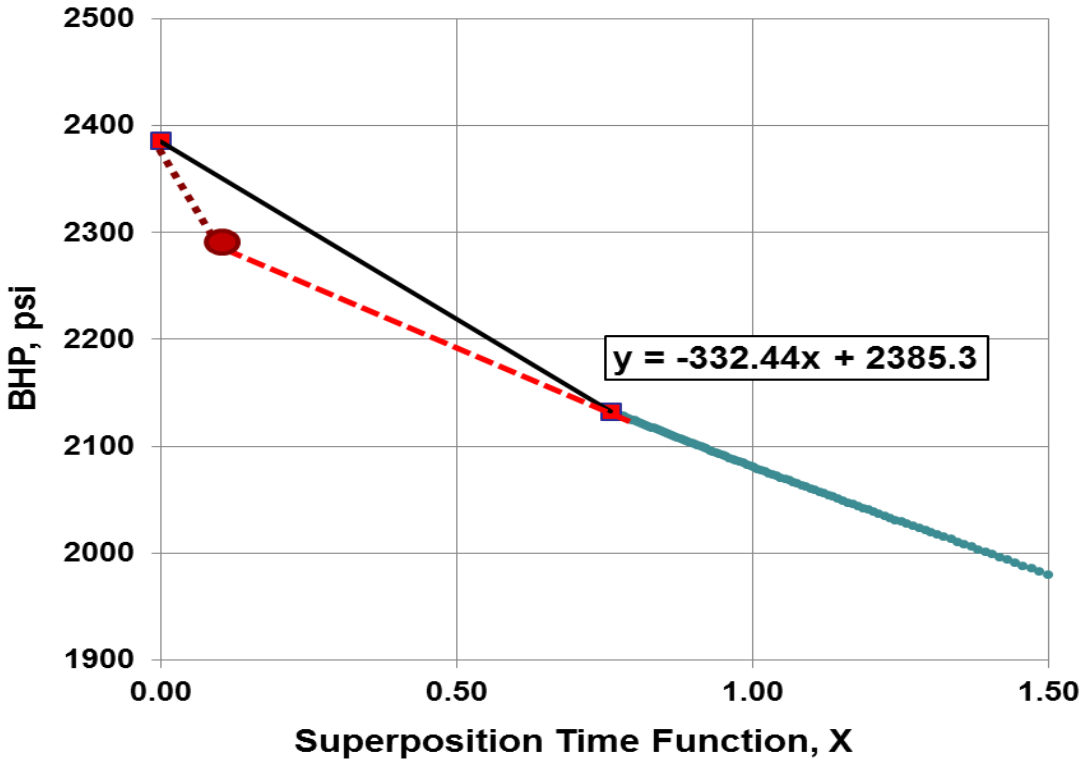

Figure 4.26 Pressure buildup data on superposition function plot

A curve match using Ecrin software is shown in Figure 4.27. The model match results in a permeability of 0.0126 md and a fracture half-length of 125 ft. The other model parameters are summarized in Table 4.4. This solution is a non-unique.

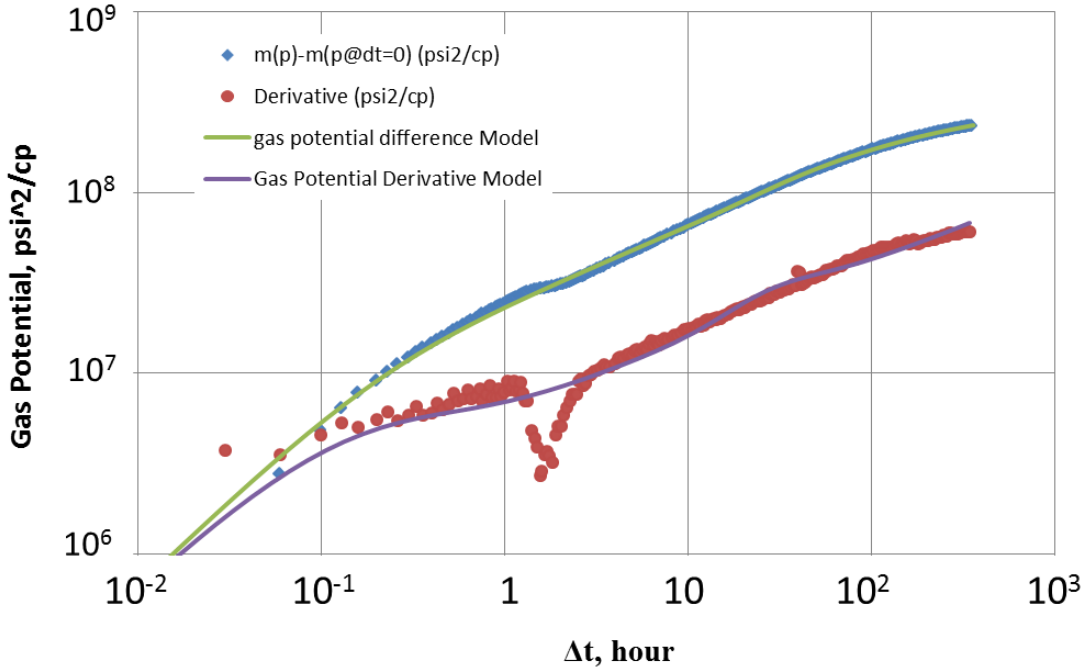

Figure 4. 27 Log-log diagnostic plot of buildup data with model generated by Ecrin–well GM

Table 4.4 Parameters match for buildup

Model Parameters		
Well & Wellbore parameters (Tested well)		
C	0.0126	bbl/psi
Skin	0.023	--
Xf	125	ft
Fc	1710	md.ft
Reservoir & Boundary parameters		
Pi	2366.31	psia
k.h	0.151	md.ft
k	0.0126	md

Table 4.5 Summary of fracture calibration test and buildup interpretations

	Falloff			Buildup	
		After-Closure			
	Before Closure, (k from empirical correlation with Gc)	pi-k relation (p from Nolte linear Flow)	pi-k relation (p from before closure)	Modeling	pi-k relation
pi, psi	2326.3	2355	2326.3	2366	2385
k, md	0.004	0.030 (upper limit)	0.026 (upper limit)	0.013	4.95 (upper limit)
kh, md-ft	0.056	0.42	0.49	0.156	69.36

Discussion

With both a FCT and a drawdown/buildup sequences completed sequentially, direct comparison of the buildup and falloff interpretations is possible.

The FCT analysis provides a set of values of formation effective permeability and initial reservoir pressure estimation. More importantly, before-closure analysis provides a means to investigate the homogeneity of the formation. From log-log plot, it indicates the pressure dependent leakoff which is related to the prediction of natural fracture dilation or reopening. The identification of a dual-porosity reservoir is crucial in productivity estimation.

In comparison, the subsequent drawdown-buildup sequence provides very few knowledge about the reservoir. In this case, even though the well is shut-in for more than half a month, the pressure buildup still hasn't nearly reached radial flow. The reason for the permeability overestimation is that the buildup using the p_i-k relation is that the shut-in time is not long enough to give a more precise permeability upper-limit estimation.

This case greatly demonstrates the efficacy and efficiency of a fracture calibration test in formation evaluation in low permeability reservoir.

CHAPTER V

CONCLUSIONS

- Fracture calibration test is a more effective and efficient way for formation permeability estimation than a drawdown-buildup sequence, especially in a low permeability formations.
- The log-log diagnostic plot offers a powerful, unified approach for before- and after- closure analysis, thus eliminating the necessity of multiple piecewise plots.
- The two common abnormal leakoff types in shale and tight gas (pressure dependent leakoff and transverse storage) can be diagnosed on the log-log diagnostic plot, thus eliminating the necessity of G-function plot.
- The characteristics manifested on the pressure semi-log derivative curve that traditionally being interpreted as pressure dependent leakoff can sometimes be interpreted as two closures.
- The utility of relation of pi-k on Horner Plot or Superposition function plot enables a better estimate of upper-limit of permeability than assuming an apparent radial flow when radial flow is absent. This approach can be applied both on fracture calibration test analysis and on conventional buildup test. The longer the falloff/buildup period (or the more approach to radial flow), the more accurate the estimation.

REFERENCES

Barree, R.D. 1998. Applications of Pre-Frac Injection/Falloff Tests in Fissured Reservoirs - Field Examples. Paper SPE 39932 presented at the SPE Rocky Mountain Regional/Low-Permeability Reservoirs Symposium, Denver, Colorado. DOI: 10.2118/39932-ms.

Barree, R.D., Barree, V.L., and Craig, D. 2009. Holistic Fracture Diagnostics: Consistent Interpretation of Prefrac Injection Tests Using Multiple Analysis Methods. SPE 107877-pa SPE Production & Operations **24** (3): pp. 396-406.

Benelkadi, S. and Tiab, D. 2004. Reservoir Permeability Determination Using after-Closure Period Analysis of Calibration Tests. SPE 88640-pa SPE Reservoir Evaluation & Engineering **7** (3): 230-237. DOI: 10.2118/88640-pa.

Carter, R.D. 1957. App. Of:" Optimum Fluid Characteristics for Fracture Extension". Drilling and Prod. Prac. API.

Cinco-Ley, H. and Samaniego-V., F. 1981. Transient Pressure Analysis for Fractured Wells. SPE Journal of Petroleum Technology **33** (9): 1749-1766. DOI: 10.2118/7490-pa.

Craig, D.P. 2005. Analytical Modeling of Fracture Injection/Falloff Sequence and the Development of a Refracture-Candidate Diagnostic Test, Ph.D. dissertation. Texas A&M University.

Craig, D.P. and Blasingame, T.A. 2006. Application of a New Fracture-Injection/Falloff Model Accounting for Propagating, Dilated, and Closing Hydraulic Fractures.

Paper SPE 100578 presented at the SPE Gas Technology Symposium, Calgary, Alberta, Canada. DOI: 10.2118/100578-ms.

Ehlig-Economides, C.A. and Fan, Y. 1994. Interpretation of Fracture Calibration Tests in Naturally Fractured Reservoirs. Paper SPE 28690 presented at the International Petroleum Conference and Exhibition of Mexico, Veracruz, Mexico. DOI: 10.2118/28690-ms.

Goodman, C.L., Howell, R.C., and Gabbard, J.M. 2005. Injection Testing to Determine Reservoir Properties. Paper SPE 93958 presented at the SPE Production Operations Symposium, Oklahoma City, Oklahoma. DOI: 10.2118/93958-ms.

Gu, H., Elbel, J.L., Nolte, K.G. et al. 1993. Formation Permeability Determination Using Impulse-Fracture Injection. Paper SPE 25425 presented at the SPE Production Operations Symposium, Oklahoma City, Oklahoma. DOI: 10.2118/25425-ms.

Gulrajani and Nolte. 2000. Reservoir Stimulation Third Edition. In Reservoir Stimulation Third Edition, ed. Economides, M.J. and Nolte, K.G.: Wiley.

Horner, D.R. 1967. Pressure Buildups in Wells. Richardson, Texas: SPE.

Marongiu-Porcu, M., Ehlig-Economides, C.A., and Economides, M.J. 2011. Global Model for Fracture Falloff Analysis. SPE-144028-MS. Paper presented at the North American Unconventional Gas Conference and Exhibition, The Woodlands, Texas, USA. Society of Petroleum Engineers. DOI: 10.2118/144028-ms.

Mayerhofer, M.J. and Economides, M.J. 1993. Permeability Estimation from Fracture Calibration Treatments. Paper SPE 26039 presented at the SPE Western Regional Meeting, Anchorage, Alaska. DOI: 10.2118/26039-ms.

Mayerhofer, M.J. and Economides, M.J. 1997. Fracture-Injection-Test Interpretation: Leakoff Coefficient Vs. Permeability. Paper SPE 28562. SPE Production & Operations **12** (4): 231-236. DOI: 10.2118/28562-pa.

Mayerhofer, M.J., Ehlig-Economides, C.A., and Economides, M.J. 1995. Pressure-Transient Analysis of Fracture Calibration Tests. Paper SPE 26527. SPE Journal of Petroleum Technology **47** (3): 229-234. DOI: 10.2118/26527-pa.

Mohamed, I.M., Nasralla, R.A., Sayed, M.A., Marongiu-Porcu, M., and Ehlig-Economides, C.A. 2011.Evaluation of After-Closure Analysis Techniques for Tight and Shale Gas Formations. Paper SPE 140136 presented at the Hydraulic Fracturing Technology Conference, 24-26 January 2011, The Woodlands, Texas, USA.

NEB. 2009. A Primer for Understanding Canadian Shale Gas - Energy Briefing Note. National Energy Board, Calgary, Alberta, Canada (November).

Nolte, K.G. 1979. Determination of Fracture Parameters from Fracturing Pressure Decline. Paper SPE 8341 presented at the SPE Annual Technical Conference and Exhibition, Las Vegas, Nevada. DOI: 10.2118/8341-ms.

Nolte, K.G., Maniere, J.L., and Owens, K.A. 1997. After-Closure Analysis of Fracture Calibration Tests. Paper SPE 38676 presented at the SPE Annual Technical Conference and Exhibition, San Antonio, Texas. DOI: 10.2118/38676-ms.

Reynolds, M.M. and Munn, D.L. 2010. Development Update for an Emerging Shale Gas Giant Field - Horn River Basin, British Columbia, Canada. Paper SPE 130103 presented at the SPE Unconventional Gas Conference, Pittsburgh, Pennsylvania, USA, 23-25 February. DOI.org/10.2118/130103-ms.

Soliman, M.Y., Craig, D.P., Bartko, K.M. et al. 2005. Post-Closure Analysis to Determine Formation Permeability, Reservoir Pressure, Residual Fracture Properties. Paper SPE 93419 presented at the SPE Middle East Oil and Gas Show and Conference, Kingdom of Bahrain. DOI: 10.2118/93419-ms.

Soliman, M.Y. and Gamadi, T.D. 2012. Testing Tight Gas and Unconventional Formations and Determination of Closure Pressure. Paper SPE150948 presented at the SPE/EAGE European Unconventional Resources Conference and Exhibition, Vienna, Austria. DOI: 10.2118/150948-ms.

Talley, G.R., Swindell, T.M., Waters, G.A. et al. 1999. Field Application of after-Closure Analysis of Fracture Calibration Tests. Paper SPE 52220 presented at the SPE Mid-Continent Operations Symposium, Oklahoma City, Oklahoma. DOI: 10.2118/52220-ms.

Thompson, J.W., Fan, L., Grant, D. et al. 2010. An Overview of Horizontal Well Completions in the Haynesville Shale. Paper SPE-136875-MS presented at the Canadian Unconventional Resources and International Petroleum Conference, Calgary, Alberta, Canada. Society of Petroleum Engineers. DOI: 10.2118/136875-ms.

Valko, P.P. and Economides, M.J. 1999. Fluid-Leakoff Delineation in High-Permeability Fracturing.Paper SPE 56135. SPE Production & Operations **14** (2): 110-116. DOI: 10.2118/56135-pa.

Shlyapobersky, J., Walhaug, W.W., Sheffield, R.E., Huckabee, P.T.1998. Field Determination of Fracturing Parameters for Overpressure Calibrated Design of Hydraulic Fracturing. paper SPE 18195, 1998 63rd Annual Technical Conference and Exhibition. Houston, 2-5 Oct.

Younes, A., Moore, H., Suumeyer, N. 2010. Sweet Spotting the Haynesville-Bossier Shale Gas Play, Northwestern Louisiana, an Integrated study. AAPG Search and Discovery Article 90122, Hedberg Conference. 5- 10 December.

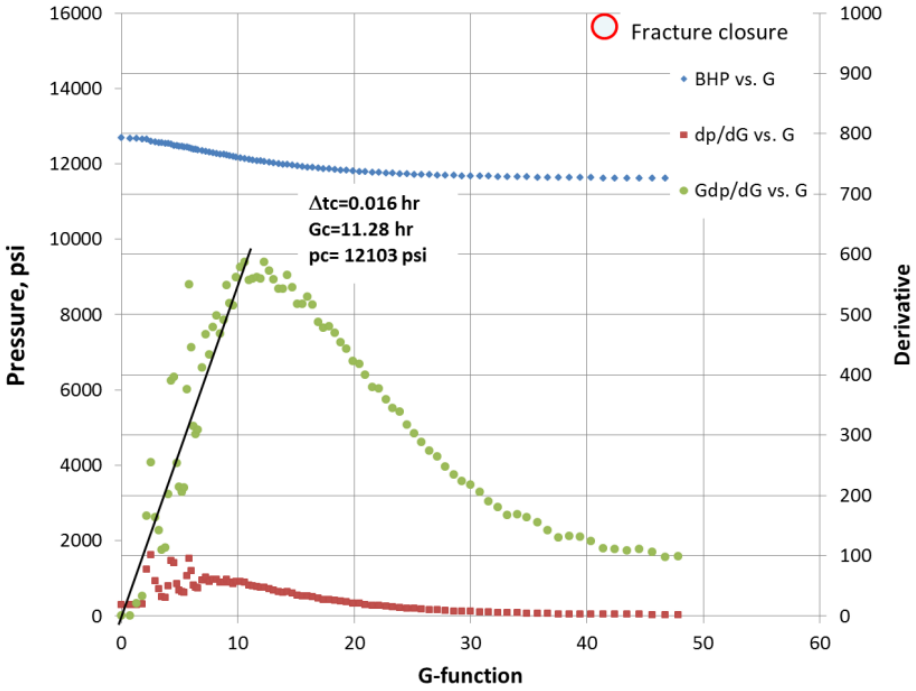

Figure Appendix 1--G-function diagnostic plot for data of Haynesville Well A

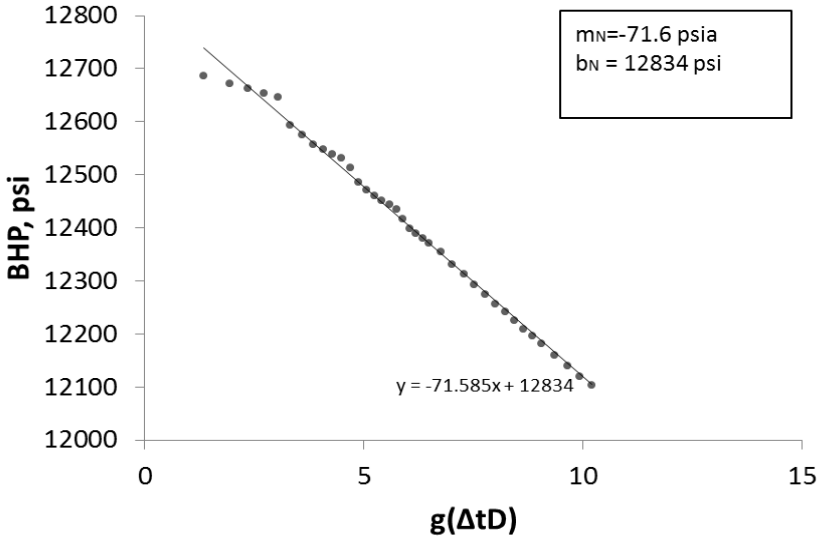

Figure Appendix 2--BHP vs. g-function Plot Well A

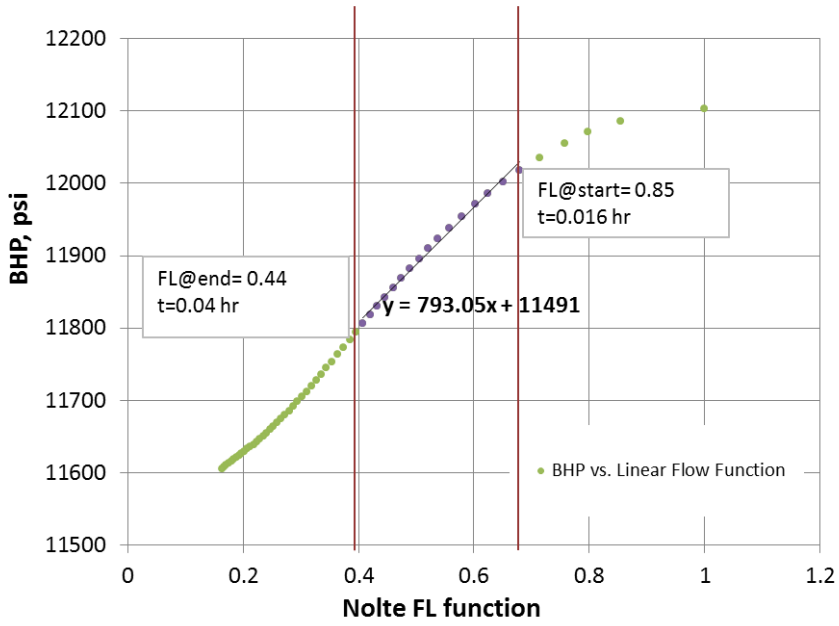

Figure Appendix 3--Bottom-hole Pressure vs. Nolte FL Plot, Well A

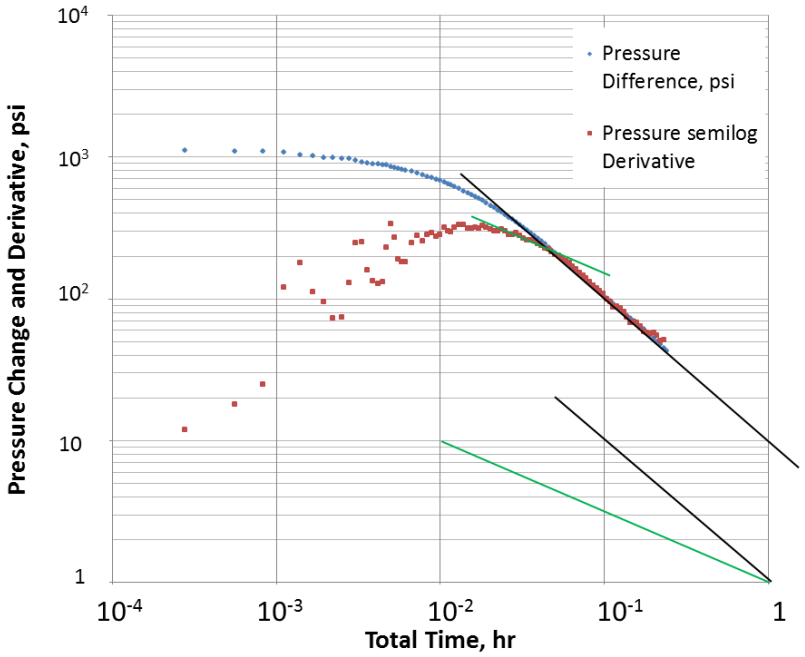

Figure Appendix 4--Pressure change and the semi-log derivative vs. time plot, Well A

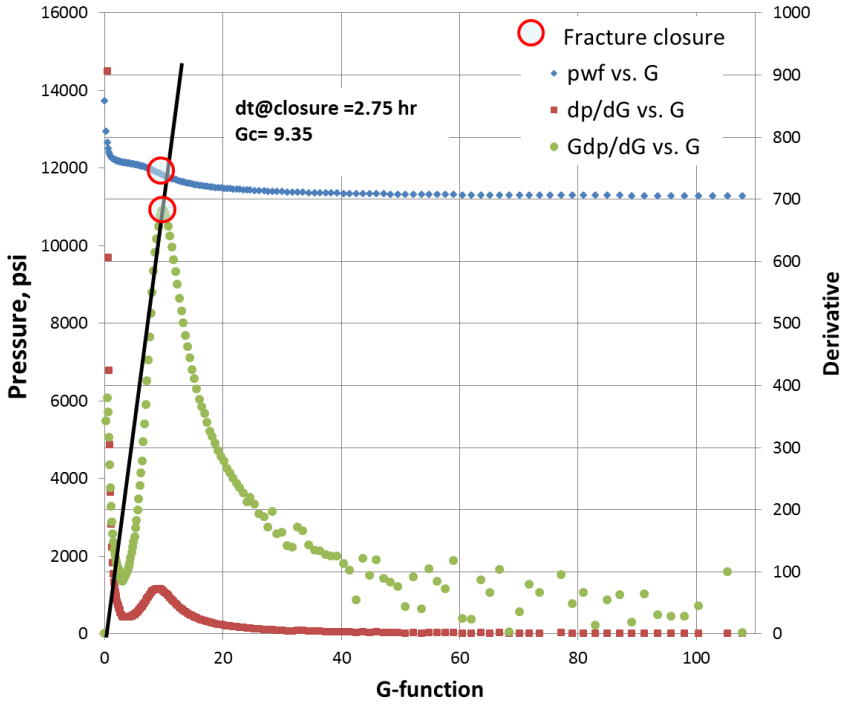

Figure Appendix 5--G-function diagnostic plot for data of Haynesville Well B

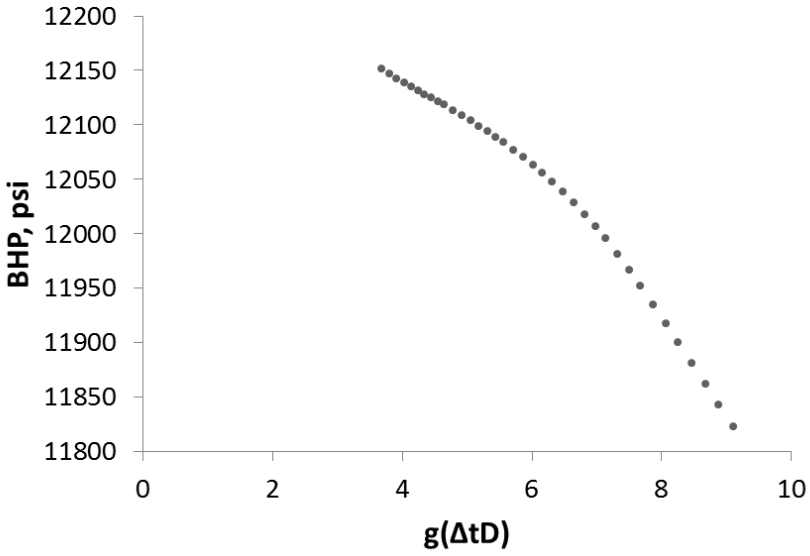

Figure Appendix 6--BHP vs. g-function Plot Well B

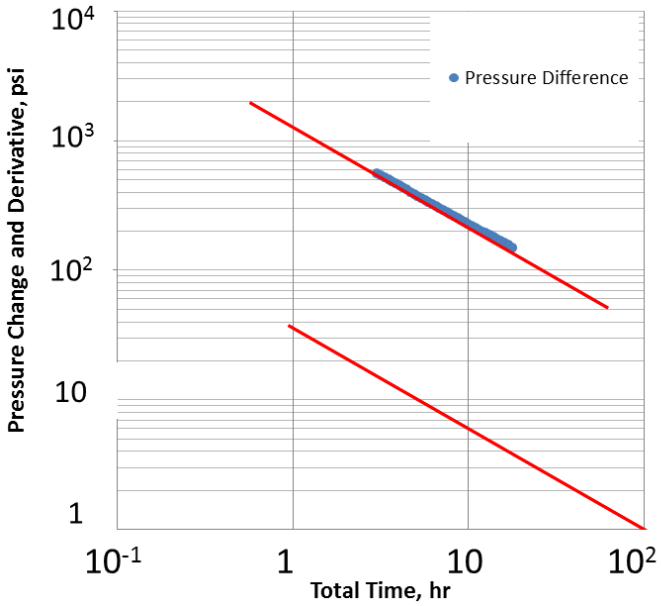

Figure Appendix 7--Pressure change and the semi-log derivative vs. time Plot for Bilinear Flow, Well B

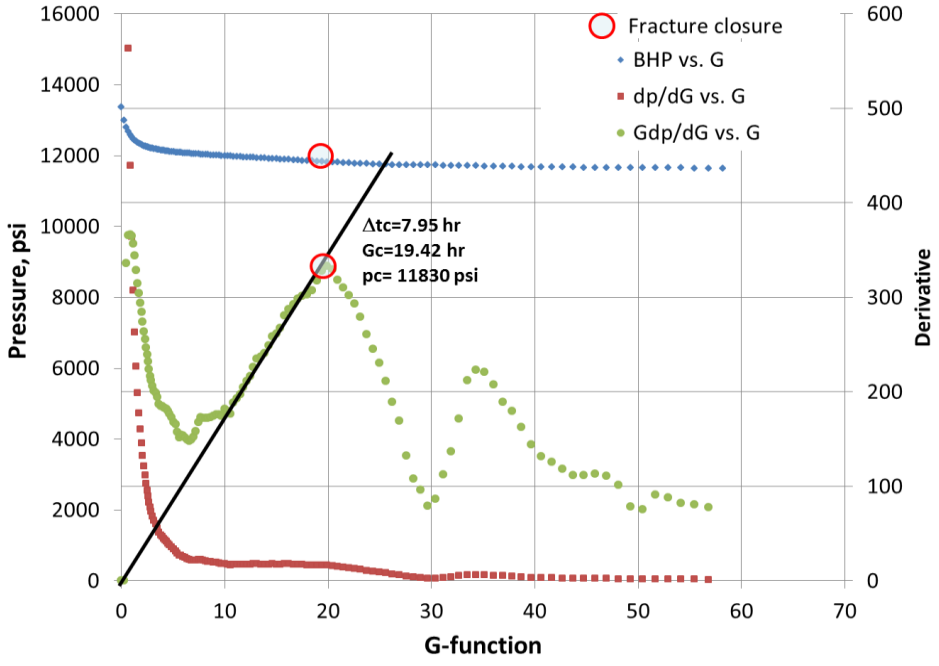

Figure Appendix 8--G-function diagnostic plot for data of Haynesville Well C FCT test

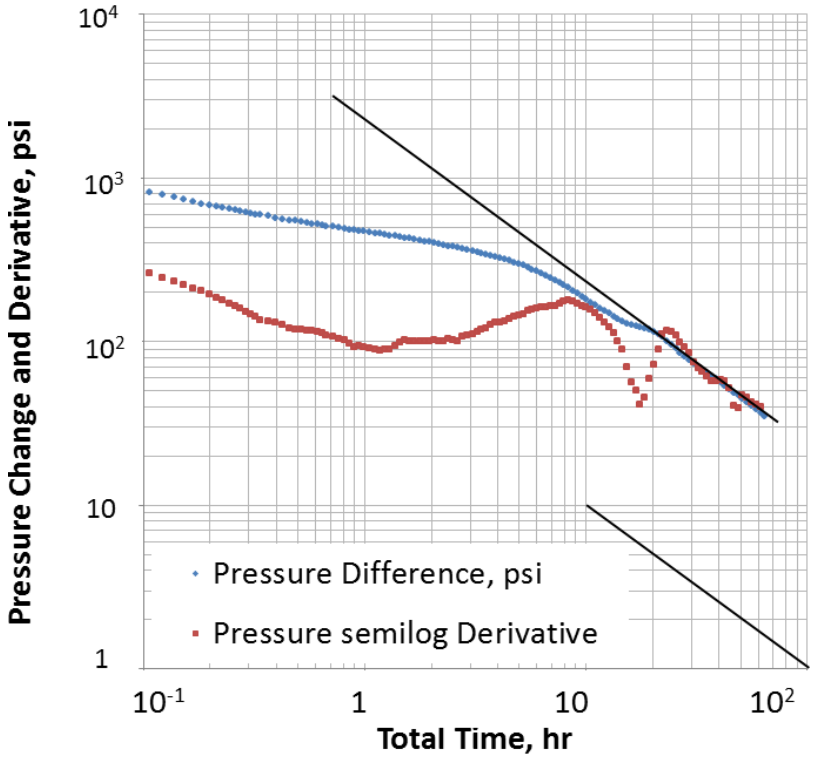

Figure Appendix 9--Pressure difference and the semi-log derivative vs. time plot, Well C

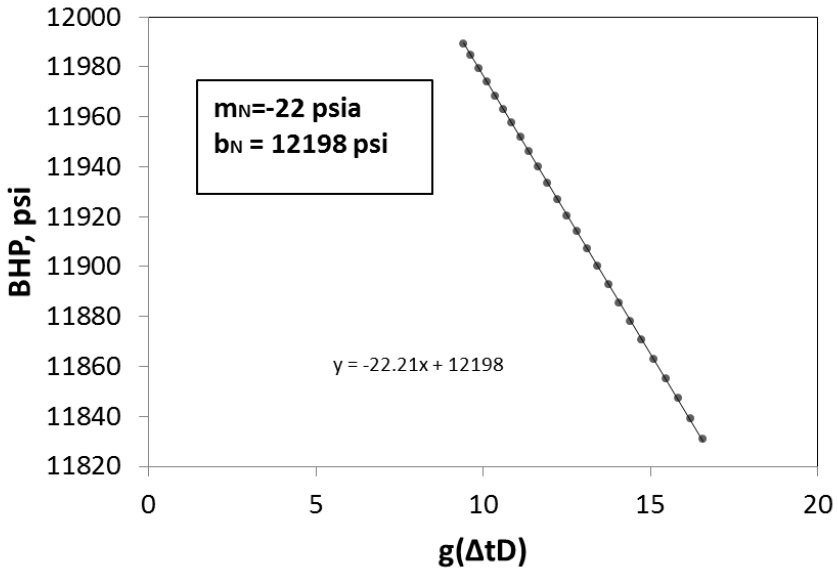

Figure Appendix 10--BHP vs. g-function plot, Well C

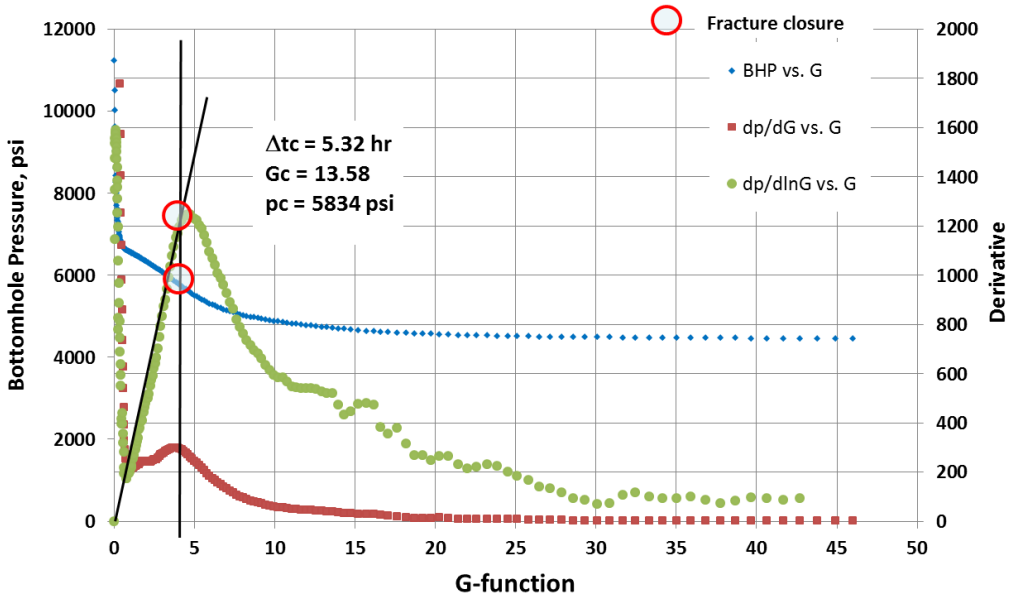

Figure Appendix 11--G-function diagnostic plot for data of HornRiver WellX FCT test

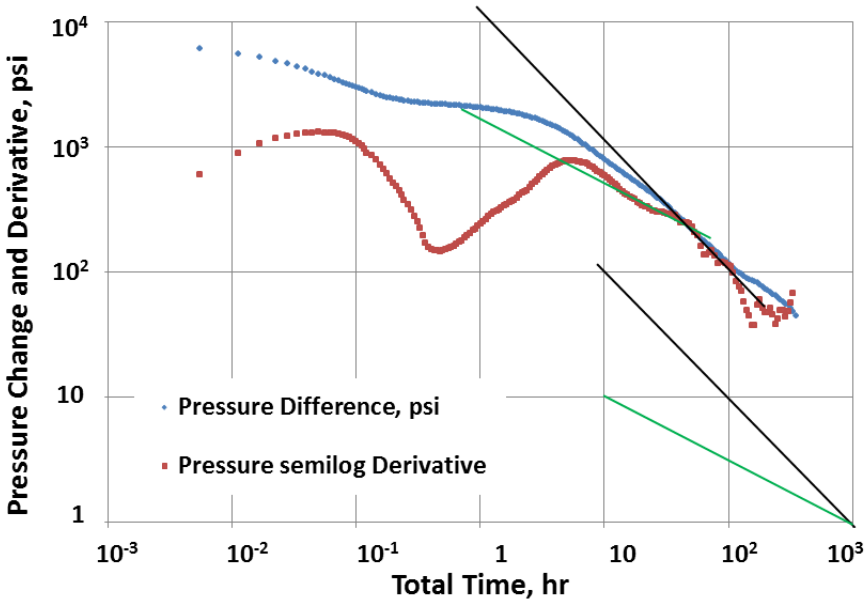

Figure Appendix 12--Pressure change and the semi-log derivative vs. time Plot for HornRiver Well Z

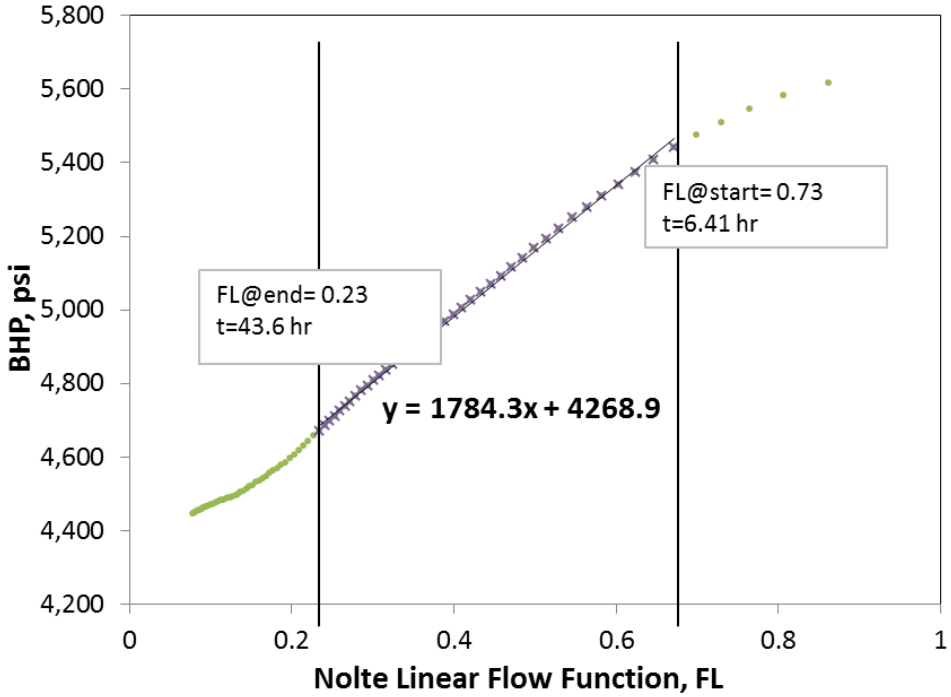

Figure Appendix 13--Bottom-hole Pressure vs. Nolte FL Plot, HornRiver Well Z

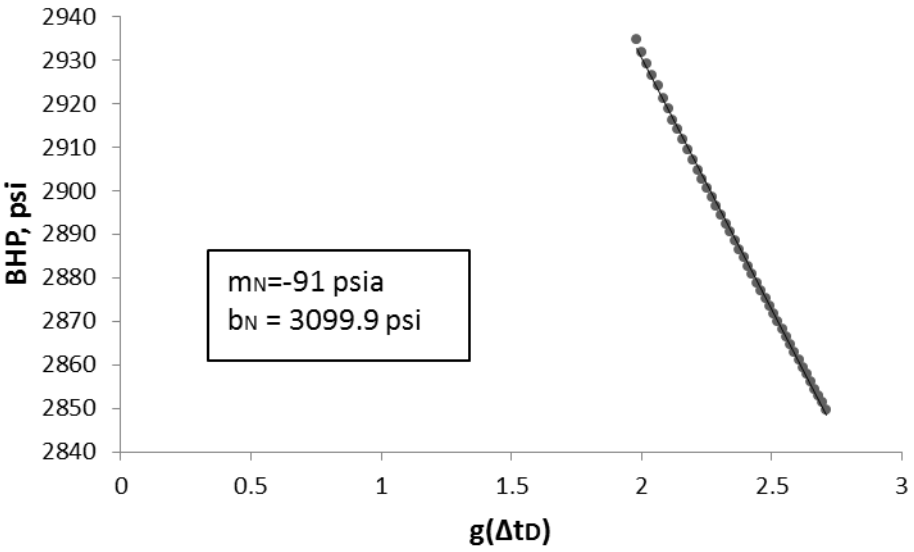

Figure Appendix 14--BHP vs. g-function plot Well GM

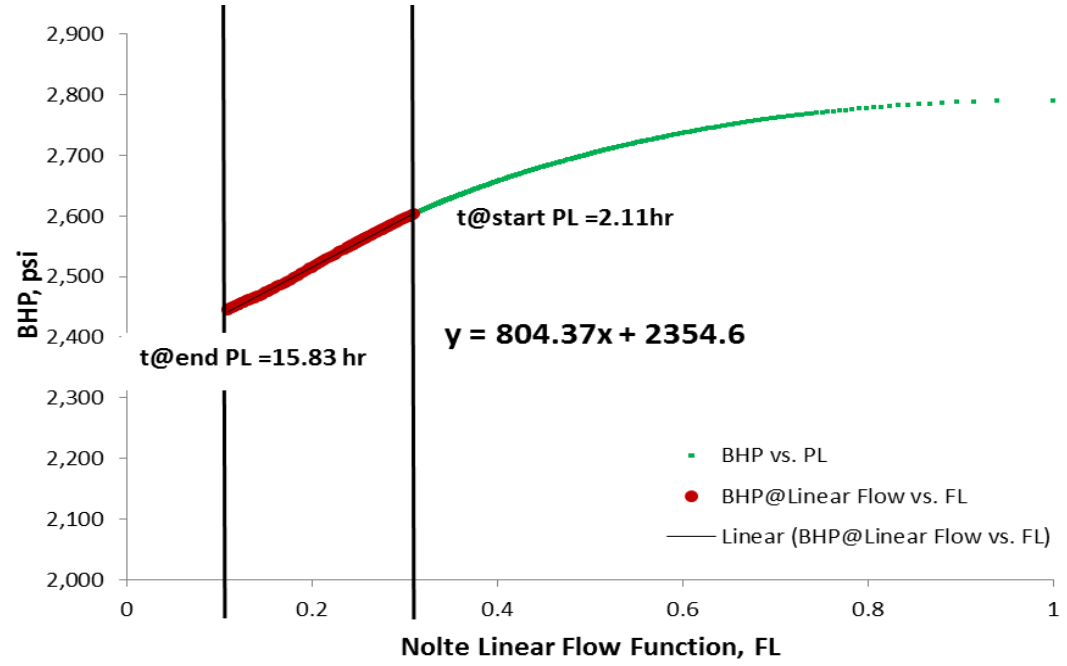

Figure Appendix 15--Bottom-hole pressure vs. Nolte F_L plot, Well GM

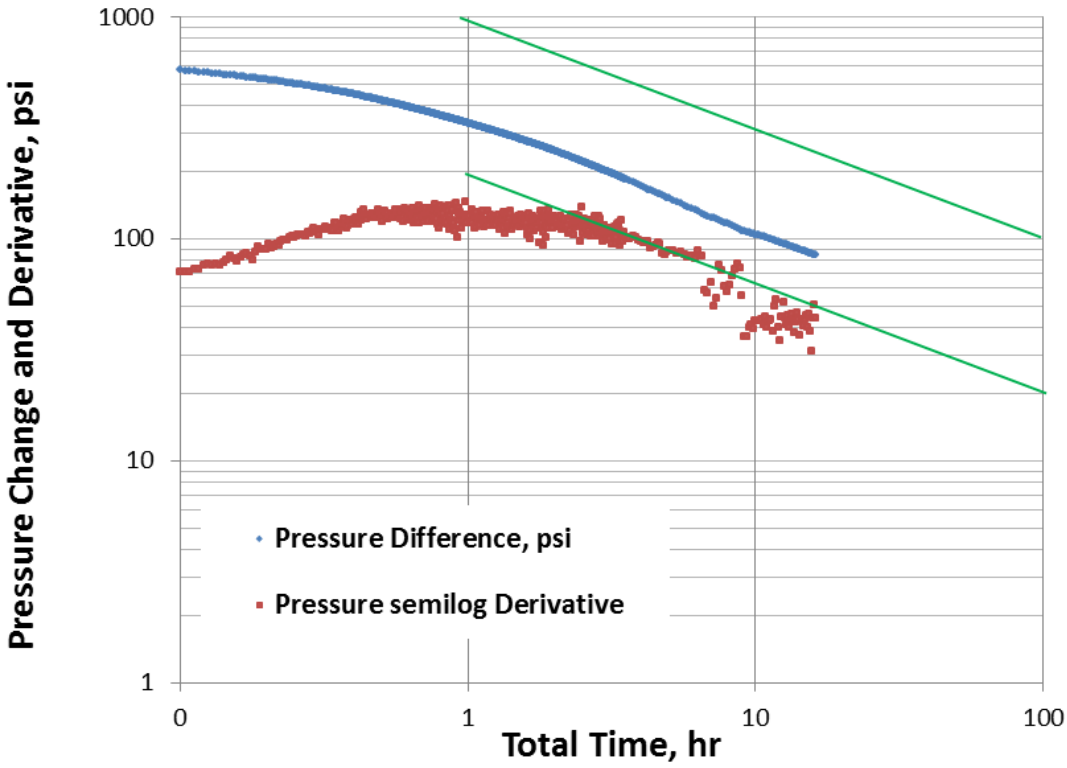

Figure Appendix 16--Pressure change and the semi-log derivative vs. time Plot-buildup, Well GM

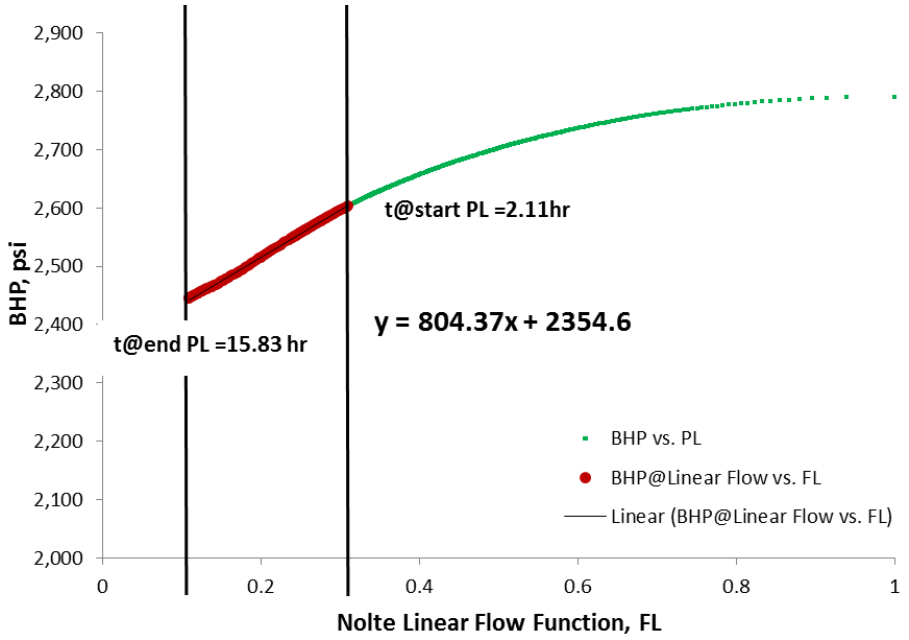

Figure Appendix 17--Bottom-hole Pressure vs. Nolte FL Plot, Well GM

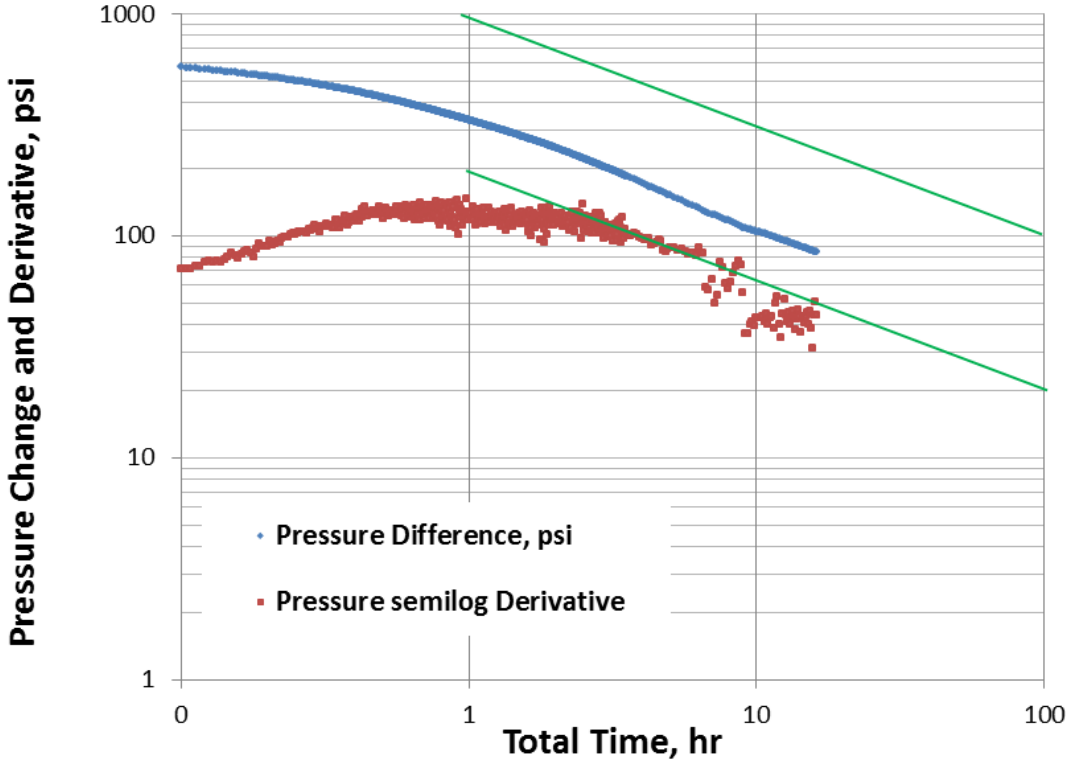

Figure Appendix 18--Pressure change and the semi-log derivative vs. time plot-buildup, Well GM

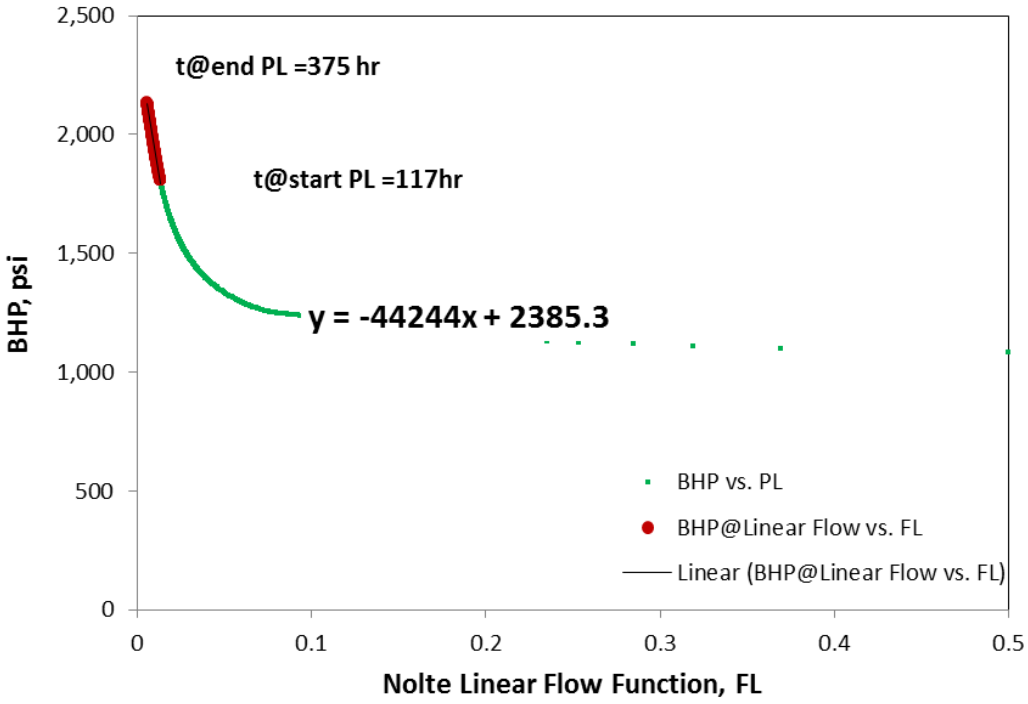

Figure Appendix 19--Bottom-hole pressure vs. Nolte F_L plot, buildup, Well GM